ANALYSIS OF COLD ROLLING OF SINTERED POROUS METAL STRIP BY UPPER BOUND TECHNIQUE

by

DESHMUKH. A. R.

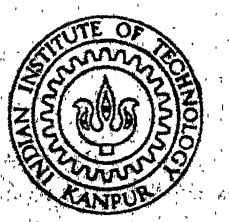

DEPARTMENT OF METALLURGICAL ENGINEERING

INDIAN INSTITUTE OF TECHNOLOGY KANPUR

SEPTEMBER, 1990

ANALYSIS OF COLD ROLLING OF SINTERED POROUS METAL STRIP BY UPPER BOUND TECHNIQUE

A Thesis Submitted

in Partial Fulfilment of the Requirements
for the Degree of

MASTER OF TECHNOLOGY

by

DESHMUKH. A. R.

to the

DEPARTMENT OF METALLURGICAL ENGINEERING
INDIAN INSTITUTE OF TECHNOLOGY KANPUR

SEPTEMBER, 1990

ME-1990-M-DES-ANA

To

My Father

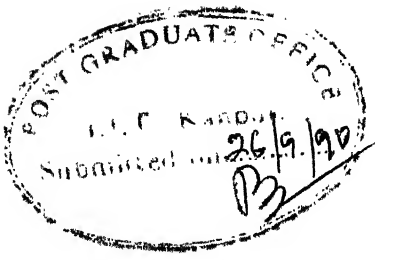

CERTIFICATE

Certified that the work presented in this thesis has been carried out under our supervision and that the work has not been submitted elsewhere for a degree.

Dr.R.K.Dube
Professor
Dept.of Met. Engg.
I.I.T. Kanpur-208016

Dr.T. Sundararajan
Assistant Professor
Dept. of Mech. Engg.
I.I.t. Kanpur - 208016

ACKNOWLEDGEMENTS

I express my deep sense of gratitude to Dr. R.K. Dube and Dr. T. Sundararajan, for their expert guidance and constant encouragement throughout the course of this thesis.

I am grateful to Dr. S. Bhargava for his valuable suggestions and discussions at every stage of this work.

I am thankful to Dr. Batra for having given me access to the excellent facilities in the Computer Centre. I would also like to thank Mr. S.C. Soni, Powder Metallurgy Lab. for his cooperation.

I would particularly like to express my appreciation to Mr. V.R. Kanetkar, for his continuous encouragement while carrying out this work.

Mr. U.S. Misra deserves my warmest thanks for the excellent typing. Thanks to Mr. Ganguly for the neat sketches.

Finally, I wish to thank to many friends who helped and encouraged the work in various ways.

CONTENTS

LIST OF FIGURES

LIST OF TABLES

LIST OF SYMBOLS

f = The degree of influence of the hydrostatic stress component on the onset of yielding

f' = The ratio of the apparent stress applied to the porous body and the effective stress applied to the mnatrix

V_i = Prescribed velocity over the portion of surface A_v in upper bound theorem

$\dot{F}_i$ = Prescribed surface traction over surface area A_F

V^*_i = Any kinematically admissible velocity field satisfying $V^*_i = V_i$ on A_v

x = x-direction coordinate

y = y-direction coordinate

z = z-direction coordinate

L = Projected length of arc of contact in the rolling direction

V_n = Normal velocity to the roll surface

u = Longitudinal or horizontal velocity of the strip

v = Transverse or vertical velocity of the strip at any point in the domain

u_1 = Entrance velocity of the strip

y_1 = Half entry thickness of the strip

y_2 = Half exit thickness of the strip

y_o = Entry strip thickness

y = Local strip thickness

W = Total power

W_p = Power required for plastic deformation

W_F = Friction power

W_s = Shear power loss at the discontinuity

U = Roll speed

m = Friction factor

b = Density exponent

K = Critical shear stress

Greek Symbols

$\sigma_1, \sigma_2, \sigma_3$ = Principal stresses

σ_m = Hydrostatic stress

$\bar{\sigma}_{eq}$ = Equivalent stress to which the matrix metal is suabjected

$\bar{\varepsilon}_{eq}$ = Equivalent strain corresponding to the stress state $\bar{\sigma}_{eq}$

$d\varepsilon_1, d\varepsilon_2, d\varepsilon_3$ = Principal strain increments

ε_v = Volumetric strain

$\dot{\varepsilon}_{ij}$ = Exact strain rate in upper bound theorem

σ_{ij} = Exact stress state

ε^*_{ij} = Strain rate derived from V^*_i

σ^*_{ij} = Stress state which does not violate yield condition and is connected to $\dot{\varepsilon}^*_{ij}$

$\dot{\varepsilon}_x, \dot{\varepsilon}_y, \dot{\varepsilon}_z$ = Normal strain rates in x, y and z-direction respectively

$\dot{\gamma}_{xy}, \dot{\gamma}_{xz}, \dot{\gamma}_{yz}$ = Shear strain rates

$\dot{\varepsilon}_v$ = Volumetric strain rate

ρ = Relative density at any point in the deformation zone

ρ_1 = Initial relative density of strip

ξ = Streamliane coordinate

Ψ = Stream function

τ = Boundary shear stress

ξ, η = Local coordinates for four noded isoparametric element

SYNOPSIS

An upper-bound solution methodology has been developed for the cold densification rolling of sintered porous metal strips. Based on the recently derived plasticity theory for porous metals, the density and velocity fields during rolling have been estimated by minimizing the rolling power. The effects of rolling parameters such as friction between the rolls and the strip, roll diameter, roll speed, strip thickness and percentage reduction and also the material characteristic such as initial relative density of the porous metal, on the densification behaviour and rolling power are investigated. The other process variables such as roll pressuure and percentage slip are also calculated. The multi-pass cold densification rolling with and without intermediate annealing is analysed. The effect of work hardening is also taken into account. The density and strains have been verified experimentally for multi-pass rolling of poros copper strip.

In the upper bound analysis, a stream function form which produces a kinematically admissible velocity field is assumed. The total power for rolling, which is the sum of the internal power for plastic deformation, frictional power and shear power losses along the surface of velocity discontinuity, is minimized to find the velocity and density distributions. It is also shown that, there exists an optimal entrance strip velocity which corresponds to minimum power consumed.

The distributions of density, velocity and strain indicate that the deformation is homogeneous. The results for roll pressure clearly show that the roll pressure is much smaller for porous metal than that of solid material under similar rolling conditions. It is seen that the exit relative density of strip increases with increase in friction factor. Also, the power required to deform the material is higher for large friction factors. The roll speed and roll radius do not affect the densification. However, the results show a marked increase in the power consumed at higher speeds. The effect of initial strip thickness is also investigated. It is shown that densification is larger for smaller strip thickness. It is also observed that the densification behaviour is significantly influenced by initial relative density of strip.

The calculated results for density and strains are in good agreement with the experimental ones for multi-pass rolling of porous copper strip. It is also shown that the densification of porous copper strip is not affected by the mode of cold rolling i.e. cold rolling with intermediate annealing or cold rolling without annealing. However, the work almost increases by factor of two, if annealing is not performed.

CHAPTER I

INTRODUCTION

1.1 ROLLING OF POROUS METALS:

For making products via traditional powder metallurgy technique, powders are compacted in dies and subsequently sintered at elevated temperatures. The products thus obtained usually contain porosity of the order 3-10%, and are characterised by poor ductility value, which limit their usage to low stress applications. Various methods such as forging, extrusion and rolling are used to improve the strength, and in particular ductility, of the sintered product. Hot or cold rolling of sintered green strip is done to produce strip of full density.

The entire process of making strip by powder metallurgy method consists of making a green strip from metal powder. This is generally done by roll compaction of loose metal powder. Alternatively green strip can also be obtained by slurry method [1]. The green strip is then sintered at the appropriate temperature to increase the strength. Subsequently the sintered strip is densified by either hot rolling in one pass or repeated cold rolling-annealing cycles. Finally, the strip is cold rolled and annealed to improve surface finish and mechanical properties.

The deformation behaviour of sintered porous metal is greatly influenced by the presence of voids. The analytical methods that are used to study the deformation of ordinary pore-free metals cannot be applied directly to porous metals, due to the additional problems created by these voids. Kuhn [2] and

Green [3] independently proposed yield criteria and stress-strain relations, which take into account density changes during the deformation of porous metals. However, the application of these theories was limited to uni-axial compression and tension or plane-strain compression, and could not be extended to analyse the complicated deformation processes. Shima and Oyane [4] later proposed a plasticity theory by extending the yield criterion to a general stress state.

Most of the studies carried out in the area of powder metallurgy processing of fully dense strip have been concerned with the feasibility of the process for producing a sound product. A number of analytical studies have also been carried out on roll compaction of loose powder to produce green strip. However, very little information is available on the densification rolling of a sintered porous strip. The present study concerns with the cold densification rolling of a porous copper strip and describes a theoretical methodology to analyse the various aspects of material deformation and densification characteristics.

1.2 REVIEW OF THE PREVIOUS WORK:

The densification of sintered P/M products have been widely studied experimentally. However, only a few theoretical studies on this area are available in the literature. Most of the earlier analysis, have dealt with forging of sintered powder compacts. While, considerable amount of work has been done on solid metal strip rolling for a wide range of rolling parameters, very little information is available at present on the

densification rolling of porous metal strips. So far no attempt has been made to study the importance of various rolling parameters on the densification rolling of P/M sintered strip.

A major objective of mathematical modelling of metal forming processes is to provide the necessary information for proper design and control of these processes. Therefore, the method of analysis must be capable of determining the effects of various process parameters on the metal deformation characteristics. A wide spectrum of solution techniques have been emplouyed in the past to analyse the metal forming processes. The most popular among these are the upper bound analysis and the finite element method. The finite element method has received considerable attention as being the most powerful technique for the analysis of metal forming processes. The major advantage of the finite element method is that the method can be applied to a wide class of boundary value problems without restrictions of workpiece geometry. It is possible to take into account the realistic boundary conditions and material properties. However, the amount of computational effort required for FEM analysis is often very high. The upper bound technique is also a useful analytical tool for metal forming problems. One of the major advantages of this method is that it is relatively simpler than FEM and yet is powerful enough to predict the values of important design parameters or operational variables.

The rolling of fully dense material has been analysed extensively by various authors using the upper bound theorem or the finite element method [5-14]. The effects of rolling parameters such as friction factor, roll diameter, roll speed,

percentage reduction, front and back tension etc. have been studied in detail. Avitzur [5] analysed the cold strip rolling of an ideal plastic material using the upper bound approach. The conditions of constant Columb friction coefficient were investigated. Recently, Avitzur and co-workers [6] have proposed the use of two triangular velocity fields for the upper bound solution of strip rolling. The effects of various process parameters upon the total power has also been studied in this work.

The finite element analysis of cold strip rolling was attempted by Rao and Kumar [7]. A plane strain problem was treated using the incremental displacement method. The stress and strain histories along the material path were traced and a nonlinear analysis of the problem was carried out. The deformation and pressure distributions in the plastic zone were obtained. The elasto-plastic finite element modelling of cold strip rolling was investigated by Liu and co-workers [8,9]. Assuming plane strain conditions, the elastic and plastic deformations both inside and outside the nominal contact zone have been predicted. Solutions for nonsteady and steady state rolling have been obtained for a wide range of rolling parameters. Mori et al. [10] have simulated the deformation characteristics for plane strain rolling by the rigid plastic finite element method. A slightly compressible material with and without work hardening has been considered. Both steady and nonsteady state strip rolling have been analysed. The three-dimensional deformation in rolling has been studied using FEM by Mori and Osakada [11]. A constant coefficient of friction have

been assumed between the plate and the rolls.

As compared to solid metal rolling, the strip rolling of porous material has not yet been analysed in so much detail. Mori and Osakada [15] developed a finite element model for analysing the plastic deformation of sintered powder metals. The plane strain hot rolling of sintered powder plates were considered and the distribution of density, strain, strain rate and stress in the plate as well as roll pressure, were calculated. Using a variational formulation by rigid plastic material along with the plasticity theory of Shima and Oyane [4], they performed a transient analysis in which the calculation was repeated from the initial state till the final steady state rolling was achieved. The non-steady state rolling was treated because the authors experienced difficulties in achieving a good convergence for the steady state scheme. It was found that, the computed stresses and strains were greatly influenced by the density distribution. In other related studies [16,17] the same authors have studied upsetting and the indenting of cylindrical billets. They have employed the rigid plastic finite element method to predict the stresses and the relative density distributions within the deformed material.

It is clear from the review of literature presented above that considerable gap exists in the theoretical understanding of cold densification rolling of porous metal strips. In particular, simple analysis based on the upper bound technique are not available. The present study is a modest attempt to bridge the gap in the theoretical knowledge on this subject.

1.3 OBJECTIVE AND SCOPE OF THE STUDY:

The present study aims to achieve the following objectives:

(i) To analyse the densification behaviour of porous metals during cold rolling, using the upper bound technique.

(ii) To provide estimates of the total power required for rolling and the break-down of rolling power into its various components.

(iii) To predict the variations of velocity, strain components, and density within the deformation zone, and roll pressure and percentage slip.

(iv) To conduct a detailed parametric study and investigate the effects of process and material parameters such as roll diameter, roll speed, friction factor, percentage reduction, strip thickness and the inlet strip density.

(v) To analyse single-pass and multi-pass cold rolling; studying multi-pass rolling with and without intermediate annealing.

(vi) To verify the theoretical predictions on densification and strains experimentally.

Due to limitations on the range of published data on material properties the scope of the study has been restricted as follows:

(i) Simulation has been carried out for copper strips in the relative density range of $0.7 < \rho < 0.995$.

(ii) The range of parameter values considered are:

roll radius: 67.5 mm - 350 mm

roll speed: 550 mm/s - 800 mm/s

friction factor: 0.3 - 0.6

percentage reduction: single pass: 5% - 35%

multi-pass : upto 86.6% (theoretical)

upto 61.4% (experimental)

initial strip thickness: 0.5 mm - 6.6 mm

(iii) Steady state rolling has been analysed. The stress-strain relationship proposed by Shima and Oyane [4] have been considered.

(iv) Density has been assumed to be uniform over each cross-section within the plastic zone. A power function form of density variation with the strip thickness has been assumed as proposed by Bhargava [18].

(v) Only densification and strain characteristics have been measured experimentally.

CHAPTER II

MATHEMATICAL MODEL OF COLD DENSIFICATION ROLLING

2.1 PLASTICITY THEORY FOR POROUS METALS:

Powder metallurgical techniques, combined with conventional deformation processes, have become quite useful for the fabrication of various engineering products. Sintered powder metals are employed as starting materials in many of the common working processes such as forging and extrusion. In the modelling of these deformation processes, in general,plasticity theory has been found to be an invaluable tool for the calculation of forming loads and stress distributions. Powder metal working processes, however, do not come under the purview of common plasticity theories, since during the plastic deformation of porous metals, the material volume undergoes a drastic change. Moreover, conventional yield criteria are not applicable and the constitutive relations between stress aand strains are complex with a strain dependence on density. Analysis of powder metal working, therefore, requires the use of special plasticity theories. In recent years, the plastic deformation characteristics of porous materials have aroused wide research interest. Yield criteria and stress-strain relations for porous materials in uniaxial tension/compression have been proposed by Kuhn [2] and Green [3]. These have, later been extended to a general stress state by Oyane [4].

2.1.1 Yield behaviour of P/M materials:

It is a well-known fact that plastic deformation of a fully dense material does not involve any volume change. Also, hydrostatic stress has no influence on the yield behaviour of a fully dense material. The yield criterion for such a material, is therefore, only a function of the second invariant (J'_2) of the stress deviator throughout the expression

$$f = (3\,J'_2)^{1/2} \tag{2.1}$$

where, f is the yield surface. The invariant J'_2 is, in turn given by the expression

$$J'_2 = [(\sigma_1 - \sigma_2)^2 + (\sigma_2 - \sigma_3)^2 + (\sigma_3 - \sigma_1)^2]/6 \tag{2.2}$$

with σ_1, σ_2 and σ_3 being the principal stresses. It is evident from the equation (2.2) that yielding depends only on the stress difference for a dense material and that a pure hydrostatic stress will not influence yielding.

In the sintered powder metal, however, there is a change in material volume after deformation and the yield behaviour if sensitive to the hydrostatic stress. A criteron was proposed by Green [3], which was based on elastic-plastic deformation of a volume element containing spherical pores. The criterion is given by

$$\delta Y^2 = J'_2 + \alpha J_1^2 \tag{2.3}$$

where, α and δ are the functions of the porosity and Y is the

yield strength of the material. However, it was found that the above relationship overestimates the Poisson's ratio at low densities and predicts a much lower sensitivity to increasing density as compared to experimental measurements. The Poisson's ratio for solid metal is equal to 0.5, while it is smaller for porous metals and increases till it attains a value of 0.5 when the density approaches 100%.

Another criterion for the yielding of porous materials as proposed by Kuhn and Downey was based on the observed relationship between and density [2]. This relationship is given by

$$\nu = \frac{\text{lateral strain}}{\text{longitudinal strain}} = 0.5\ \rho^{a} \qquad (2.4)$$

where, a = 1.92 for room temperature deformation and a = 2.0 for hot deformation. Kuhn and Downey modified the yield criterion for a fully dense material and proposed the following criterion for porous materials:

$$f = [3\ J'_2 - (1 - 2\nu)\ J_2\ ]^{1/2} \qquad (2.5)$$

where, J_2 is the second invariant of stress given by $J'_2 - J_1^2/3$. The effect of hydrostatic stress was also included in the form of a quadratic term through J_2 and thus, satisfying the requirement that the yield criterion should be an even function of hydrostatic stress. Evidently the second term in equation (2.5) vanishes as $\nu \rightarrow 0.5$, for a fully dense material.

Both the theories so far discussed have been used only for simple stress states such as uni-axial compression and tension or plane-strain compression. It has not been possibale to apply these approaches for the analysis of practical deformation processes.

Shima and Oyane [4] later proposed a yield criterion which has been successfully applied to analyse complicated deformation processes. The present theoretical simulation is also based on plasticity theory derived by Shima and Oyane. The yield criterion proposed by these authors is given by

$$F \quad [\{(\sigma_1 - \sigma_2)^2 + (\sigma_2 - \sigma_3)^2 + (\sigma_3 - \sigma_1)^2\}/2 + (\sigma_m/f)^2]^{1/2} \tag{2.6}$$

where, the factor f represents the degree of influence of the hydrostatic stress component σ_m, on the onset of yielding of the porous material and it may be a function of the relative density. F in the above equation can be related to the yield stress of the matrix metal $\bar{\sigma}_{eq}$, which is a materiala parameter. The equation (2.6) can, therefore be rewritten as,

$$f^*\sigma_{eq} = [\{(\sigma_1 - \sigma_2)^2 + (\sigma_2 - \sigma_3)^2 + (\sigma_3 - \sigma_1)^2\}/2 + (\sigma_m/f)^2]^{1/2} \tag{2.7}$$

In the above equation, f* represents the ratio of the apparent stress applied to the porous body and the effective stress applied to the matrix and is again a function of the relative density. The functions f and f* can be determined experimentally [4] from uni-axial compression test. For porous copper,

$$f = \frac{1}{2.49\ (\ 1\ -\ \rho\ )^{0.514}} \qquad (2.8)$$

and

$$f' = \rho^{2.5} \qquad (2.9)$$

However, these forms of expressions for f and f' are also applicable to sintered iron and sintered alluminium.

The yield surface of a porous body given by equation (2.7) is an ellipsoid, the major axis of which coincides with the σ_m axis. On the other hand, for solid materials, the yield surface is a cyalinder whose axis coincides with σ_m axis.

2.2.2 Stress-strain relations:

For a porous material, the principal strain increments d ε_1, d ε_2 and dε_3 can be obtained by partially differentiating the plastic potential (g) with respect to σ_1, σ_2 and σ_3. Thus,

$$d\varepsilon_1 = d\lambda' \frac{\partial g}{\partial \sigma_1} = d\lambda \{\ \sigma_1 - (1 - 2/g\ f^2)\ \sigma_m\ \}$$

$$d\varepsilon_2 = d\lambda' \frac{\partial g}{\partial \sigma_2} = d\lambda \{\ \sigma_2 - (1 - 2/g\ f^2)\ \sigma_m\ \}$$

$$d\varepsilon_3 = d\lambda' \frac{\partial g}{\partial \sigma_3} = d\lambda \{\sigma_3 - (1 - 2/g\ f^2)\ \sigma_m\} \qquad (2.10)$$

The volumetric strain d $_v$ can be written as

$$d\varepsilon_v = d\varepsilon_1 + d\varepsilon_2 + d\varepsilon_3 = -\frac{d\rho}{\rho} = d\lambda(2/3\ f^2)\ \sigma_m \qquad (2.11)$$

where, $d\lambda$ is a proportionality constant. If W_p is the incremental plastic work done per unit volume of the porous body, then

$$dW_p = \sigma_1 \, d\varepsilon_1 + \sigma_2 \, d\varepsilon_2 + \sigma_3 \, d\varepsilon_3 \qquad (2.12)$$

Alternately,

$$dW_p = \rho \bar{\sigma}_{eq} \, d\bar{\varepsilon}_{eq} \qquad (2.13)$$

where, $d\bar{\varepsilon}_{eq}$ is the equivalent strain corresponding to the stress state of $\bar{\sigma}_{eq}$. Substituting equation (2.10) into equation (2.13) and rearranging the terms, we have

$$d\lambda = \frac{3\rho}{2(f^*)^2} \, \frac{d\bar{\varepsilon}_{eq}}{\bar{\sigma}_{eq}} \qquad (2.14)$$

Finally, $d\bar{\varepsilon}_{eq}$ can be written as

$$d\bar{\varepsilon}_{eq} = \frac{f^*}{\rho} \left[(2/9)\{(d\varepsilon_1-d\varepsilon_2)^2+(d\varepsilon_2-d\varepsilon_3)^2+(d\varepsilon_3-d\varepsilon_1)^2\}+(f d\varepsilon_v)^2\right]^{1/2} \qquad (2.15)$$

Summarising the above equations we have

$$\bar{\sigma}_{eq} = \frac{1}{\rho^{2.5}} \left[\{(\sigma_1-\sigma_2)^2+(\sigma_2-\sigma_3)^2+(\sigma_3-\sigma_1)^2\}/2+(q_m/f)^2\right]^{1/2} \qquad (2.16)$$

$$d\varepsilon_1 = \frac{3}{2} \, \frac{1}{\rho^{2(2.5)-1}} \, \frac{d\bar{\varepsilon}_{eq}}{\bar{\sigma}_{eq}} \{\sigma_1-(1-2/9f^2)\sigma_m\}$$

$$d\varepsilon_2 = \frac{3}{2} \, \frac{1}{\rho^{2(2.5)-1}} \, \frac{d\bar{\varepsilon}_{eq}}{\bar{\sigma}_{eq}} \{\sigma_2-(1-2/9f^2)\sigma_m\}$$

$$d\varepsilon_3 = \frac{3}{2} \frac{1}{\rho^{2(2.5)-1}} \frac{d\bar{\varepsilon}_{eq}}{\bar{\sigma}_{eq}} \{\sigma_3 - (1 - 2/9f^2)\,\sigma_m\} \qquad (2.17)$$

$$d\varepsilon_v = -\frac{d\rho}{\rho} = \frac{1}{\rho^{2(2.5)-1)}} \cdot \frac{d\bar{\varepsilon}_{eq}}{\bar{\sigma}_{eq}} \cdot \frac{\sigma_m}{f^2}$$

and further

$$d\bar{\varepsilon}_{eq} = \rho^{2.5-1} [(2/9)\{(d\varepsilon_1 - d\varepsilon_2)^2 + (d\varepsilon_2 - d\varepsilon_3)^2 + (d\varepsilon_3 - d\varepsilon_1)^2\} + (f d\varepsilon_v)^2]^{1/2}$$

(2.18)

when the relative density (ρ) → 1, then $f \to \infty$, $f \to 1$ and $d\varepsilon_v = 0$, and these equations reduce to the well-known stress-strain equations of conventional plasticity theory of a fully dense material.

2.1.3 Stress-strain curve for the matrix material:

In the basic equations of plasticity theory for porous materials given above, $\bar{\sigma}_{eq}$ and $\bar{\varepsilon}_{eq}$ refer to the equivalent stress and the equivalent strain respectively, to which the matrix material is subjected. Therefore, if a stress-strain curve for a sintered material is known, it can be converted to a stress-strain curve for the matrix material by utilizing the basic equations (2.16 - 2.18) [4].

The flow curve of the copper matrix was obtained from the simple compression test of sintered copper cylinders by Mori and Osakada [15]. The expression for the flow curve for copper is

$$\bar{\sigma}_{eq} = 431 \, (\bar{\varepsilon}_{eq} + 0.01)^{0.32} \ \text{MPa} \qquad (2.19)$$

The present theoretical simulation has been carried out in the relative density range $0.7 < \rho < 0.995$. The plasticity theory proposed by Shima and Oyane is valid in this range of relative density.

2.2 UPPER BOUND TECHNIQUE FOR POROUS METALS

The upper bound technique is one of the simplest and most powerful tools used for analytical modelling of most of the metal forming problems. The upper bound theorem is based on a kinematically admissible velocity field which minimizes the total power required for the process. A kinematically admissible velocity field, in turn, must satisfy the following conditions:

(i) The velocity components and their first derivative must be continuous except at allowable surfaces of velocity discontinuity.

(ii) The velocity boundary conditions required by the geometry must be met.

The upper bound solution provides a value for the power equal to or greater than the actual power required to deform the material. The conditions in the solution procedure are relaxed to the extent that the equations of equilibrium, the stress-

strain relations, the stress boundary conditions are not necessarily satisfied at every point. However, the total force applied by prescribed surface tractions is a satisfied parameter. There are infinite number of kinematically admissible velocity fields that satisfy the velocity boundary conditions. The true solution is the one which corresponds to the minimum power. In the application of the upper bound solution, the plastic boundaries of some chosen form are assumed which define the plastically deforming region. Once the plastic boundaries are fixed, a kinematically admissible velocity field is assumed which satisfies the velocity boundary constraints. In this regard, a physical understanding of the flow of metal is quite useful. The derivation of the upper bound theorem for the plastic deformation of a porous metal is briefly discussed below.

The yield surface for a porous metal is an ellipsoid in the principal stress space, which is concave to the origin. Thus, the principle of maximum plastic work can be applied which states that the true increment in plastic work δW required to bring about a given set of strain increments $d\varepsilon_{ij}$ is greater than the increment in plastic work δW^* which would abe required to bring about the same strain increment by any other distribution of stresses throughout a volume V, which confirms to the same yield criterion. Thus,

$$\delta W - \delta W^* = \int_V (\sigma_{ij} - \overset{*}{\sigma}_{ij})\ d\,\varepsilon_{ij}\ dV$$

In terms of strain rate and rate of work,

$$\dot{W} - \dot{W}^* = \int_V (\sigma_{ij} - \overset{*}{\sigma}_{ij})\ d\dot{\varepsilon}_{ij}\ dV$$

The principle of maximum plastic work leads to

$$\int_V (\sigma_{ij} - \overset{*}{\sigma}_{ij})\, d\dot{\varepsilon}_{ij}\, dV \geq 0 \qquad (2.20)$$

This criterion is always satisfied by the rigid plastic material, if its yield locus is convex outwards. In equation (2.20), σ_{ij} is the exact stress or the true stress condition during the deformation, $\overset{*}{\sigma}_{ij}$ is any other stress which does not violate the yield criterion and $\dot{\varepsilon}_{ij}$ is the exact strain rate.

Thus, we have

$$\int_V \sigma_{ij}\, \dot{\varepsilon}_{ij}\, dV \geq \int_V \overset{*}{\sigma}_{ij}\, \dot{\varepsilon}_{ij}\, dV \qquad (2.21)$$

The prescribed velocity boundary conditions and surface tractions for any plastically deforming region are shown in Fig. 2.1. Using the equation (2.13), the above equation can be rewritten as

$$\int_V \overset{*}{\sigma}_{ij}\, \dot{\varepsilon}_{ij}\, dV \leq \int_V \sigma_{ij}\, \dot{\varepsilon}_{ij}\, dV = \int_V \rho\, \sigma_{eq}\, \dot{\varepsilon}_{eq}\, dV \qquad (2.22)$$

On a porous body of volume V and total surface A, the stress, strain rate, and other relevant quantities are denoted as follows:

V_i = prescribed velocity over the portion of surface A_V

F_i = surface traction prescribed over the surface area A_F

$\dot{\varepsilon}_{ij}$ = exact strain rate

σ_{ij} = exact stress state

$\overset{*}{V}_i$ = any kinematically admissible velocity field satisfying

$\overset{*}{V}_i = V_i$ on A_V

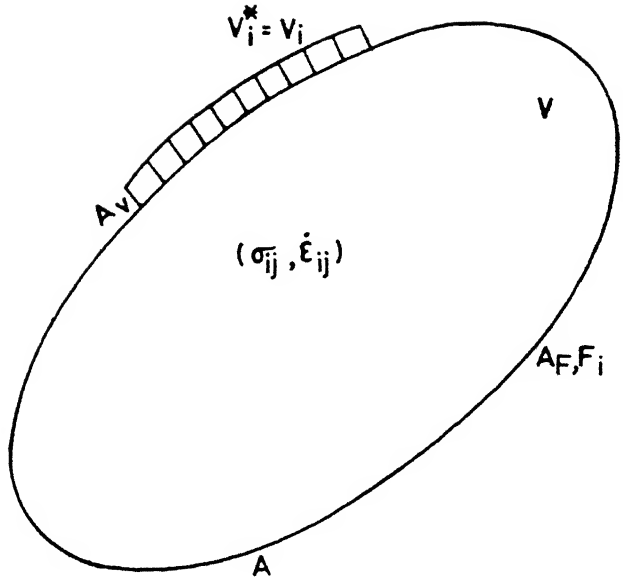

FIG. 2.1 DEFINATION OF TERMS USED FOR THE UPPER BOUND THEOREM

$\dot{\varepsilon}^{*}_{ij}$ = strain rate derived from V^{*}_{i}

σ^{*}_{ij} = any stress which does not violate the yield condition and is connected to $\dot{\varepsilon}^{*}_{ij}$.

The principle of virtual work leads to

$$\int_V \sigma_{ij} \; \varepsilon^{*}_{ij} \; dV = \int_A F_i \; V^{*}_{i} \; dA \qquad (2.23)$$

The equation (2.23) can be rewritten as

$$\int_V \sigma_{ij} \; \dot{\varepsilon}^{*}_{ij} \; dV = \int_{A_V} F_i \; V^{*}_{i} \; dA + \int_{A_F} F_i \; V^{*}_{i} \; dA \qquad (2.24)$$

Setting $V^{*}_{i} = V_i$ on A_V, the above equation becomes,

$$\int_V \sigma_{ij} \; \dot{\varepsilon}^{*}_{ij} \; dV = \int_{A_V} F_i \; V_i \; dA + \int_{A_F} F_i \; V^{*}_{i} \; dA \qquad (2.25)$$

Now,

$$\sigma^{*}_{ij} \; \dot{\varepsilon}^{*}_{ij} = \rho \sigma^{*}_{eq} \; \dot{\varepsilon}^{*}_{eq} = \rho \sigma_{eq} \; \dot{\varepsilon}^{*}_{eq}$$

Also,

$$\int_V \sigma_{ij} \; \dot{\varepsilon}^{*}_{ij} \; dV \leq \int_V \sigma^{*}_{ij} \; \dot{\varepsilon}^{*}_{ij} \; dV = \int_V \rho \sigma_{eq} \; \dot{\varepsilon}^{*}_{eq} \; dV \qquad (2.26)$$

Using equation (2.25) in equation (2.26)

$$\int_{A_V} F_i \; V_i \; dA + \int_{A_F} F_i \; V^{*}_{i} \; dA \leq \int_V \rho \sigma_{eq} \; \dot{\varepsilon}^{*}_{eq} \; dV$$

or,

$$\int_{A_V} F_i \; V_i \; dA \leq \int_V \rho \sigma_{eq} \; \dot{\varepsilon}^{*}_{eq} \; dV - \int_{A_F} F_i \; V^{*}_{i} \; dA \qquad (2.27)$$

Equation (2.27) defines the upper bound theorem for a porous metal. The right hand side of this equation gives an upper bound

for the work rate of the unknown surface traction action on A_V. If the frictional shear stress τ_f is specified at the roll workpiece interface A_T, the upper bound theorem for porous metals can be stated by the following equation:

$$\int_{A_V} F_i \, V_i \, dA \leq \int_V \rho \, \sigma_{eq} \, \dot{\varepsilon}^*_{eq} \, dV - \int_{A_F} F_i \, V_i^* \, dA + \int_{A_T} \tau_f \, \Delta u^* \, dA \qquad (2.28)$$

where, Δu^* is the relative velocity at the roll-workpiece interface. The power $\dot{W}$, derived from a kinematically velocity field is given by the right hand side of equation (2.28). Thus,

$$\dot{W} = \int_V \rho \sigma_{eq} \, \dot{\varepsilon}^*_{eq} \, dV + \int_{A_T} \tau_f \, \Delta u^* \, dA - \int_{A_F} F_i \, V_i^* \, dA \qquad (2.29)$$

The equation above describes the generalized upper bound theorem for a porous metal. It gives an upper bound for the total power required to plastically deform a porous metal. The true density and velocity distributions are obtained by minimizing this total power.

2.3 MODEL ASSUMPTIONS:

The following assumptions have been made in the present work while obtaining upper bound solution for cold densification rolling of sintered metal strips.

(i) It is assumed that, the material remains perfectly rigid before it comes under the rolls and also after

emerges out. In other words, the deformation zone lies within the entry and exit sections as shown in Fig. (2.3).

(ii) A velocity discontinuity has been assumed only at the entrance due to the sudden change in the direction of metal flow lines. At the exit from the rolls, metal flow velocity is continuous and lies in the direction of the tangent to the roll surface.

(iii) At each cross-section the relative density is uniform in the thickness direction because of the small thickness value encountered in strip rolling. Practically speaking, there is a slight variation in density across a section, with higher density near the roll surface as compared to that in the interior. However, this small variation can be neglected without much loss in accuracy.

(iv) The lateral spread in strip rolling is very small as the width of the strip is large compared to its thickness. Hence, strain in width direction is assumed to be zero and rolling becomes a case of plane strain rolling.

(v) Isothermal conditions are assumed as appropriate for the cold rolling of thin strips.

(vi) The rolls are assumed to be perfectly rigid.

2.4 DERIVATION OF KINEMATICALLY ADMISSIBLE FLOW FIELD:

The Figure 2.2 shows a unit volume of porous metal undergoing progressive deformation along the flow line. It can

be seen that the relative density increases in the direction of rolling due to compression and contact growth. Referring to Fig. (2.3), zone-II represents the deformation zone and ξ is a normalized cross-stream coordinate which varies from the value of zero at the axis to unity at the roll surface. If the streamline connecting ξy_1 and ξy_2 is to have smooth transition at the exit, the slope of this streamline should be zero at the exit section. It has been assumed that there is a velocity discontinuity at the entrance to the roll which results in a sharp turn of the streamlines at that cross section. The effect of velocity discontinuity has been taken into account during the evaluation of work according to upper bound theorem.

In the deformation zone, each ξ = constant curve represents a streamline. In order to derive the streamline shapes, it is important to note the facts that the roll surface is circulasr with radius R and due to symmetrical rolls, the mid-plane of the strip is straight. Thus, continuous smooth transition of streamline shapes is possible if one assumes. Streamlines of circular form with centre lying along the exit section are assumed. The streamline $\xi = 1$ represents the strip surface, which is a circular with centre placed at the roll centre. As one proceeds towards the mid-plane of the strip, the centre of the circular streamline moves away from the strip surface. The streamline $\xi = 0$ is the mid-plane whose radius is infinity, see Fig. (2.3).

The assumed streamline pattern satisfies all the velocity boundary conditions. For instance, at the roll surface the normal velocity $V_n = 0$, this comes from the definition of

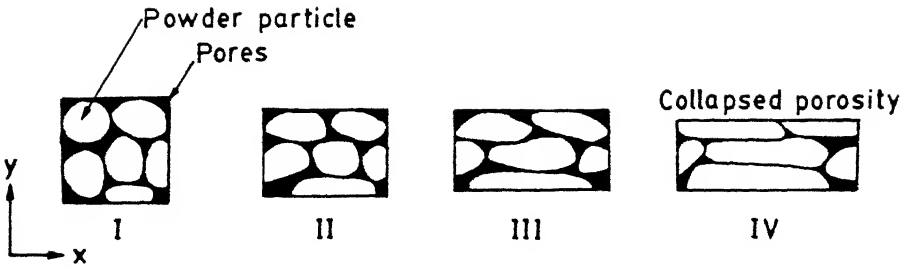

FIG. 2·2 PROGRESSIVE DEFORMATION OF A UNIT VOLUME OF POROUS METAL SHOWING CONTACT GROWTH

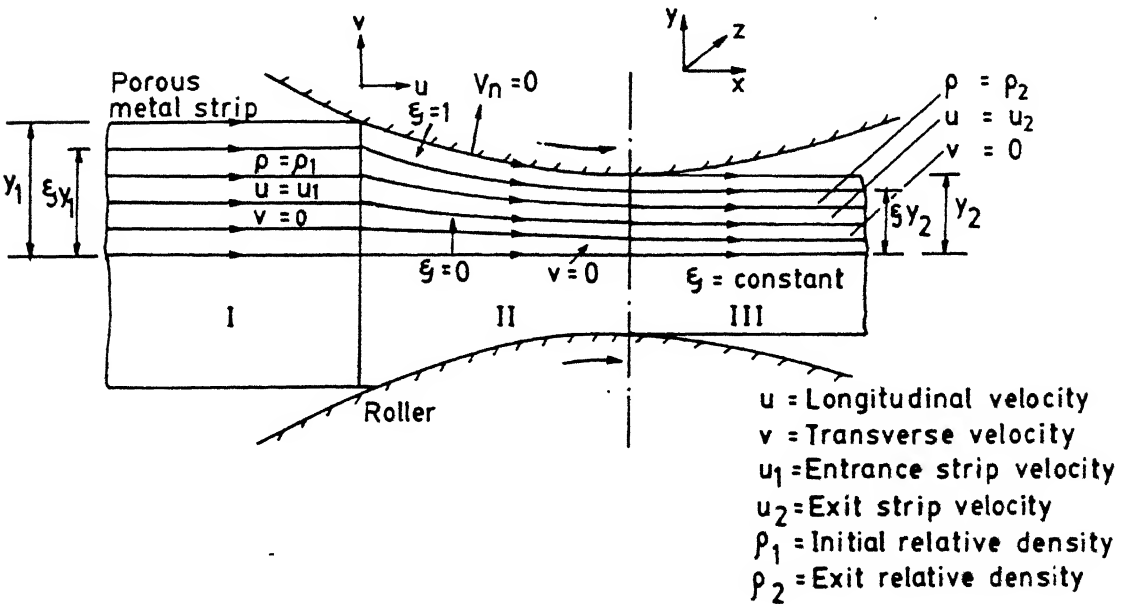

FIG. 2·3 SCHEMATIC REPRESENTATION OF VELOCITY FIELD

streamline, as there is no metal flow across the streamline. At the mid-plane and exit sections vertical component of velocity v = 0, because streamlines are horizontal. Thus, the concept of a streamline not only facilitates satisfaction of velocity boundary conditions but also gives a clear idea about the shape of flow lines in the deformation zone.

The equation of a circular streamline can be written as

$$(x - L)^2 + (y - y_0)^2 = r^2 \qquad (2.30)$$

where,

L = projected length of the arc of contact in the flow direction

r = radius of the streamline under consideration

y_0 = y-coordinate of the centre of streamline arc = $r + \xi y_2$.

It may be noted that the coordinates of the centre of the streamline are given by (L, y_0). From the Fig. (2.3), it is evident that at $x = 0$, $y = \xi y_1$. Substituting this value in equation (2.30) yelds the following expression for the radiuus r of the streamline,

$$r = \frac{L^2}{2\xi(y_1 - y_2)} + \frac{\xi(y_1 - y_2)}{2} \qquad (2.31)$$

The mass flow rate per unit width of the strip can be expressed as follows:

$$\Psi = \xi \rho_1 u_1 y_1 \qquad (2.32)$$

where,

ρ_1 = initial relative density of strip,

u_1 = entrance velocity of the strip,

y_1 = entry thickness of the strip.

For a compressible flow, it is possibale to define a stream function such that

$$\rho u = \left(\frac{\partial \Psi}{\partial y}\right) \qquad (2.33)$$

where,

u = longitudinal or horizontal velocity of the strip at any point in the domain,

ρ = the alocal relative density of the strip

Ψ = stream function = mass flow rate between a given streamline and the mid-plane of the strip

$$\rho V = - \left(\frac{\partial \Psi}{\partial x}\right) \qquad (2.34)$$

V = transverse or vertical velocity of the strip at any point in the domain.

ρ_1, u_1 and y_1 are constants and can be considered as inlet parameters. However unlike ρ_1 and y_1, the inlet velocity u_1 can not be chosen arbitrarily for any rolling situation, as one does not have any external control in selecting a particular value for this parameter. In the present work, u_1 has been treated as an unknown parameter which is determined from the upper bound theorem.

Thus, defining $C = \rho_1 u_1 y_1$, equation (2.32) can be rewritten as,

$$\Psi = C \xi \qquad (2.35)$$

The above equation indicates that mass flow rate is directly proportional to the streamline coordinate ξ. Combining

equations (2.33 - 2.35), we can deduce following equations:

$$\frac{\partial \Psi}{\partial x} = C \quad \frac{\partial \xi}{\partial x} = - \rho v .$$

$$\frac{\partial \Psi}{\partial y} = C \quad \frac{\partial \xi}{\partial y} = \rho u \tag{2.36}$$

Differentiating the streamline aradius r partially with respect to

$$\frac{\partial r}{\partial y} = \frac{-L^2}{2\xi^2 (y_1 - y_2)} \frac{\partial \xi}{\partial y} + \frac{(y_1 - y_2)}{2} \frac{\partial \xi}{\partial y} \tag{2.37}$$

$$(y-y_0)\left[1 - y_2 \frac{\partial \xi}{\partial y}\right] = \frac{\partial r}{\partial y}\left[r + (y - y_0)\right] \tag{2.38}$$

$$(y-y_0)\left[1 - y_2 \frac{\partial \xi}{\partial y}\right] = \left[\frac{-L^2}{2\xi^2 (y_1-y_2)} + \frac{(y_1-y_2)}{2}\right](r+y-y_0) \frac{\partial \xi}{\partial y} \tag{2.39}$$

$$\frac{\partial \xi}{\partial y} = \frac{(y - y_0)}{\left[y_2(y-y_0)+(r + y - y_0)\left\{\frac{-L^2}{2\xi^2 (y_1 - y_2)} + \frac{(y_1 - y_2)}{2}\right\}\right]} \tag{2.40}$$

Similarly, differentiating equastions (2.30) and (2.31) partially with respect to x, and simplifying

$$\frac{\partial \xi}{\partial x} = \frac{(x - L)}{\left[y_2(y-y_0)+(r + y - y_0)\left\{ \frac{-L^2}{2 \xi^2 (y_1-y_2)} + \frac{(y_1-y_0)}{2}\right\}\right]} \tag{2.41}$$

Now, substituting for $\frac{\partial \xi}{\partial x}$ and $\frac{\partial \xi}{\partial y}$ from equations (2.40) and (2.41) into equation (2.36), the following expressions for u and V are obtained:

$$u = \frac{\rho_1 u_1 y_1}{\rho} \left[\frac{y - (r + \xi y_2)}{y_2(y-(r+\xi y_2)) + (y - \xi y_2) \left\{ \frac{-L^2}{2\xi^2 (y_1 - y_2)} + \frac{(y_1 - y_2)}{2} \right\}} \right] \tag{2.42}$$

$$V = - \frac{\rho_1 u_1 y_1}{\rho} \left[\frac{x - L}{y_2(y-(r+\xi y_2)) + (y - \xi y_2) \left\{ \frac{-L^2}{2\xi^2 (y_1 - y_2)} + \frac{(y_1 - y_2)}{2} \right\}} \right] \tag{2.43}$$

It may be noted that at the exit all the streamlines become horizontal and this condition is satisfied as seen from equation (2.43) which gives $V = 0$ at $x = L$. The centre line is a streamline with $\xi = 0$ and the velocity component normal to it becomes zero because $r \to \infty$ for $\xi = 0$. It can also be verified that for $\xi = 1$ (roll surface) the normal avelocity is zero. Thus, it is clear that the above velocity pattern represents a kinematically admissible velocity field. It may be noted, however, that the proper density distribution is not known as yet and it is determined by work minimization as stated by the upper bound theorem.

2.5 NATURE OF DENSITY VARIATION IN POROUS METAL STRIP ROLLING:

It has been shown by Bhargava [18] that the densification rolling of powder metals is dominated by two processes, namely, the compression of particles which increases the interparticular contact area and the sliding of the particles at their neck regioans without causing any substantial plastic deformation. Considering homogeneous compression and grains with an initial spherical shape, he derived that the relative density variation can be represented by the expression

$$\frac{\left(\frac{1-\rho}{\rho}\right)}{\left(\frac{1-\rho_1}{\rho_1}\right)} = \left(\frac{\bar{y}}{y_\phi}\right)^b \qquad (2.44)$$

where,

ρ = local relative density

ρ_1 = inalet relative density

$\bar{y}$ = local strip thickness

and,

y_ϕ = inlet strip thickness.

The exponent b takes a value of 2 when there is no slip between the particles for the forming processes such as forging and upsetting. In the present work also, density is taken as a constant over each cross-section (homogeneous compression) with a power function form of dependence on the local strip thickness. The exponent b, however, is left as an unknown to be determined as a part of the solution.

The assumption of uniform density over each cross-section is reasonably valid for the rolling of thin strips as used in the

present study. The value of b, in general, can be dependent on rolling parameters friction factor, percentage reduction, roll speed, roll diameter and initial strip thickness and relative density. For each set of parameters, the true value of b will be determined from the minimum work principle according to the upper bound theorem. This, in turn, will result in the true density distribution for the given set of rolling conditions.

2.6 STRAIN-RATE CALCULATIONS

The strain rates in the deformation zone are given by the following equations:

$$\dot{\varepsilon}_x = \frac{\partial u}{\partial x} = \text{strain rate in x-direction}$$

$$\dot{\varepsilon}_y = \frac{\partial v}{\partial y} = \text{strain rate in y-direction}$$

$$\dot{\gamma}_{xy} = \frac{\partial u}{\partial y} + \frac{\partial v}{\partial x} = \text{shear strain rate} \qquad (2.45)$$

The other strain rates are zero due to plane-strain rolling condition, i.e. $\dot{\gamma}_{xz} = \dot{\gamma}_{yz} = \dot{\varepsilon}_z = 0$. It is very cumbersome to analytically evaluate expressions for the strain rate components from the equations for u and v. Therefore, the strain rates are evaluated numerically in the present study.

2.7 EVALUATION OF THE TOTAL ENERGY DISSIPATION RATE:

The total power required to perform the strip rolling process is made up of three separate contributions. They are,

(i) power expended for internal plastic deformation within the

strip

ii) power to overcome friction at the strip surface.

iii) power losses due to shearing along the surface of velocity discontinuity.

Internal Power of deformation:

The equivalent strain rate for porouus metal plane strain olling is given by the expression:

$$\dot{\varepsilon}_{eq} = \rho^{2.5-1}\sqrt{\frac{2}{9}\{(\dot{\varepsilon}_x-\dot{\varepsilon}_y)^2+(\dot{\varepsilon}_y-\dot{\varepsilon}_z)^2+(\dot{\varepsilon}_z-\dot{\varepsilon}_x)^2+\frac{3}{2}\dot{\gamma}_{xy}^2\} + (f\,\dot{\varepsilon}_v)^2} \qquad (2.46)$$

here, $\dot{\varepsilon}_v$ is the volumetric strain rate, is expressed as

$$\dot{\varepsilon}_v = \dot{\varepsilon}_x + \dot{\varepsilon}_y \qquad (2.47)$$

nd $\dot{\varepsilon}_z = 0$, for the present case of plane strain rolling of orous copper strip also, for copper, we have

$$f = \frac{1}{2.49\,(1-\rho)^{0.514}} \qquad (2.48)$$

hus, equation (2.46) becomes

$$\dot{\varepsilon}_{eq} = \rho^{2.5-1}\sqrt{\frac{2}{9}\{(\dot{\varepsilon}_x-\dot{\varepsilon}_y)^2+\dot{\varepsilon}_x^2+\dot{\varepsilon}_y^2+\frac{3}{2}\dot{\gamma}_{xy}^2\}+\{\frac{\dot{\varepsilon}_x+\dot{\varepsilon}_y}{2.49(1-\rho)^{0.514}}\}^2} \qquad (2.49)$$

e equivalent stress can be written from the plasticity theory

$$\bar{\sigma}_{eq} = \frac{1}{\rho^{2.5}} \sqrt{\frac{1}{2}\{(\sigma_x - \sigma_y)^2 + (\sigma_y - \sigma_z)^2 + (\sigma_z - \sigma_x)^2 + 6\tau_{xy}^2\} + (\sigma_m/f)^2} \qquad (2.50)$$

The power necessary for plastic deformation $\dot{W}_p$ is given by

$$\dot{W}_p = \int\int \rho \, \dot{\bar{\varepsilon}}_{eq} \, \bar{\sigma}_{eq} \, dx \, dy \qquad (2.51)$$

The present analysis is carried out for porous copper in the relative density range $0.7 < \rho < 0.995$. The equivalent stress-strain curve for copper [15] is expressed as

$$\bar{\sigma}_{eq} = 431 \, (\bar{\varepsilon}_{eq} + 0.01)^{0.32} \quad MPa \qquad (2.52)$$

Using equation (2.52) in equation (2.52),

$$\dot{W}_p = 431 \int\int \rho \, \dot{\bar{\varepsilon}}_{eq} \, (\bar{\varepsilon}_{eq} + 0.01)^{0.32} \, dx \, dy \qquad (2.53)$$

The cumulative equivalent strain $\bar{\varepsilon}_{eq}$ undergone by a particle is determined by integrating the equivalent strain rate $\dot{\bar{\varepsilon}}_{eq}$ along the streamliane corresponding to the motion of the particle.

Friction Power:

In porous metal rolling, the actual friction conditions are quite complex. The frictional condition is usually represented by a coefficient of friction or a friction factor. The frictional shear stress is a function of the contact pressure,

location, slip velocity etc. It reverses its direction at the neutral point. The frictional shear stress is usually expressed by the product of contact pressure and the coefficient of friction. The other simple approach for representing the interfacial friction phenomenon is through the prescription of a friction factor. The friction factor is defined as the ratio of the frictional to the yield shear strength of the material. Metal rolling is a friction aided process and therefore, one can expect a high value of friction factor. The value of friction factor can be chosen on the basis of the surface roughness of rolls and the lubricating conditions. The higher the friction, the larger the power needed to perform the process. The larger value of friction factor makes the rolling process more stable [5]. However, it becomes less efficient from the point of power required for rolling.

In the present work, the frictional resistance on the interface is assumed to be constant for the sake of simplicity, a constant friction factor is considered over the whole arc of contact. Also it has been assumed that both the rolls have same surface conditions.

The frictional stress is expressed by

$$\tau = m K \qquad (2.54)$$

where, K is the criatical shear stress of the material whose value is obtained by setting the normal stress components in equation (2.50) to zero. Thus,

$$K = \frac{\bar{\sigma}_{eq}\,\rho^{2.5}}{\sqrt{3}} \qquad (2.55)$$

The velocity of slip at the roll-strip interface is,

$$\Delta V = \left(U - \sqrt{u^2 + v^2}\right)\Big|_{\xi=1} \qquad (2.56)$$

where U is the roll speed. The frictional power is calculated as

$$\dot{W}_f = \int \tau \Delta V \; dl \qquad (2.57)$$

The friction power is evaluated along the arc of contact. Substituting the relative velocity V into equation (2.57), we get,

$$\dot{W}_f = \frac{m}{\sqrt{3}} \int \rho^{2.5}\, \bar{\sigma}_{eq} \left(U - \sqrt{u^2 + v^2}\right) dl \qquad (2.58)$$

assuming constant m along the arc of contact.

Shear power losses at entry:

A velocity discontinuity exists at the entry because all the streamlines bend suddenly at entrance to the roll. This discontinuity has been considered taking into account the straight boundaries of deformation zone. It has been assumed here that, the plastic deformation starts immediately after the strip enters the roll. In actual practice, plastic deformation starts even before the strip is gripped between the rolls and plastic boundaries are not straight.

The shear losses at the discontinuity are given by

$$\dot{W}_s = \frac{1}{\sqrt{3}} \int \bar{\sigma}_{eq}\, \rho^{2.5}\, \Delta v \; dl \qquad (2.59)$$

where Δv is the difference in v component of the velocity at the discontinuity.

Expression for total power:

The total power required for rolling is given by,

$$\dot{W} = \dot{W}_p + \dot{W}_f + \dot{W}_s \qquad (2.60)$$

For a given reduction and friction conditions, the work is optimized with respect to exponent b and the entrance velocity u_1 of the strip.

CHAPTER III

NUMERICAL SOLUTION PROCEDURE

3.1 OVERALL SOLUTION STRATEGY

In order to obtain the true density and velocity distributions through the upper bound technique, the primary quantity which needs to be evaluated is the total rolling power. This has been accomplished by numerical integration of the various components of power over the deformation zone, using a kinematically admissible velocity field and a guess density distributions, given by equations (2.42 - 2.44). For a given set of rolling conditions, the minimum rolling power has been evaluated by systematically varying the two free parameters of the problem, namely: the exponent (b) of the density distribution and the strip velocity (u_1) at the inlet cross-section of the deformation zone. The velocity and density distributions corresponding to minimum power have been taken as the true distributions.

Due to the strong non-linear nature of the problem, it is not possible to evaluate the total power integral analytically in an exact manner. For this reason, numerical integration based on Gauss-Legendre quadrature has been resorted to. The numerical quadrature requires that for evaluating the area integral of internal plastic deformation power, the deformation zone be discretized into several small area elements; similarly, for calculating the friction and shear loss power contributions on boundary curves, these boundaries need to be discretized into several line segments. Both these requirements are met by

discretizing the whole plastic deformation region into a finite element type mesh consisting of several small elements. All the elements have quadrilateral shape with 4 nodes each (see Fig. 3.1). The nodes (which are placed at the vertices of the quadrilateral) aid in the computation of both the area and line integrals via numerical quadrature. A mesh consisting of 21 elements in X-direction and 10 elements in y-direction (with 21 x 10 total elements) has been used in the present study for performing all the computations. Only half the strip thickness (upto the mid-plane has been considered due to symmetry). The shapes of the elements are such that two opposite sides of each element are aligned with particle stream lines while the other two sides are normal to the metal flow direction (See, Fig. 3.2). The total rolling power has been computed as the sum of the following quantities:

(i) Internal plastic power over the 21x10 area elements.

(ii) Friction power over the 21 line segments lying on the strip surface.

(iii) Shear losses over the 10 line segments of the entry section.

3.2 CALCULATION OF FIELD VARIABLES AT NODES

In order to evaluate the elemental integrals, it is necessary to find the values of the field variables density, x and y-direction velocities, strain components etc.) at the nodes of each element. This is easily achieved, if one recognizes the fact that all the nodes lie on one streamline or the other. Since each stream line is identified by a constant value of ξ

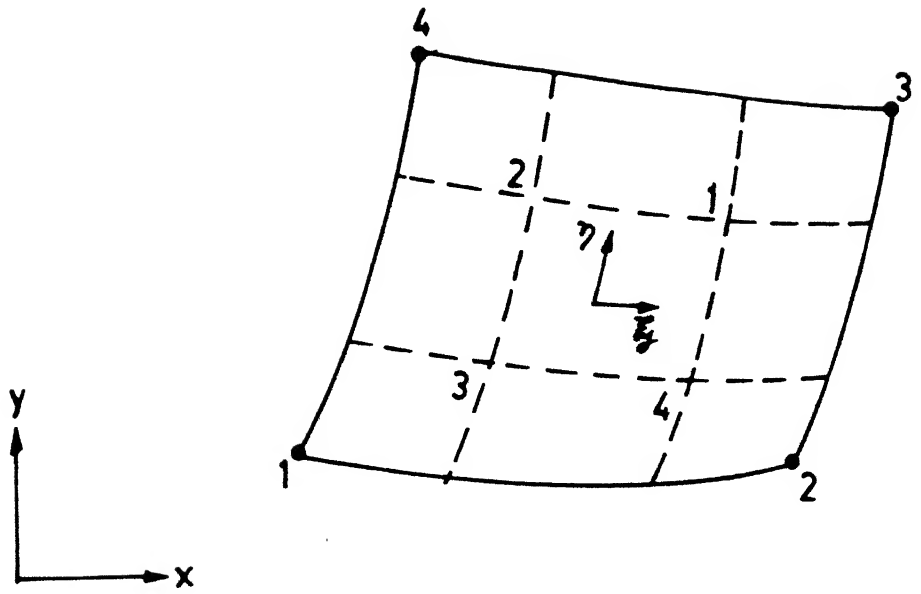

x, y = Global coordinates
η, ξ = Local coordinates

G. 3.1 ORDER OF GAUSS POINT SAMPLING POSITION FOR FOUR-NODED ISOPARAMETRIC ELEMENT

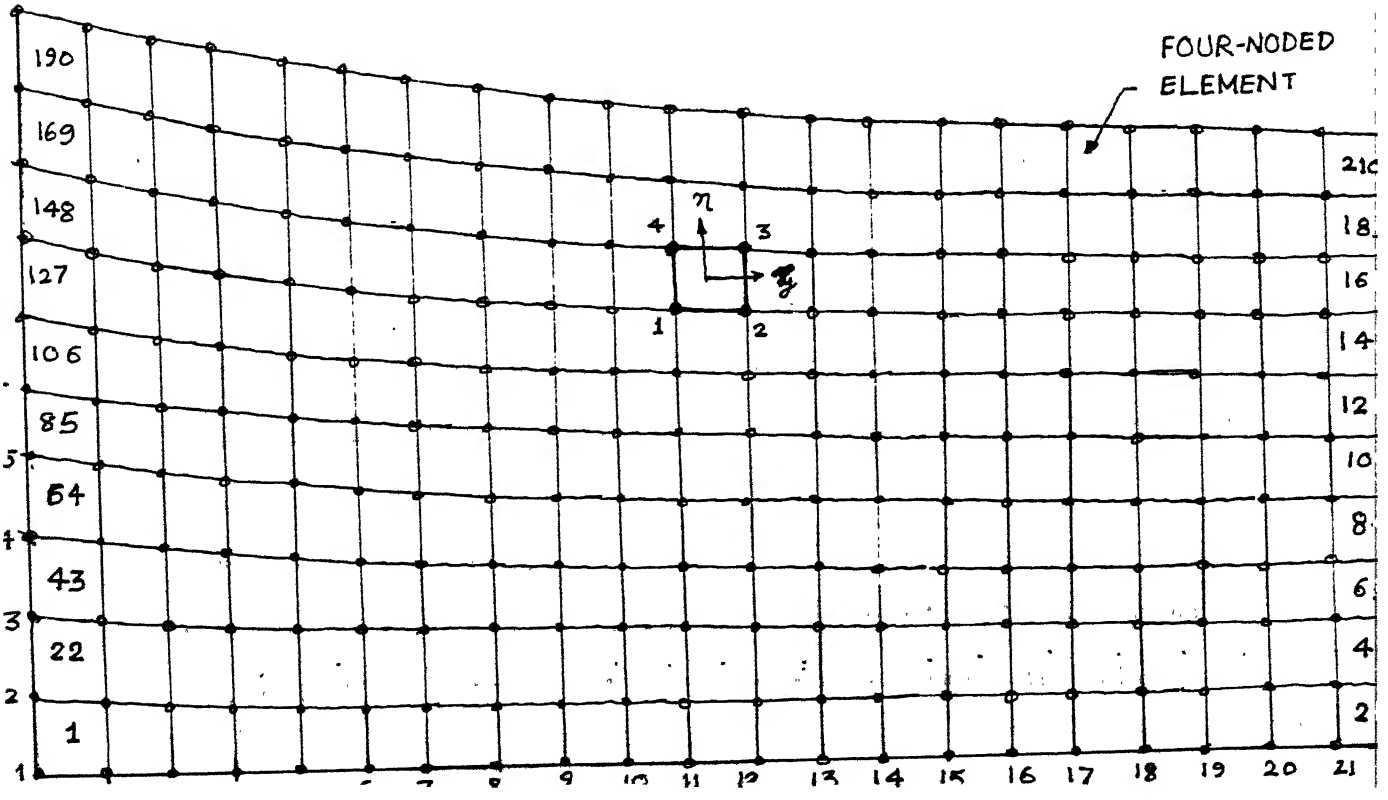

(stream-line coordinate), the field variables are sequentially computed as described below:

(i) For the 21x10 mesh, the x-direction and ξ-direction increments are respectively given by $\Delta x = L/21$ and $\Delta\xi = 1/10$. From this, the x and ξ values at each node are calculated.

(ii) Knowing x and ξ, from equations (2.30) and (2.31), the values of y and r for each node are determined.

(iii) Using equations (2.42 - 2.44), the velocity components u and v and the density ρ are evaluated at all the nodes.

(iv) In order to compute the strain rate components $\dot{\varepsilon}_x$, $\dot{\varepsilon}_y$ and $\dot{\gamma}_{xy}$, and the corresponding cumulative strains ε_x, ε_y and γ_{xy} under gone by a particle, the following procedure is adopted. The strain rate components are related to the velocity derivatives $\frac{\partial u}{\partial x}$, $\frac{\partial v}{\partial x}$, $\frac{\partial u}{\partial y}$, and $\frac{\partial v}{\partial x}$ through the expressions of eq.(2.45).

The velocity derivatives, in turn, are evaluated using 4-noded interpolation of u and v variation within each element. After obtaining the strain rate components $\dot{\varepsilon}_x$, $\dot{\varepsilon}_y$ and $\dot{\gamma}_{xy}$, the nodal values of cumulative strain components are evaluated by tracing the strain history of each particle along its stream line path. The incremental value of a particular strain component is obtained by integrating the corresponding strain rate component with respect to time. The evaluation procedure for the strain rate and strain components at each node is described in the next section in greater detail. The

various steps involved in the evaluation of the true distributions are graphically shown in Fig. (3.3).

3.3 CALCULATION OF STRAIN RATE AND STRAIN COMPONENTS

From the nodal values of u,v and ρ, it is possible to obtain the values of these variables at any interior point of an element through interpolation. For 4-noded quadrilateral elements, one can employ the following interpolation schemes within each element:

$$u = \sum_{i=1}^{4} N_i \; u_i$$

$$v = \sum_{i=1}^{4} N_i \; v_i \qquad (3.1)$$

$$\rho = \sum_{i=1}^{4} N_i \; \rho_i$$

where u_i, v_i and ρ_i are the nodal values of the velocity components and density respectively, and N_i are the interpolation functions. It is more convenient to represent the interpolation fnctions in terms of normalized local coordinates ξ and η, rather than in terms of actual coordinates x and y. The expressions for the interpolation functions in local coordinates (ξ, η) are:

$$N_1 = \frac{1}{4}(1-\xi)(1-\eta); \quad N_2 \; \frac{1}{4}(1+\xi)(1-\eta)$$

$$N_3 = \frac{1}{4}(1+\zeta)(1+\eta); \qquad N_4 \frac{1}{4}(1-\zeta)(1+\eta)$$

(3.2)

The local coordinates are defined in such a way that they vary from −1 to +1 for all elements; thus, all quadrilateral elements (regardless of their shape) can be represented as squares of size 2x2, in terms of their respective local coordinates. Such a feature is extremely useful in performing numerical integration.

Now, for a quadrilateral element, it is possible to interpolate the global coordinates x and y at any point in terms of the values of nodal coordinates.

It can be shown that

$$x = \sum_{i=1}^{4} N_i \, x_i \qquad (3.3)$$

$$y = \sum_{i=1}^{4} N_i \, y_i$$

For the four-noded quadrilateral element, the conversion between the (x,y) and (ζ , η) coordinates can be achieved as follows. From chain rule,

$$\frac{\partial N_i}{\partial \zeta} = \frac{\partial N_i}{\partial x}\frac{\partial x}{\partial \zeta} + \frac{\partial N_i}{\partial y}\frac{\partial y}{\partial \zeta}$$

$$\frac{\partial N_i}{\partial \eta} = \frac{\partial N_i}{\partial x}\frac{\partial x}{\partial \eta} + \frac{\partial N_i}{\partial y}\frac{\partial y}{\partial \eta}$$

or,

$$\begin{bmatrix} \frac{\partial N_i}{\partial \zeta} \\ \\ \frac{\partial N_i}{\partial \eta} \end{bmatrix} = \begin{bmatrix} \frac{\partial x}{\partial \zeta} & \frac{\partial y}{\partial \zeta} \\ \\ \frac{\partial x}{\partial \eta} & \frac{\partial y}{\partial \eta} \end{bmatrix} \begin{bmatrix} \frac{\partial N_i}{\partial x} \\ \\ \frac{\partial N_i}{\partial y} \end{bmatrix} = [J] \begin{bmatrix} \frac{\partial N_i}{\partial x} \\ \frac{\partial N_i}{\partial y} \end{bmatrix} \qquad (3.4)$$

In eq. (3.4), [J] is the Jacobian matrix for coordinate transformation. The inverse transformation from (ζ , η) coordinates to (x,y) coordinates is given by:

$$\begin{bmatrix} \frac{\partial N_i}{\partial x} \\ \\ \frac{\partial N_i}{\partial y} \end{bmatrix} = [J]^{-1} \begin{bmatrix} \frac{\partial N_i}{\partial \zeta} \\ \\ \frac{\partial N_i}{\partial \eta} \end{bmatrix} \qquad (3.5)$$

Using eq.(3.3), the Jacobian matrix and its inverse can be evaluated as:

$$[J] = \begin{bmatrix} \frac{\partial x}{\partial \zeta} & \frac{\partial y}{\partial \zeta} \\ \\ \frac{\partial x}{\partial \eta} & \frac{\partial y}{\partial \eta} \end{bmatrix} = \begin{bmatrix} \sum_{i=1}^{4} \frac{\partial N_i}{\partial \zeta} x_i & \sum_{i=1}^{4} \frac{\partial N_i}{\partial \zeta} y_i \\ \\ \sum_{i=1}^{4} \frac{\partial N_i}{\partial \eta} x_i & \sum_{i=1}^{4} \frac{\partial N_i}{\partial \eta} y_i \end{bmatrix}$$

$$[J]^{-1} = \frac{1}{|J|}\begin{bmatrix} \frac{\partial y}{\partial \eta} & \frac{-\partial y}{\partial \zeta} \\ -\frac{\partial x}{\partial \tau_i} & \frac{\partial x}{\partial \zeta} \end{bmatrix} = \frac{1}{|J|}\begin{bmatrix} \sum_{i=1}^{4} \frac{\partial N_i}{\partial \eta} y_i & -\sum_{i=1}^{4} \frac{\partial N_i}{\partial \zeta} y_i \\ -\sum_{i=1}^{4} \frac{\partial N_i}{\partial \eta} x_i & \sum_{i=1}^{4} \frac{\partial N_i}{\partial \zeta} x_i \end{bmatrix} \tag{3.7}$$

where,

$$|J| = \frac{\partial x}{\partial \zeta}\frac{\partial y}{\partial \eta} - \frac{\partial x}{\partial \eta}\frac{\partial y}{\partial \zeta}$$

$$= \left(\sum_{i=1}^{4} \frac{\partial N_i}{\partial \zeta} x_i\right)\left(\sum_{j=1}^{4} \frac{\partial N_i}{\partial \eta} y_j\right) - \left(\sum_{i=1}^{4} \frac{\partial N_i}{\partial \eta} x_i\right)\left(\sum_{i=1}^{4} \frac{\partial N_i}{\partial \zeta} y_j\right) \tag{3.8}$$

The derivatives of interpolation functions $\partial N_i/\partial \zeta$ and $\partial N_i/\partial \eta$, in turn, are obtained by differentiating the expressions for N_i in eq. (3.2) with respect to ζ or η.

Now, the strain rate components can be evaluated using equations (3.1) - (3.8), as follows:

$$\dot{\varepsilon}_x = \frac{\partial u}{\partial x} = \sum_{i=1}^{4} \frac{\partial N_i}{\partial x} u_i$$

$$= \frac{1}{|J|} \sum_{i=1}^{4} \{ (\sum_{k=1}^{4} \frac{\partial N_k}{\partial \eta} y_k) \frac{\partial N_i}{\partial \zeta} - (\sum_{k=1}^{4} \frac{\partial N_k}{\partial \zeta} y_k) \frac{\partial N_i}{\partial \eta} \} . u_i$$

(3.9)

$$= \frac{\partial v}{\partial y} = \sum_{i=1}^{4} \frac{\partial N_i}{\partial y} v_i$$

$$= \frac{1}{|J|} \sum_{i=1}^{4} \{ -(\sum_{k=1}^{4} \frac{\partial N_k}{\partial \eta} x_k) \frac{\partial N_i}{\partial \zeta} + (\sum_{k=1}^{4} \frac{\partial N_k}{\partial \zeta} x_k) \frac{\partial N_i}{\partial \eta} \} v_i$$

(3.10)

$$\gamma_{xy} = \frac{\partial u}{\partial y} + \frac{\partial v}{\partial x} = \sum_{i=1}^{4} \frac{\partial N_i}{\partial y} u_i + \frac{\partial N_i}{\partial x} v_i$$

$$\frac{1}{|J|} \sum_{i=1}^{4} \{ -(\sum_{k=1}^{4} \frac{\partial N_k}{\partial \eta} x_k) \frac{\partial N_i}{\partial \zeta} + (\sum_{k=1}^{4} \frac{\partial N_k}{\partial \zeta} x_k) \frac{\partial N_i}{\partial \eta} \} u_i +$$

$$\{ (\sum_{k=1}^{4} \frac{\partial N_k}{\partial \eta} y_k) \frac{\partial N_i}{\partial \zeta} - (\sum_{k=1}^{4} \frac{\partial N_k}{\partial \zeta} y_k) \frac{\partial N_i}{\partial \eta} \} v_i$$

(3.11)

ith the help of equations (3.4) - (3.11), it is now possible to lculate the strain rates at each of the node points of an lement. However, an examination of the mesh geometry (Fig. 3.2) ows that most of the nodes are common to two or more elements. king into account this aspect, the strain rate components at ch node within the deformation zone have been calculated as e appropriate average values between neighbouring elements.

After evaluating the strain rate components the corresponding cumulative strain components are obtained as follows. The incremental strains occuurring between two neighbouring nodes n and n+1 lying on a particular stream line, are:

$$\Delta\varepsilon_x = \varepsilon_{x,n+1} - \varepsilon_{x,n} = \dot{\varepsilon}_{x,av} \cdot \Delta t = \frac{\dot{\varepsilon}_{x,av} \cdot \Delta x}{u_{av}} \qquad (3.12)$$

$$\Delta\varepsilon_y = \varepsilon_{y,n+1} - \varepsilon_{y,n} = \dot{\varepsilon}_{y,av} \cdot \Delta t = \frac{\dot{\varepsilon}_{y,av} \Delta x}{u_{av}} \qquad (3.13)$$

$$\Delta\gamma_{xy} = \gamma_{xy,n+1} - \gamma_{xy,n} = \dot{\gamma}_{xy,av} \cdot \Delta t = \frac{\dot{\gamma}_{xy,av} \Delta x}{u_{av}} \qquad (3.14)$$

here, $\dot{\varepsilon}_{x,av}$, $\dot{\varepsilon}_{y,av}$ and $\dot{\gamma}_{xy,av}$ are the average values of the train rate components between nodes n and n+1, Δt is the time nterval required for a particle to travel from n to n+1, u_{av} is he average x-direction velocity between the two nodes and Δx s the step-size of the numerical mesh in x-direction. Using the bove expressions for incremental strain components, it is very imple to calculate the cumulative strains (or in other words, ne strain-history) of material particles. Setting, $\varepsilon_x = 0$, $\varepsilon_y = 0$ and $\gamma_{xy} = 0$ at the inlet boundary (neglecting elastic

or plastic strains the particles might have undergone before reaching this surface), the cumulative strains are progressively calculated along each streamline of the numerical mesh. The values of the strain components corresponding to all the nodes are stored as suitable arrays, for evaluating the stresses and the power integrals.

3.4 ROLLING POWER CALCULATIONS

As discussed earlier, the total rolling power is made up of three contributions, namely, the power for internal plastic deformation, power to overcome friction at the strip surface and the shear losses at the inlet boundary. The first one is an area integral over the deformation zone and the latter two are line integral computed on appropriate boundary curves.

In the present study, Gaussian quadrature is employed for calculating both the area and line integrals. The application of Gaussian quadrature for computing area and line integrals is described below:

$$\iint_{\Omega} F \; dx \; dy = \sum_{i=1}^{m} F(x_i, y_i) \; A_i \qquad (3.15)$$

and, $$\int_{C} F \; dl = \sum_{i=1}^{k} F_i \; l_i$$

where, i is an index for the sampling points (also known as Gauss points) F_i or $F(x_i, y_i)$ are the values of the integrand at the Gauss points and l_i or A_i represent the weighted length or area

corresponding to the i^{th} sampling point. In terms of the local coordinates ξ and η, the evaluation of the integrals becomes even simpler. Thus,

$$\iint_{(e)} F\,dx\,dy = \int_{-1}^{+1}\int_{-1}^{+1} F\,|J|\,d\xi\,d\eta = \sum_{i=1}^{m}\sum_{j=1}^{m} w_i w_j \{F.|J|\}_{i,j} \qquad (3.16)$$

and

$$\int_{(e)} F\,dl = L^e \int_{-1}^{+1} F\,d\xi \text{ or } L^e \int_{-1}^{+1} F\,d\eta$$

$$= L^e \sum_{i=1}^{k} F_i\, w_i \qquad (3.17)$$

where, w_i and w_j are standard weights and L^e is the length of a line element. The subscript is used in the above integrals indicates that the integration process is carried out over a quadrilateral element or the boundary line segment of an element. In the present study, consistent with the interpolation schemes employed, 2 sampling points per direction have been used. Thus, for the area integrals (2x2) areas points are used while line integrals are computed with 2 Gauss points, for each area element or line segment respectively. The weights and sampling point positions are summarized in Table 3.1.

Table 3.1

i	w_i	ζ_i, η_i
1	1.0	$-1/\sqrt{3}$
2	1.0	$+1/\sqrt{3}$

Each of the power contributions can now be evaluated as follows. For the plastic power calculations, the density, equivalent stress, equivalent strain and equivalent strain rates are required at the Gauss points of each element. These are calculated using equations (2.45) - (2.52) and (3.9) - (3.14), along with interpolations of the form

$$\dot{\varepsilon}_x = \sum_{i=1}^{4} N_i \dot{\varepsilon}_{x,i} \; ; \; \dot{\varepsilon}_y = \sum_{i=1}^{4} N_i \dot{\varepsilon}_{y,i} ; \; \dot{\gamma}_{xy} = \sum_{i=1}^{4} N_i \dot{\gamma}_{xy,i}$$

$$\varepsilon_x = \sum_{i=1}^{4} N_i \varepsilon_{x,i} \; ; \; \varepsilon_y = \sum_{i=1}^{4} N_i \varepsilon_{y,i} \; ; \; \gamma_{xy} = \sum_{i=1}^{4} N_i \gamma_{xy,i} \qquad (3.18)$$

applied at the Gauss points of the element.

In the above expressions, i denotes the index for the nodes of an element. In order to facilitate the transformation of the area integral from (x,y) coordinates to (ζ, η) coordinates, it is necessary to calculate the determinant of the Jacobian matrix $|J|$ at the Gauss points also.

Summing up the values of the product $\rho . \bar{\sigma}_{eq} . \dot{\bar{\varepsilon}}_{eq} |J|$ at the four Gauss points and multiplying with appropriate Gauss point

weights as shown in eq. (3.16), leads to the plastic deformatioan power contribution of one area element. Adding the contributions from all the 210 area elements provides the total plastic power over the whole deformation zone.

The calculation of friction power at the roll surface involves the following steps. First, the frictional stress values and the local velocityship are determined at the Gauss points (which lie on the boundary) using equations (2.56) - (2.58). The product $L^e \tau \Delta V$ is obtained at each of the two Gauss points and the frictional power contribution of one line segment is then evaluated via eq. (3.17). The sum of all such contributions from the 21 line segments on the roll surface, provides the total friction power.

The shear losses at entry section are computed from eq. (2.59). The integration is performed in a manner similar to that of the friction power integral. The shear loss contribution for each of the 10 line segments along the entry cross-section is calculated and summed up, to obtain the total shear loss. The rolling power is then obtained as the sum of all the three individual powers.

3.5 MINIMIZATION OF POWER

The integral for the total rolling power $\dot{W}$, has been evaluated numerically by Gass-Legendre quadrature, assuming an initial guuess for the value of b and u_1. The derivative dW/db is evaluated by slightly perturbing the value of b by Δb and using the central difference expression

$$\frac{d\dot{W}}{db} = \frac{\dot{W}(b + \Delta b) - \dot{W}(b - \Delta b)}{2\Delta b} \qquad (3.19)$$

To find the optimum value of b, weset:

$$\frac{d\dot{W}}{db} = f(b) \qquad (3.20)$$

and calculate the root of the expression:

$$f(b) = 0 \qquad (3.21)$$

by the Newton-Raphson technique. An improved guess value of b is obtained by the following equation:

$$b_{n+1} = b_n = \frac{f(b_n)}{f'(b_n)} \qquad (3.22)$$

where,

$$f'(b_n) = \frac{df}{db} = \frac{d^2\dot{W}}{db^2} \qquad (3.23)$$

In the above equation, the subscript n denotes the value corresponding to n^{th} iteration. The second derivative of $\dot{W}$ in eq. (3.23) is calculated through the central difference expression:

$$\frac{d^2\dot{W}}{db^2} = \frac{\dot{W}(b + \Delta b) + \dot{W}(b - \Delta b) - 2\dot{W}(b)}{\Delta b^2} \qquad (3.24)$$

During the numerical implementation, eq. (3.24) was converged to a value smaller than that of a prescribed parameter. Thus,

$$|f(b)| < \delta \qquad (3.25)$$

was used as the convergence criterion for the solution, with δ chosen as equal to 0.0001.

The entrance strip velocity u_1, is then varied systematically to identify the global minimum power for each set of rolling conditions. The distribution of density and velocity corresponding to the global minimum is then obtained and the corresponding results are taken as the true results for the given set of rolling conditions. The numerical computations have been performed over a wide range of rolling conditions, for both single pass and multi-pass rolling. For multi-pass rolling, the assuumption of no initial strains has been relaxed when intermediate annealing is not considered. For the calculations corresponding to multi-pass rolling with intermediate annealing, the initial strains have been taken as zero and it is also assumed that annealing does not cause any densification. The results predicted from the analysis are presented and discussed in Chapter V.

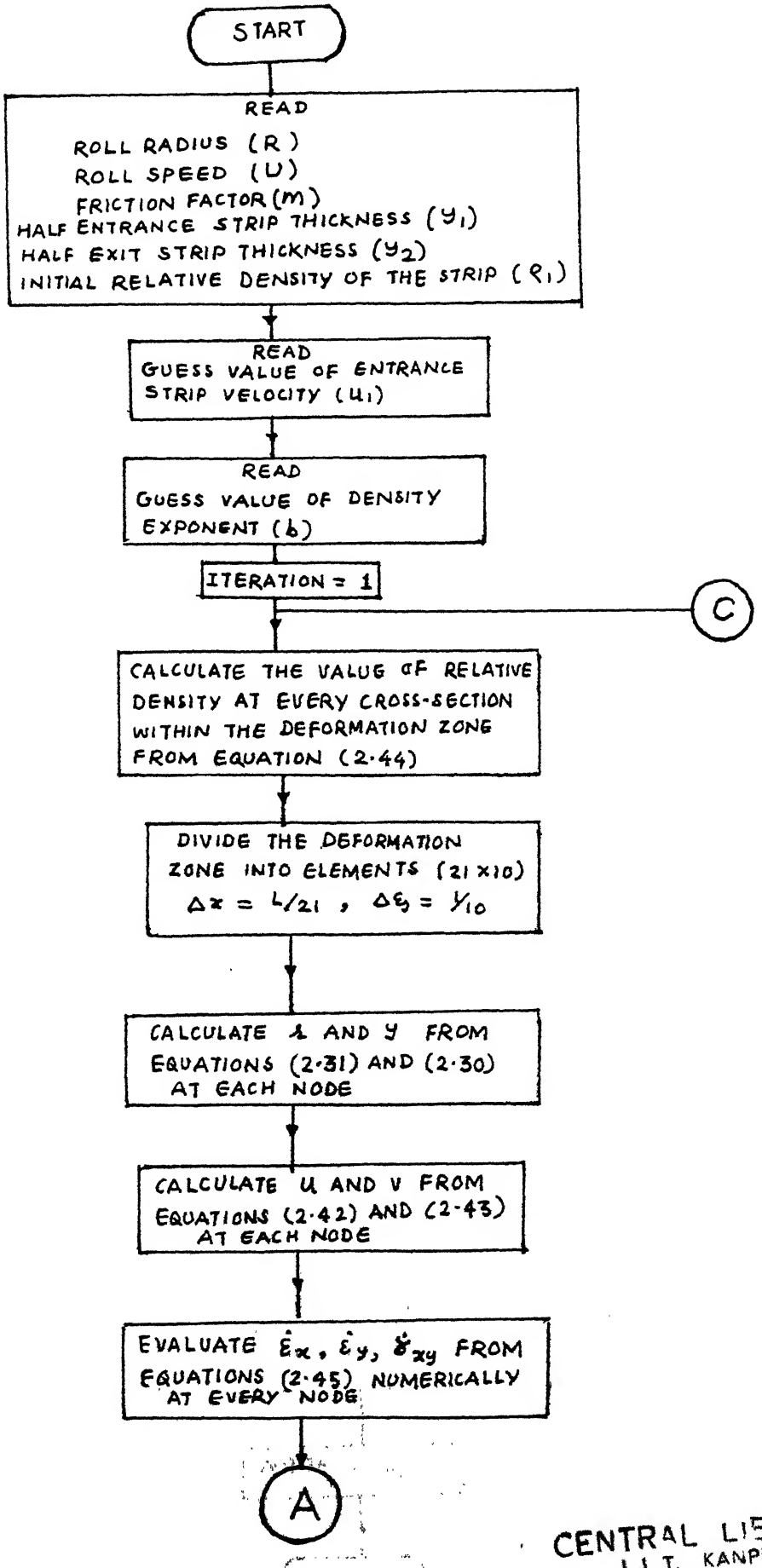

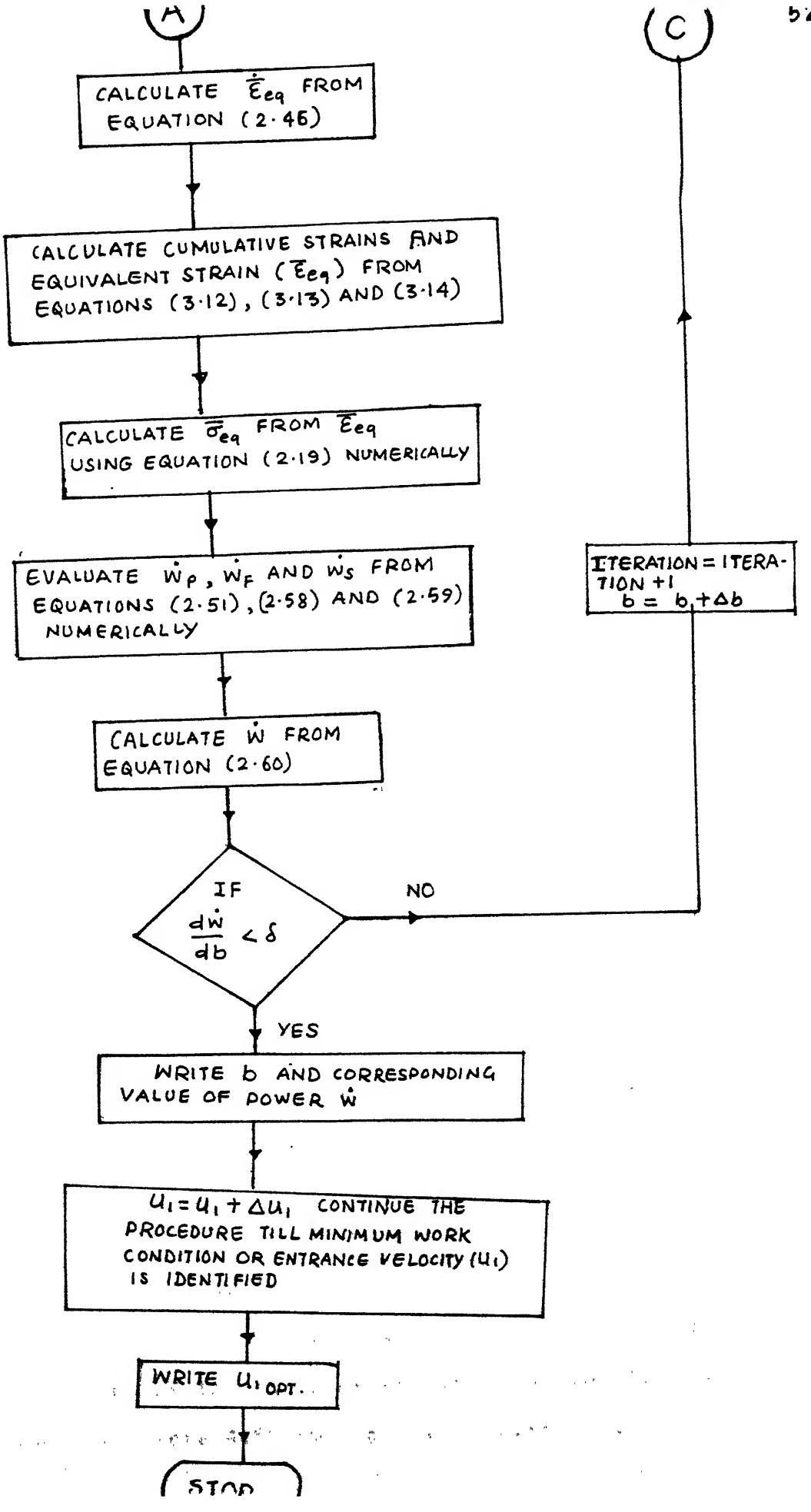
A
CALCULATE $\dot{\bar{\varepsilon}}_{eq}$ FROM EQUATION (2·46)
CALCULATE CUMULATIVE STRAINS AND EQUIVALENT STRAIN ($\bar{\varepsilon}_{eq}$) FROM EQUATIONS (3·12), (3·13) AND (3·14)
CALCULATE $\bar{\sigma}_{eq}$ FROM $\bar{\varepsilon}_{eq}$ USING EQUATION (2·19) NUMERICALLY
EVALUATE $\dot{W}_P$, $\dot{W}_F$ AND $\dot{W}_S$ FROM EQUATIONS (2·51), (2·58) AND (2·59) NUMERICALLY
CALCULATE $\dot{W}$ FROM EQUATION (2·60)
IF $\frac{d\dot{W}}{db} < \delta$
NO
YES
C
ITERATION = ITERATION +1
$b = b + \Delta b$
WRITE b AND CORRESPONDING VALUE OF POWER $\dot{W}$
$U_1 = U_1 + \Delta U_1$ CONTINUE THE PROCEDURE TILL MINIMUM WORK CONDITION OR ENTRANCE VELOCITY (U_1) IS IDENTIFIED
WRITE $U_{1\,OPT.}$
STOP

CHAPTER IV

EXPERIMENTAL PROCEDURE

Cold rolling experiments have been performed on strips prepared from atomised copper powder. The powder specifications are:

Manufacturer	-	Greenback Industries, U.S.A.
Copper content	-	99.51%
Powder size	-	63.9% of -325 mesh
Apparent density	-	2.83 kg/m^3
Hall flow meter rating	-	3.45/50 gms

The experiments have been carried out with copper strip having relative density (ρ) in the range $0.76 < \rho < 0.95$. The copper strip of required density was initially produced by the die compaction technique. Approximately 140 gms of copper powder was taken and was mixed with 1.4 gms of methyl cellulose binder. The mixture was then compacted in a die of size 4.7 cm x 7.9 cm. The die and punch were lubricated with zinc stearate. The compaction pressure used was 1451.65 kg/cm^2 (load = 53.9 tons). The strip of dimensions 4.55 cm x 6.7 cm x 0.675 cm with a relative density of 0.7465 was obtained.

The green strip thus produced was then sintered at a temperature of approximately $925^{o}C$ in hydrogen atmosphere for a period of 70 minutes and then cooled in hydrogen for about 20 minutes. After cooling, the weight and the dimensions of the strip were measured. It was found that there is some loss in the weight due to the removal of oxide film on the powder surface. The relative density of the strip after sintering was 0.7614 and the strip dimensions were 4.55 cm x 6.7 cm x 0.662 cm.

The sintered copper strip was cold rolled in a rolling mill with the following specifications:

Roll radius = 67.5 mm

Roll speed = 508.68 mm/s

Horse power = 7.8 HP

The rolls were not lubricated. The required amount of thickness reduction was carried out by multi-pass rolling. After each pass, density and dimensions of the strips were measured. Cracks were observed, after 30% reduction with respect to original thickness. The total reduction of 61.4% was carried out in seven passes. The true length and thickness strains were calculated from the obtained dimensions. The results for multi-pass rolling were summarized in Table 5.13.

CHAPTER V

RESULTS AND DISCUSSIONS

The results obtained through the upper bound technique for cold densification rolling of sintered porous copper strips are presented in this section. The main aspects studied here include the densification behaviour of the porous strip and the power consumed during the rolling process. However, some effort has also been made to gain a fundamental understanding of the deformation process by analysing the velocity field, strain field, percentage slip and the distributions of roll pressure and relative density. The effects of parameters such as friction factor, percentage reduction, roll speed, roll radius and initial density and initial strip thickness have been highlighted. Results for multipass rolling with and without intermediate annealing have also been presented.

Some of the calculated results have been verified experimentally. All the theoretical calculations have been performed for a sintered copper strip with relative density (ρ) in the range $0.7 < \rho < 0.995$, using the correlation for equivalent stress proposed by Shima and Oyane [4].

5.1 IDENTIFICATION OF MINIMUM POWER CONDITION:

As stated by the upper bound theorem (Chapter III), of all the kinematically admissible velocity fields, the true velocity field minimizes the total power. In the present study, in addition to the kinematically admissible velocity field, a density distribution with an unknown exponent (b) is assumed.

This exponent is determined by applying the minimum power criterion.

Another important variable whose value is unknown a priori, is the strip velocity at the entry (u_1). A significant finding of the present study is that there exists an optimum entrance strip velocity which leads to the global minimum of power consumed for a given set of rolling conditions (Fig. 5.1). In view of the upper bound theorem, such an optimum entry velocity may be taken to correspond to the true velocity and density distributions. Therefore, for each set of rolling conditions, the exponent (b) and the entrance strip velocity (u_1) have been systematically varied through a Neweton-Raphson search procedure for identifying the global minimum power. The typical procedure employed to track-down the point of global minimum is illustrated in Fig. 5.1 and Table 5.1.

A close examination of the power contributions in Table 5.1 shows that for $u_1 > u_{1,\,opt}$ and $b = b_{opt}$, the plastic deformation power is high due to high strain rates; on the other hand, for $u_1 < u_{1,opt}$ with $b = b_{opt}$ friction power increases due to a high value of backward slip. When these two effects exactly balance each other, the optimal flow rate occurs (i.e. $u_1 = u_{1,opt}$).

It was generally observed that as the entrance strip velocity is varied, a global minimum in rolling power does not occur for reductions greater than 35%. It appears that for a fixed friction factor, the densification is improper at high percentage reduction (25% and above) and the slip increases; these phenomena are probably responsible for no minimum existing at high reductions. However, the real reasons for the non-

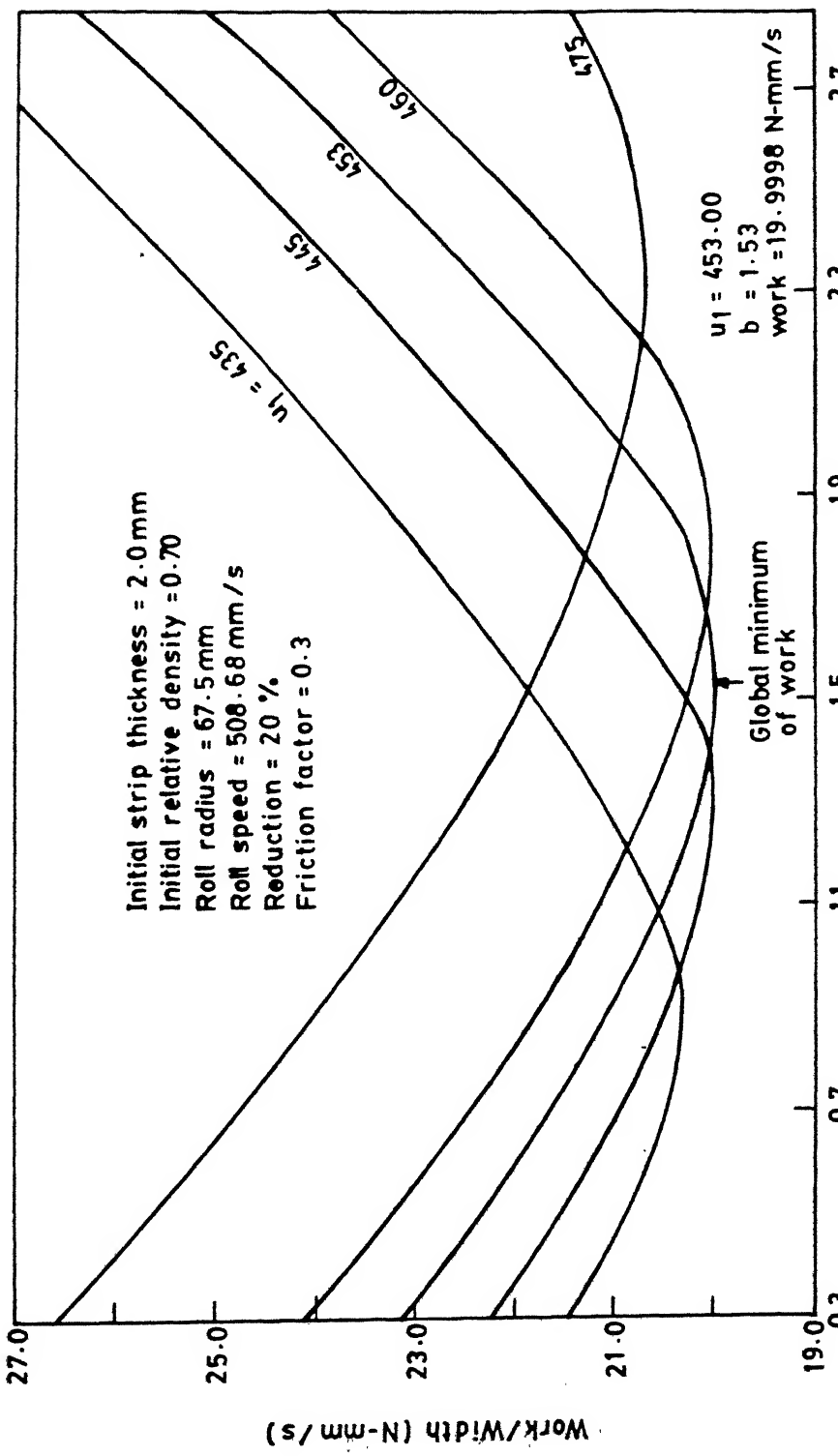

FIG. 5.1 THE GLOBAL MINIMUM OF POWER CONSUMED FOR A GIVEN SET OF ROLLING CONDITIONS

existence of a global minimum in our predictions for these conditions, are not clearly understood at this juncture.

5.2 DISTRIBUTIONS OF THE FIELD VARIABLES IN DEFORMATION ZONE:

The streamline patterns for two reductions (20% and 5%) are shown in Figure 5.2. It is observed that streamline which are equally spaced at entry remain equally spaced throughout the deformation zone. Ths feature clearly illustrates that the rolling process is homogeneous on account of the small strip thickness. The figures also indicate that for larger reduction, the arc of contact is longer and the streamlines are more curved, especially near the entrance section. This in turn, leads to larger strains.

The u and v velocity distributions are presented in Figures 5.3 and 5.4 respectively. The u-velocity distribution has been plotted only in terms of the increment over the entry velocity (u_1), for the sake of clarity. It is observed that the u-velocity is uniform while,the v-velocity decreases linearly from the surface to the centre, over any cross-section. The uniformity of u-velocity is a consequence of homogeneous compression. The v-velocity decrease towards the centre is a result of less bending of streamlines in the mid portion of the strip. In the rolling direction (x), u-velocity increases monotonically due to longitudinal elongation of material particles. The rate of elongation is high near the entry section where area reduction is also high. Towards the exit, the change in u-velocity becomes neligible. The v-velocity, on the other hand, decreases in the rolling direction. This is obviously a

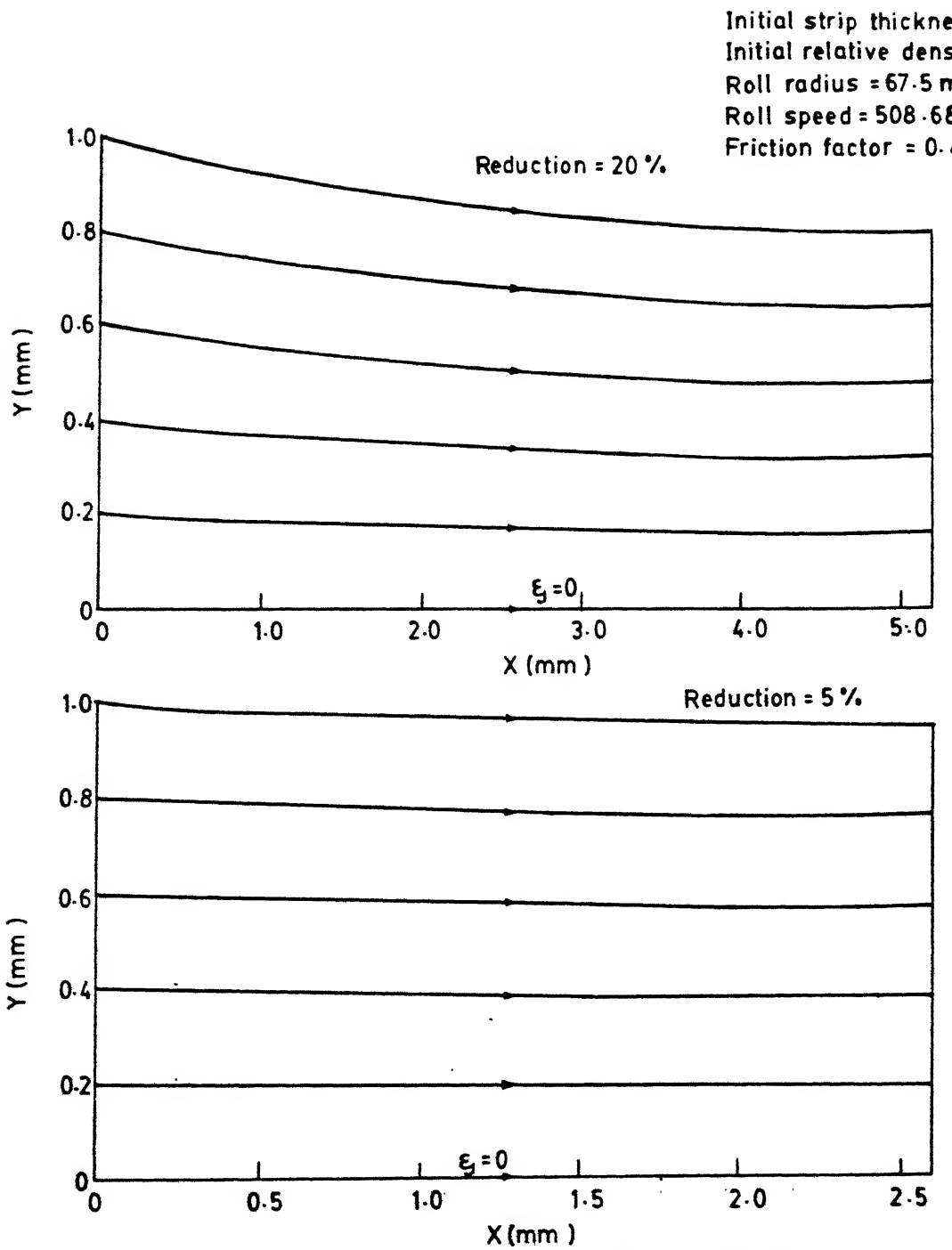

FIG. 5.2 DEFORMATION ZONE SHOWING STREAMLINES

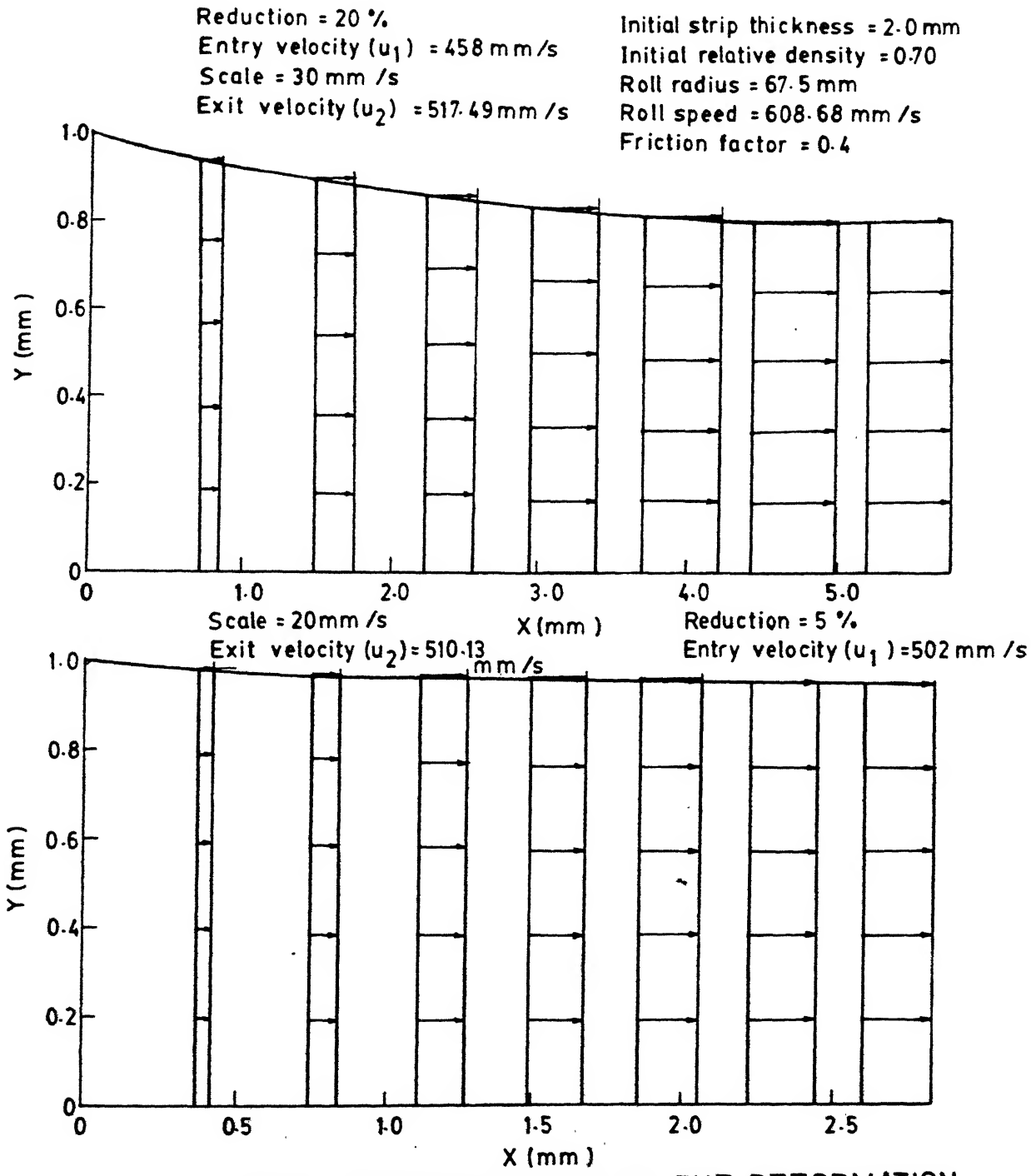

FIG. 5.3 U-VELOCITY DISTRIBUTIONS WITHIN THE DEFORMATION ZONE

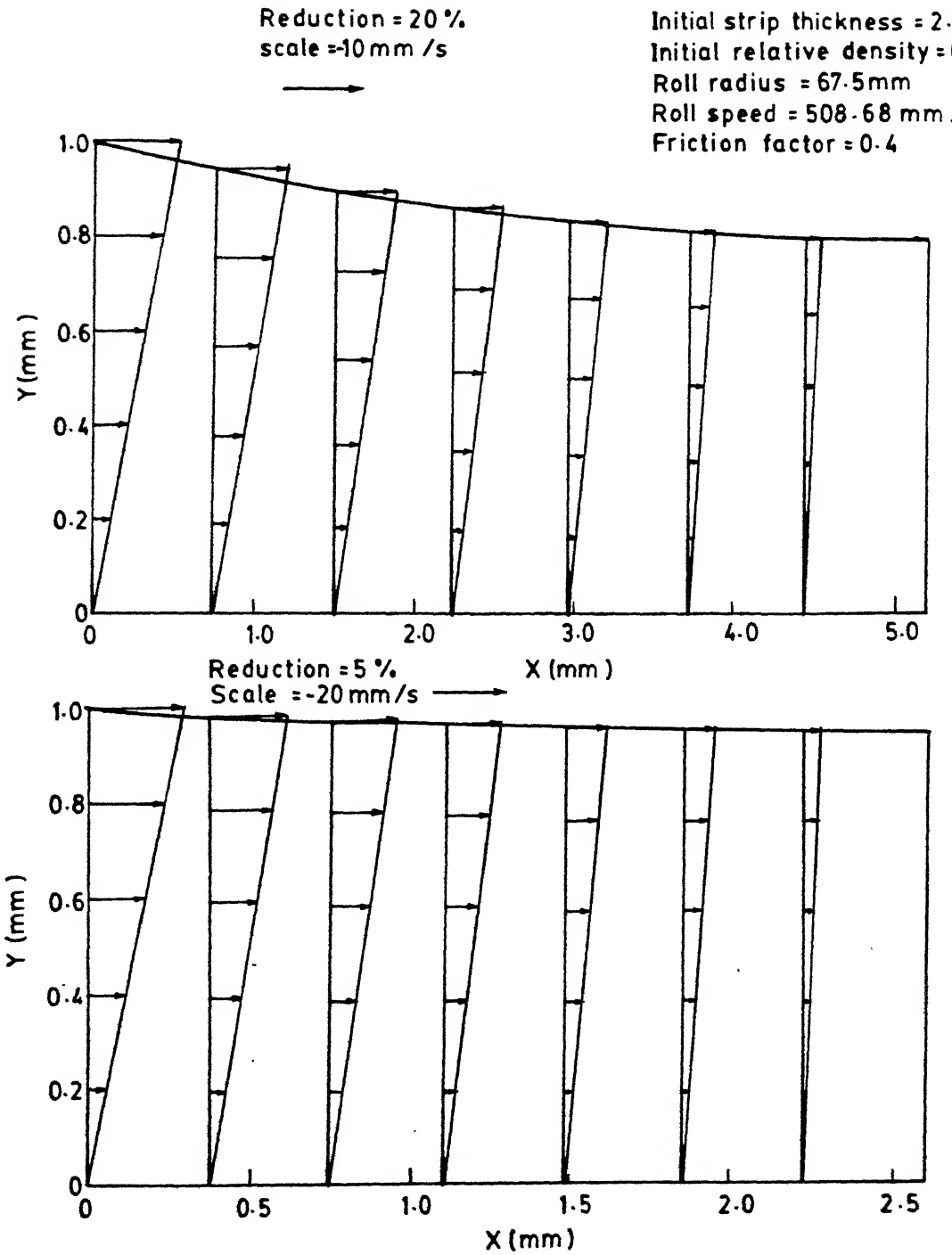

FIG. 5.4 V-VELOCITY DISTRIBUTIONS WITHIN THE DEFORMATION ZONE

esult of the streamlines becoming straight near the exit. At ower reduction, the distributions of u and v are very similasr o those at high reductions; however, the magnitudes of the hanges in u and v velocities between the inlet and exit are maller.

The strain distributions (ε_x, ε_y and γ_{xy}) are plotted in figures 5.5, 5.6 and 5.7. The normal strains in both longitudinal and lateral directions are uniform over each cross section. This feature also supports the conclusion of homogeneous compression, which was noted while discussing the streamline patterns. Both the normal strains increase rapidly near the inlet section and become almost constant towards the exit. This trend is clearly a consequence of the rapid changes in the velocity field near the inlet section. The shear strain is maximum at the surface and zero at the mid-plane, which is easily explained in terms of the larger bending of the streamlines near the surface. As expected, all the cumulative strains (ε_x, ε_y and γ_{xy}) undergone by a material particle, increase monotonically from the inlet to exit. The same strain behaviour is seen at all reductions, except that the magnitude of strains is larger at higher reductions.

The variation of density, roll pressure and slip in the rolling direction are shown in Figures 5.8a and 5.8b for the reductions of 20% and 5%. The locations of the neutral point and the maximum roll pressure are also indicated in these figures. It is observed that the maximum roll pressure occurs close to the neutral point as expected. Although theory of rolling predicts that the maximum pressure should occur at the neutral point (due

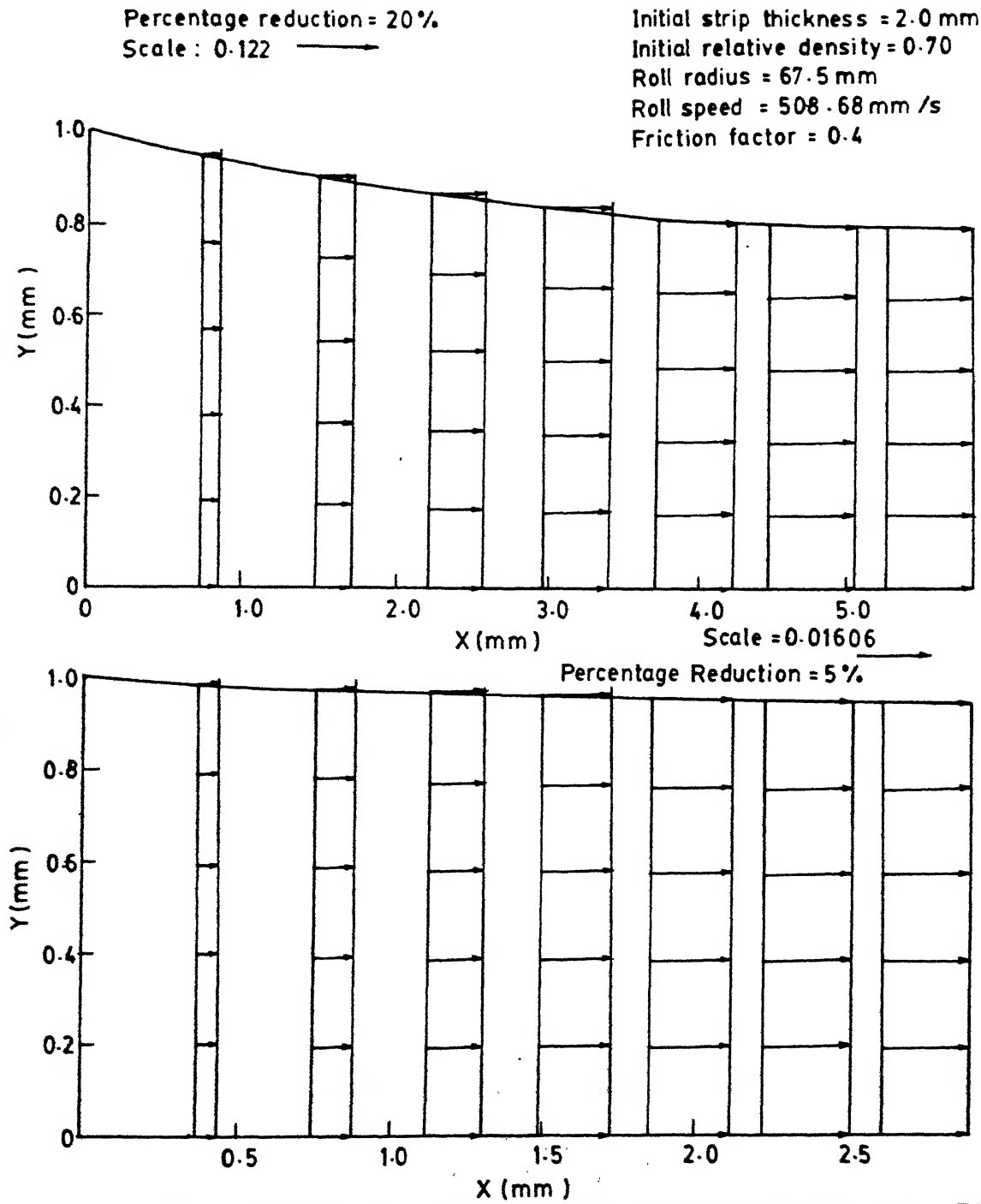

FIG.5.5 DISTRIBUTIONS OF LONGITUDINAL STRAIN(Ex) WITHIN THE DEFORMATION ZONE

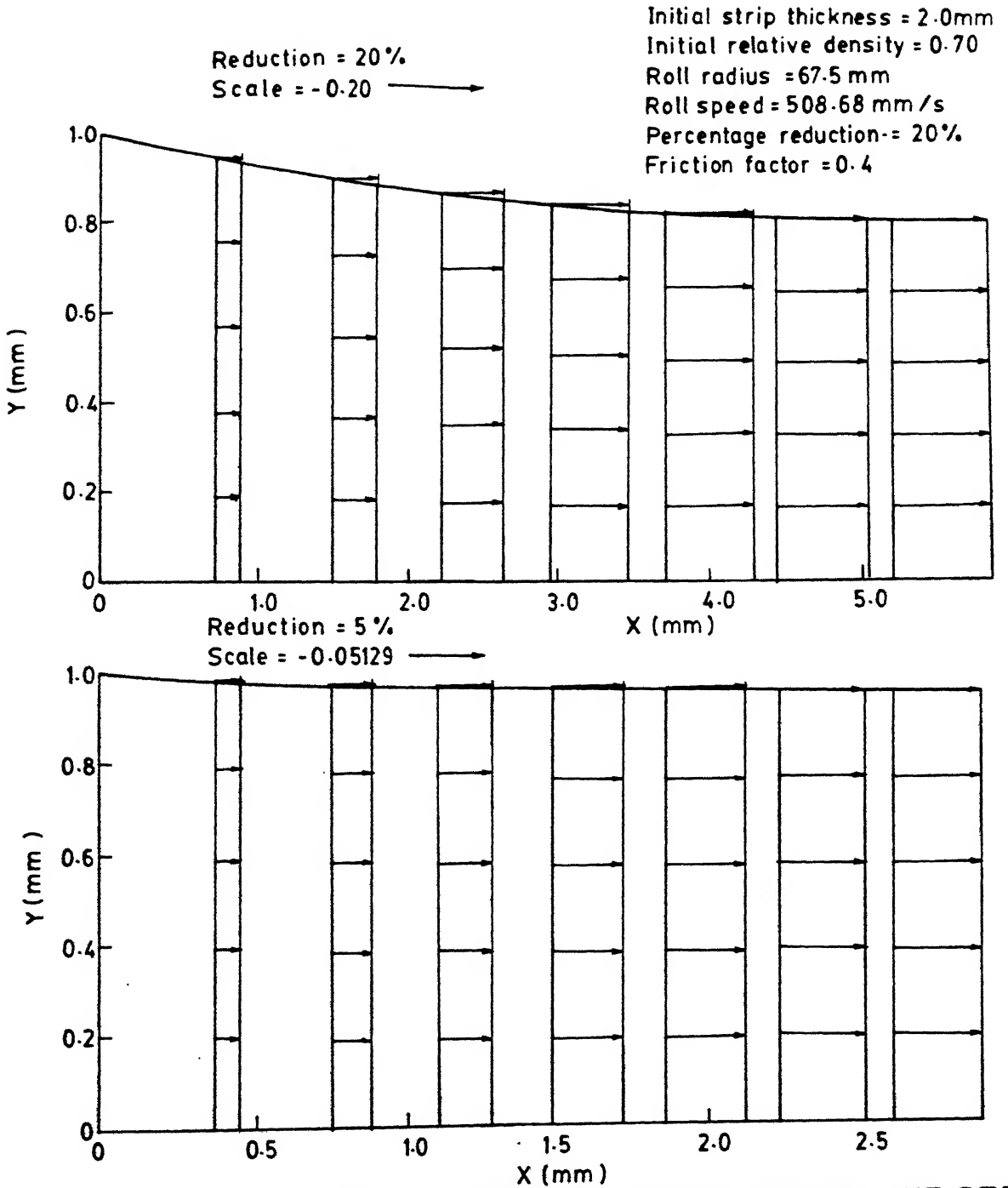

FIG. 5·6 DISTRIBUTION OF THICKNESS STRAIN WITHIN THE DEFORMATION ZONE

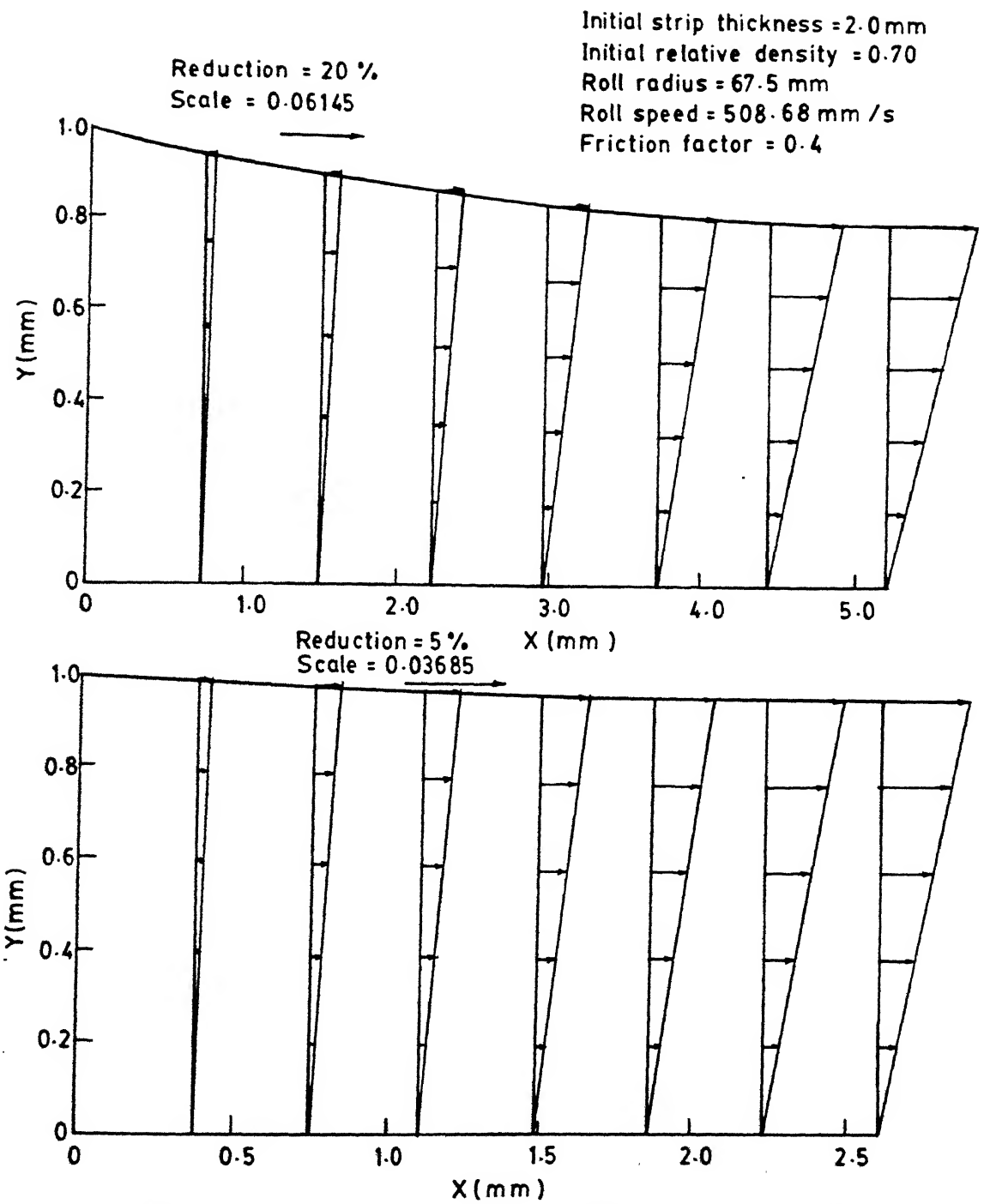

FIG. 5.7 DISTRIBUTION OF SHEAR STRAIN WITHIN THE DEFORMATION ZONE

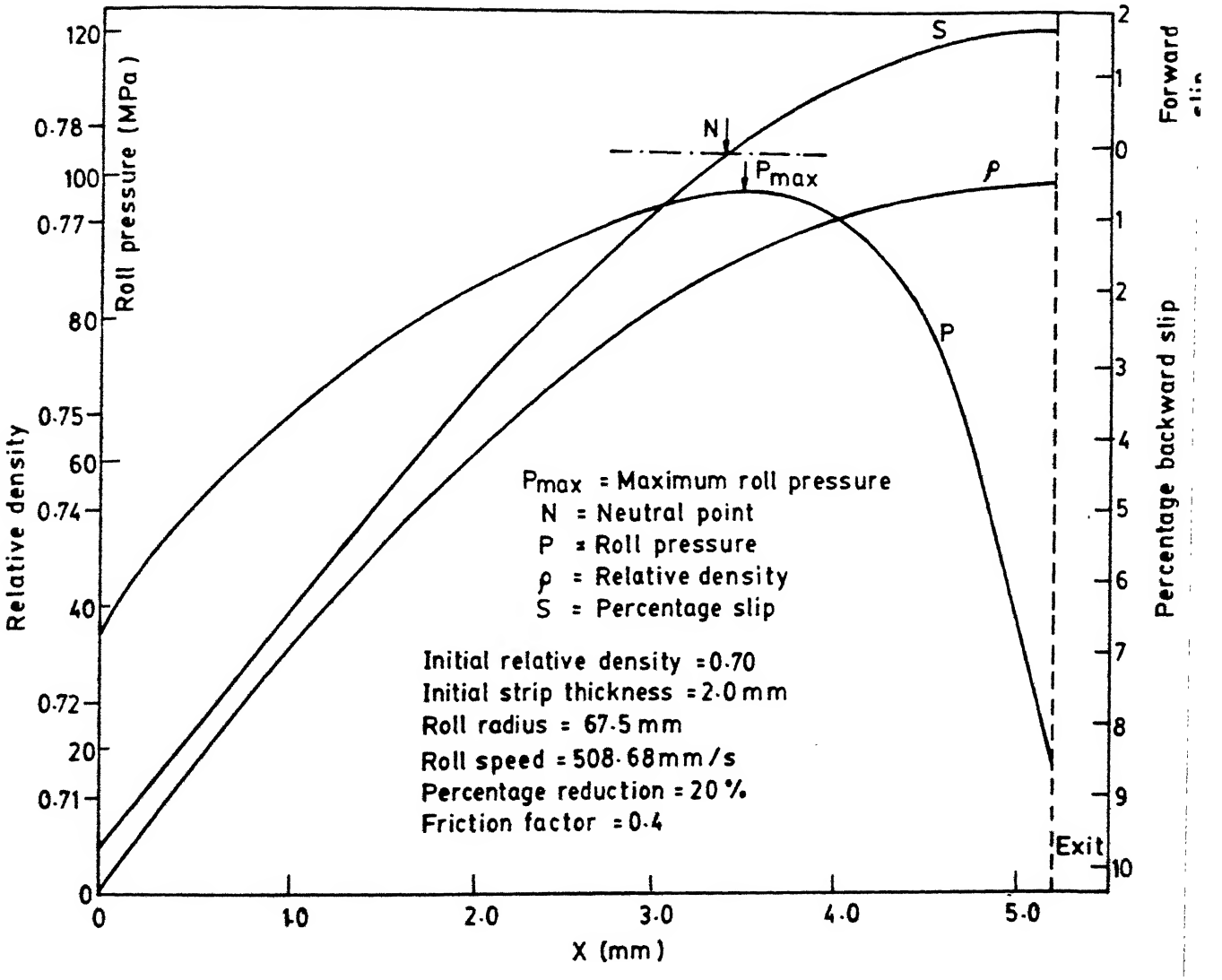

FIG. 5·8a VARIATION OF RELATIVE DENSITY ROLL PRESSURE AND PERCENTAGE SLIP IN THE ROLLING DIRECTION FOR 20% REDUCTION

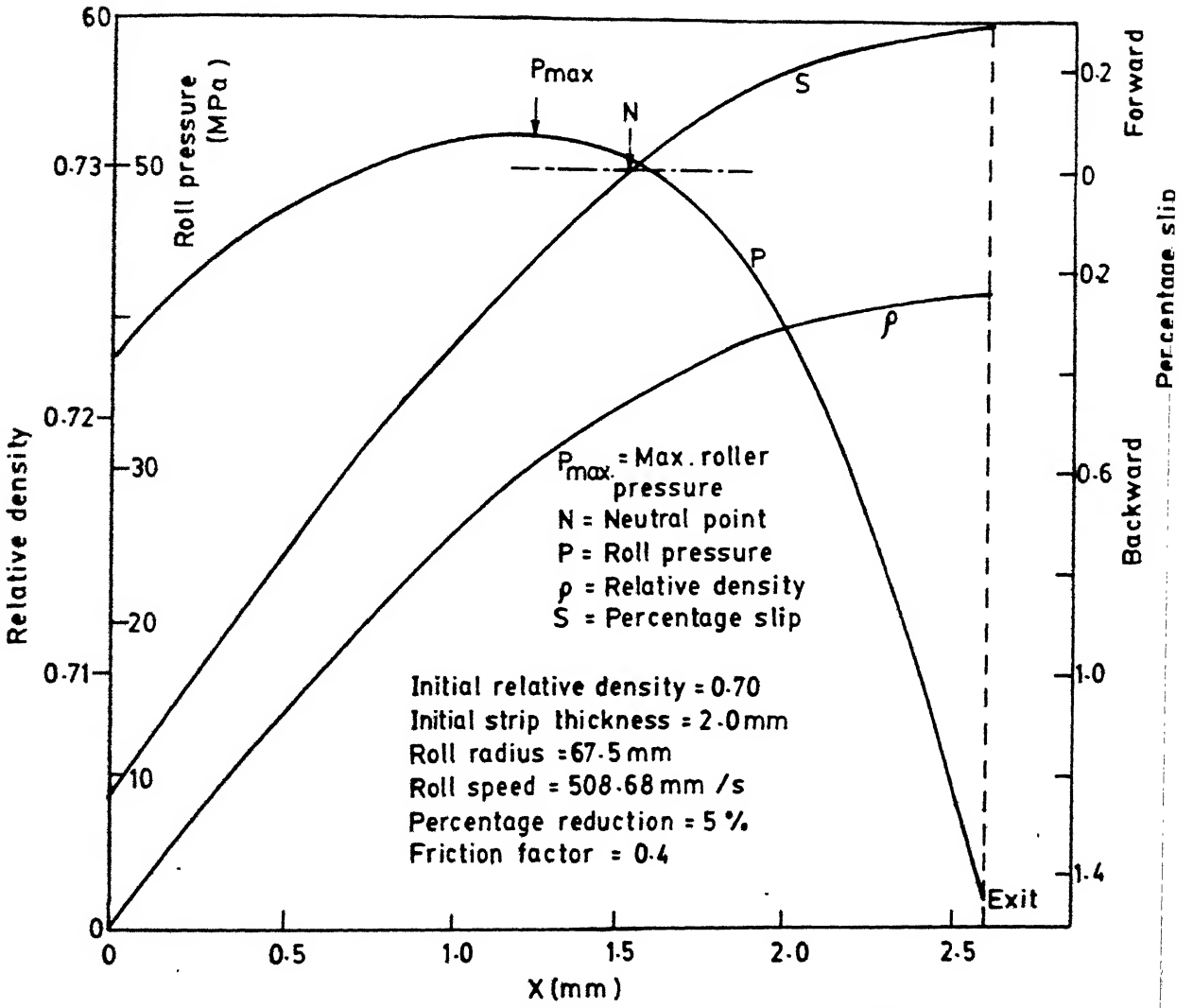

FIG. 5.8b VARIATION OF RELATIVE DENSITY, ROLL PRESSURE AND PERCENTAGE SLIP IN THE ROLLING DIRECTION FOR 5 % REDUCTION

to zero slip and zero shear stress), the upper bound analysis predicts a slight difference between the two locations. This may be due to the fact that stress balance is not applied everywhere within the deformation zone in the upper technique. It is seen that the variation of density is rapid near the entry and the curve becomes flat towards the exit. This trend is a direct consequence of the rate at which roll gap decreases with distance x, as reflected by equation (2.44) which governs the density variation. The variation of slip over the roll surface is such that the backward slip is larger in magnitude than the forward slip. The maximum backward slip which occurs at the entrance, is governed by the global minimum power criterion. It was also observed that the neutral point occurs closer to the exit than to the entry for the minimum power condition. With these facts in mind, since the velocity variation near the exit is slower, the observation that forward slip is smaller than backward slip is easily understood. A comparison of the roll pressure curve for sintered porous copper with that of solid copper [9] indicates that roll pressure is much larger for the solid material for a given reduction and friction factor; this derives from the fact that the yield stress and consequently the work required for deforming the solid metal,are higher than those for the porous material. At low reductions, the neutral point and the maximum pressure shift away from the exit section towards the mid-portion of the strip. The magnitudes of both the backward slip and forward slip are smaller, this occurs chiefly because of the smaller arc of contact. For a given initial density, smaller percentage reduction leads to lower exit density. The maximum

roll pressure is also smaller which is contributed by factors such as smaller arc of contact, less densification, lower strain hardening and smaller rolling power requirement in general.

5.3 INFLUENCE OF ROLLING PARAMETERS

(i) Friction Factor: The effects of friction upon the exit relative densdity are shown in Figure 5.9a. For the graphs shown in the figure, the initial relative density before rolling is taken to be equal to 0.7. For a given percentage reduction, the exit relative density of the strip is observed to increase with friction factor. This can be attributed to larger metal flow rate occurring because of better gripping conditions. When the friction factor is increased, the backward slip is reduced resulting in a higher metal flow rate. While, the forward slip exhibits a negligible variation (Figure 5.9b). However, the power required for rolling process increases with friction factor (Figure 5.9c). The increase in the rolling power is chiefly contributed by the frictional work. The results are shown in Tables 5.2 and 5.3.

(ii) Percentage Reduction: Figures 5.9a,b,c and d also show the influence of percentage reduction upon densification, slip and rolling power. For any given friction factor, the exit relative density is larger at higher reduction. This is easily explained in terms of greater compression as well as the elongation of the particles in rolling direction. The elongation of the particles is an important mechanism of densification for the high value of initial strip density assumed here. It is

roll pressure is also smaller which is contributed by factors such as smaller arc of contact, less densification, lower strain hardening and smaller rolling power requirement in general.

5.3 INFLUENCE OF ROLLING PARAMETERS

(i) Friction Factor: The effects of friction upon the exit relative densdity are shown in Figure 5.9a. For the graphs shown in the figure, the initial relative density before rolling is taken to be equal to 0.7. For a given percentage reduction, the exit relative density of the strip is observed to increase with friction factor. This can be attributed to larger metal flow rate occurring because of better gripping conditions. When the friction factor is increased, the backward slip is reduced resulting in a higher metal flow rate. While, the forward slip exhibits a negligible variation (Figure 5.9b). However, the power required for rolling process increases with friction factor (Figure 5.9c). The increase in the rolling power is chiefly contributed by the frictional work. The results are shown in Tables 5.2 and 5.3.

(ii) Percentage Reduction: Figures 5.9a,b,c and d also show the influence of percentage reduction upon densification, slip and rolling power. For any given friction factor, the exit relative density is larger at higher reduction. This is easily explained in terms of greater compression as well as the elongation of the particles in rolling direction. The elongation of the particles is an important mechanism of densification for the high value of initial strip density assumed here. It is

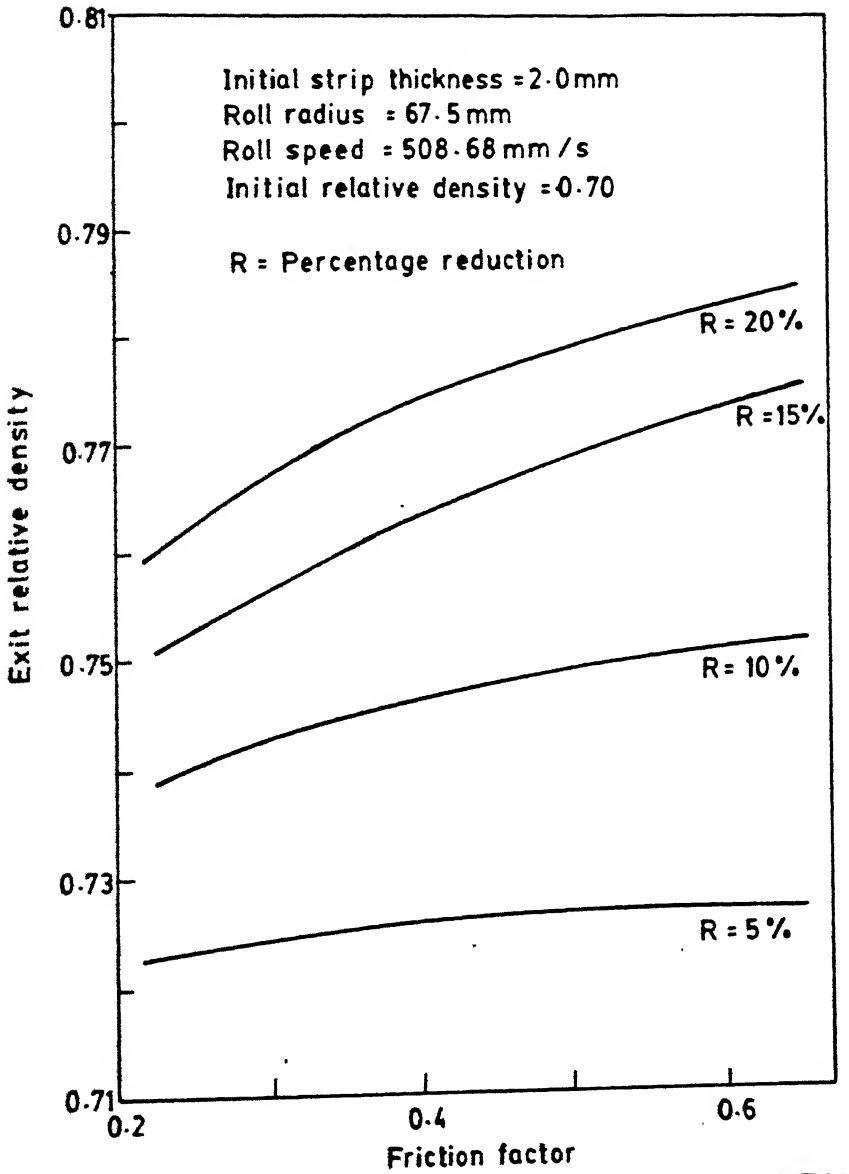

FIG. 5·9a EFFECT OF FRICTION FACTOR ON DENSIFICATION

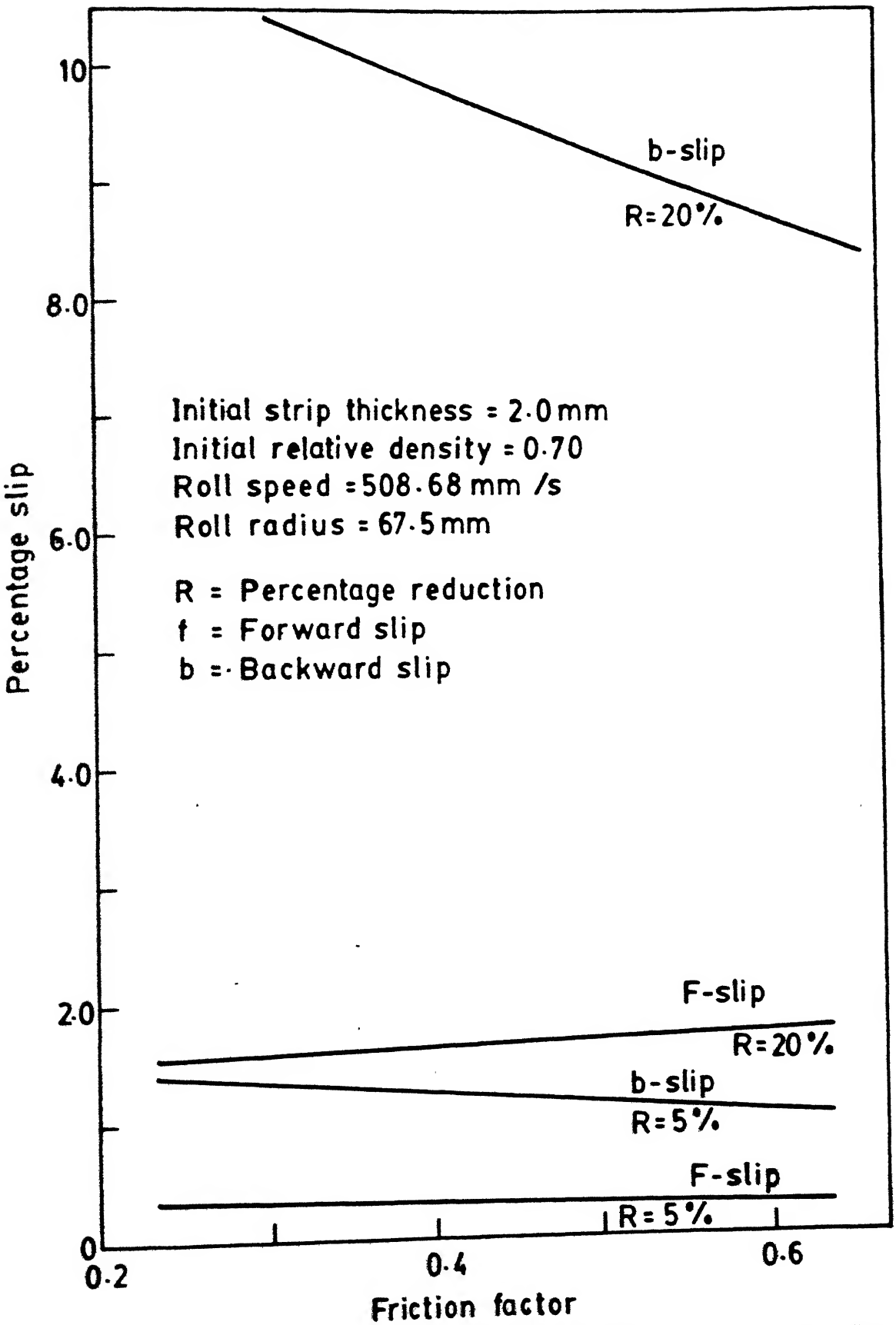

FIG. 5.9b EFFECT OF FRICTION FACTOR ON PERCENTAGE SLIP

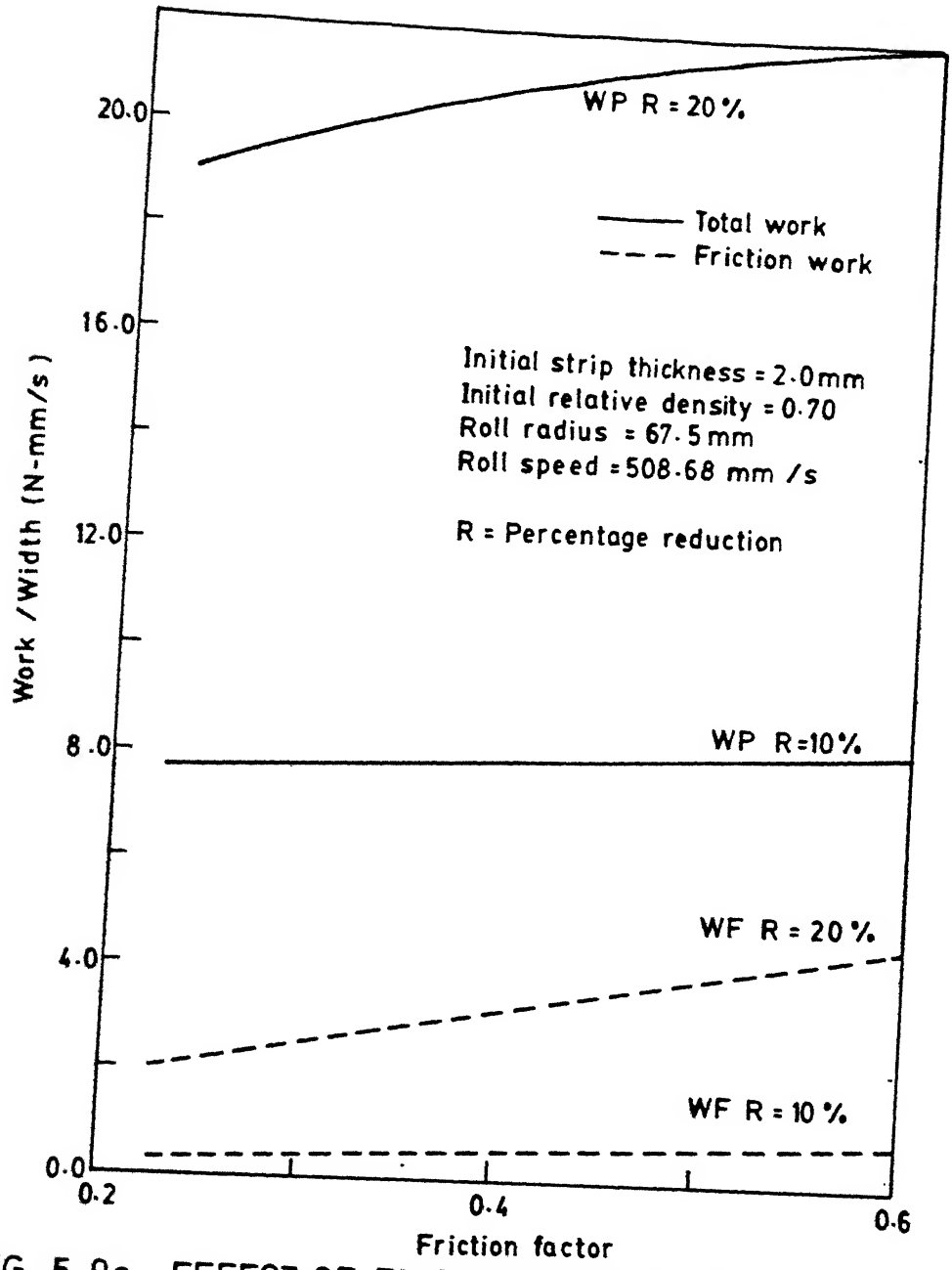

FIG. 5.9c EFFECT OF FRICTION FACTOR ON WORK

observed that the increase in densification is more sensitive to change in friction factor at higher percentage reduction. This trend can be attributed to the larger arc of contact and higher relative density . The backward and forward slip are seem to increase with percentage reduction; in particular, the backward slip becomes very high in magnitude at higher reduction for all friction factors. As regards, the rolling power, both the friction and the plastic deformation components show an increase with percentage reduction. While, friction work increases because of larger contact area, the plastic work increases due to more straining of material.

From Fig. 5.9d it can be seen that the exit relative density increases linearly with percentage reduction for a given set of rolling conditions. However, at higher reduction (25% and above) the exit relative density shows a decreasing tendency. This can be explained in terms of larger backward slip occurring at higher reductions. It is observed that the exponent (b) appearing in equation (2.44) decreases rapidly with increase in slip. This in turn, affects the densification and exit relative density falls at higher reduction. Also larger slip causes improper gripping of the strip between the rolls and thus leads to less densification.

The numerical values of exit density are summarised in Tables 5.4 for different friction factors and percentage reductions.

(iii) Roll Radius: The dependence of exit density and power components upon roll radius is shown in Figures 5.10a and 5.10b.

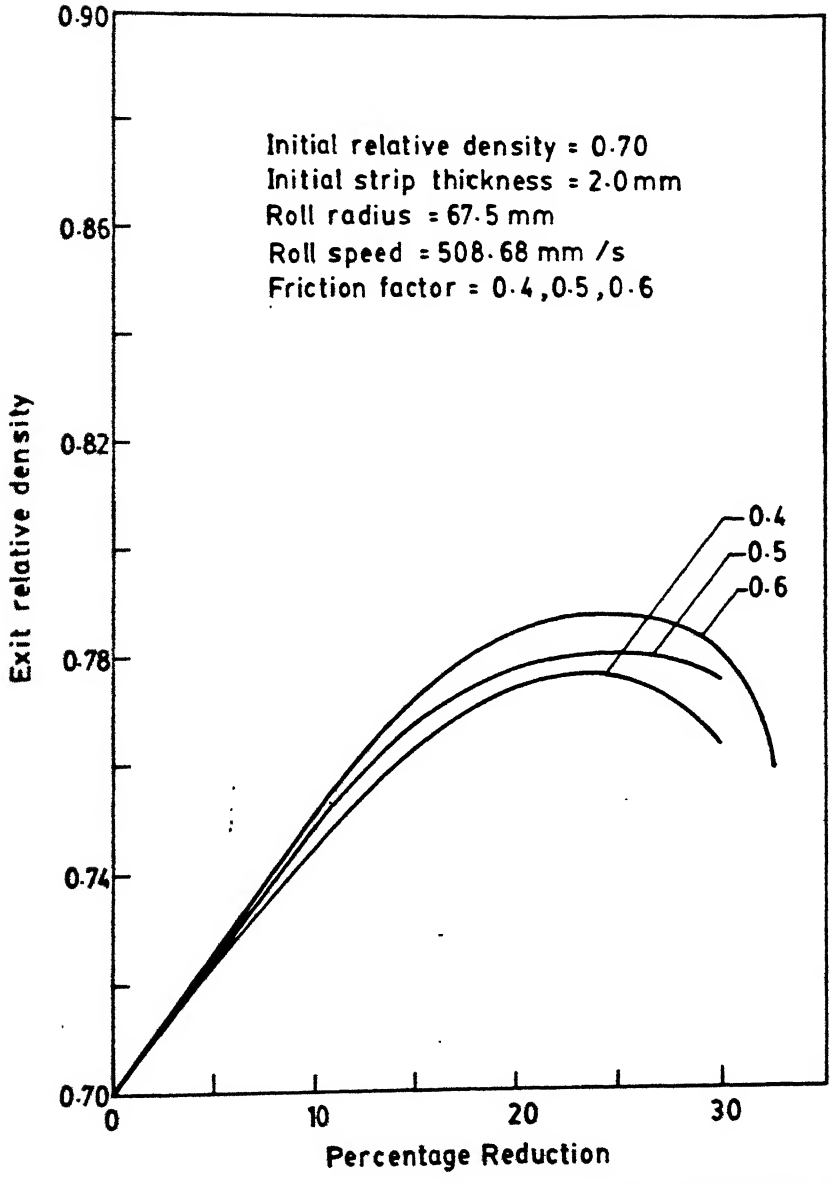

FIG. 5·9d EFFECT OF REDUCTION ON DENSIFICATION

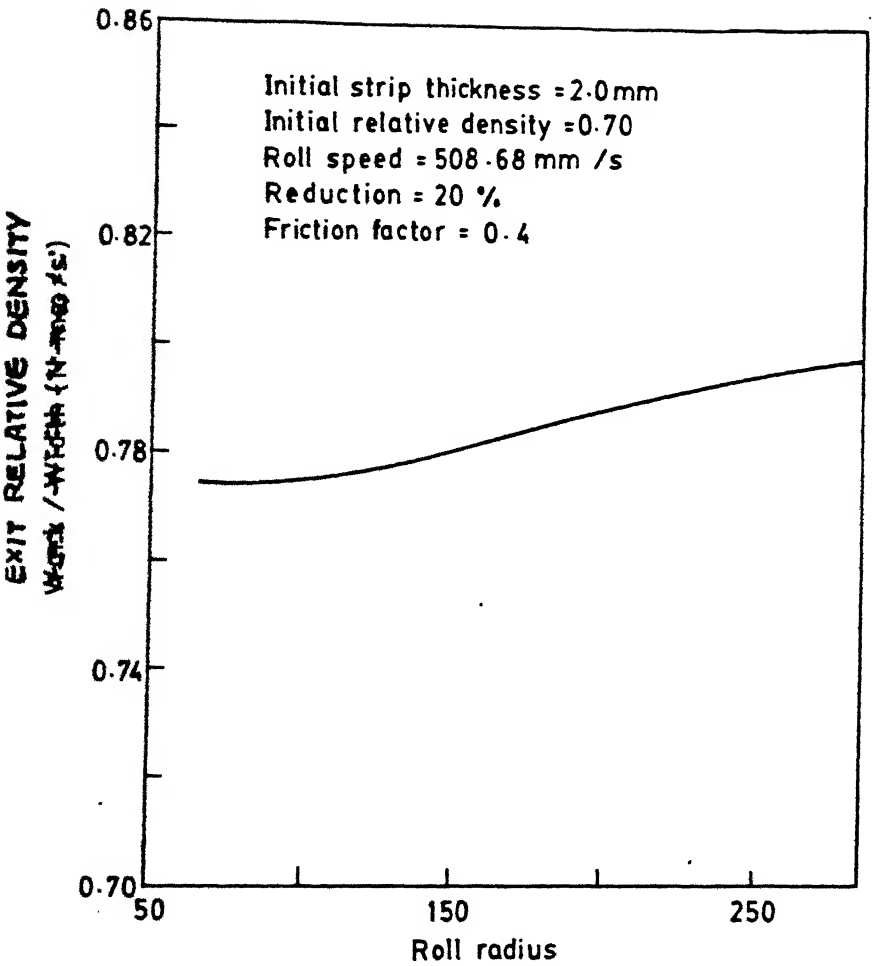

FIG. 5.10a EFFECT OF ROLL RADIUS ON DENSIFICATION

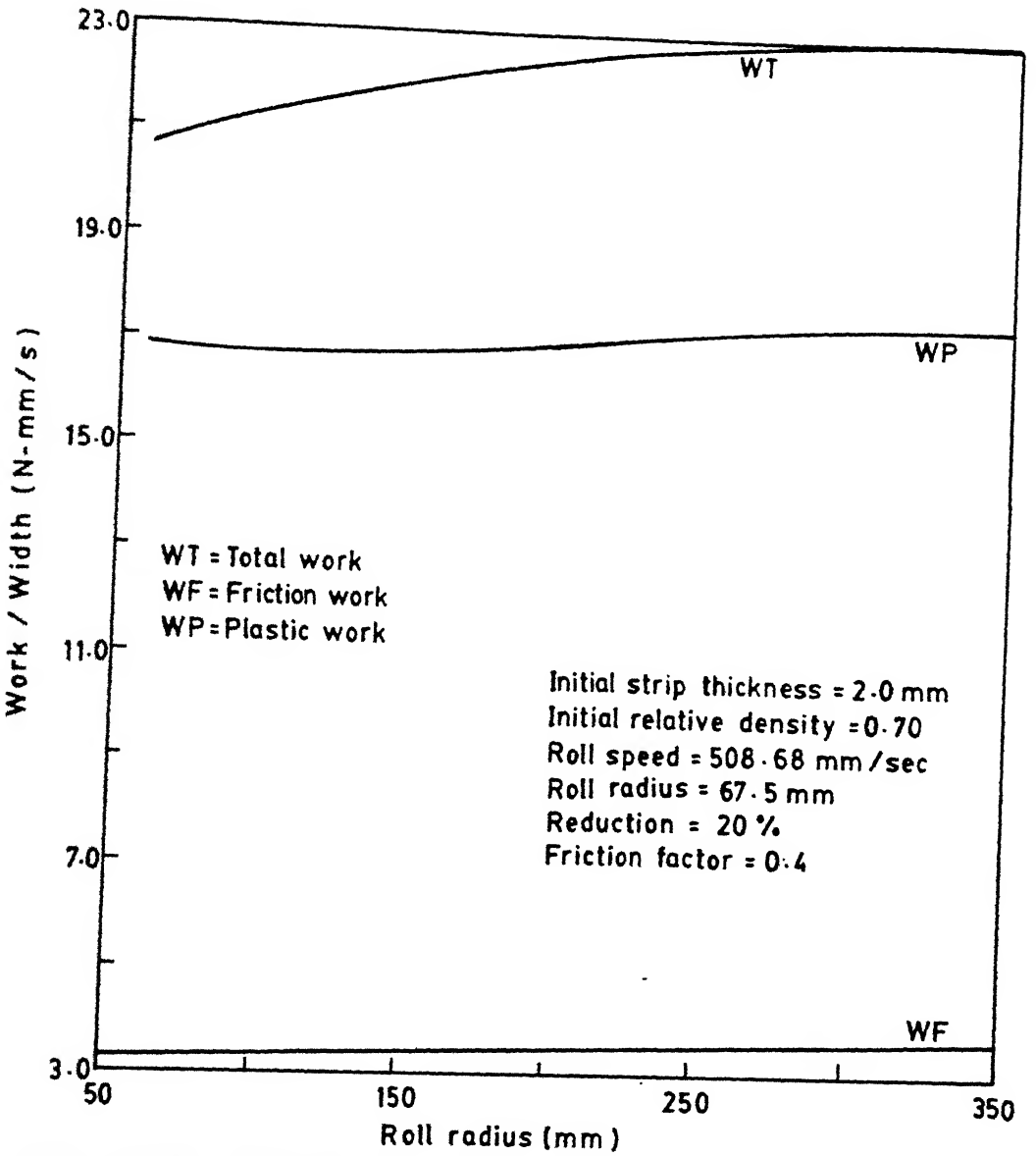

FIG. 5.10b EFFECT OF ROLL RADIUS ON WORK

It is evident that the densification behaviour is not significantly influenced by roll radius. This finding supports the conclusion derived from a microscopic view of a porous strip rolling, which indicates that the relative density is only a function of normalised contact area and slip between particles. Clearly both of these microscopic factors are not influenced by the distance travelled by the particles in the deformation zone. The exit relative density therefore is fairly insensitive to variation in roll radius.

The rolling work, on the other hand increases slightly with roll radius. This is contributed partly by friction work and partly by plastic work. The increase in friction work is due to larger arc of contact and that in the plastic work is because of the larger size of the plastic deformation zone. The results for variation of work and density with roll radius are given in Tables 5.5 and 5.6.

(iv) Roll Speed: It can be from Figures 5.11a and 5.11b that the densification is unaffected by roll speed, while power increases linearly with roll speed. The insensitivity of the densification to roll speed is again related to the microscopic features of porous metal rolling discussed in the previous section. The roll speed influences only the travel time of a particle through the roll gap and does not affect the interparticle contact area or slip between them. On the other hand, higher roll speed results in larger strain rates which in turn, leads to higher plastic deformation work. The backward slip also tends to increase with roll speed thereby causing

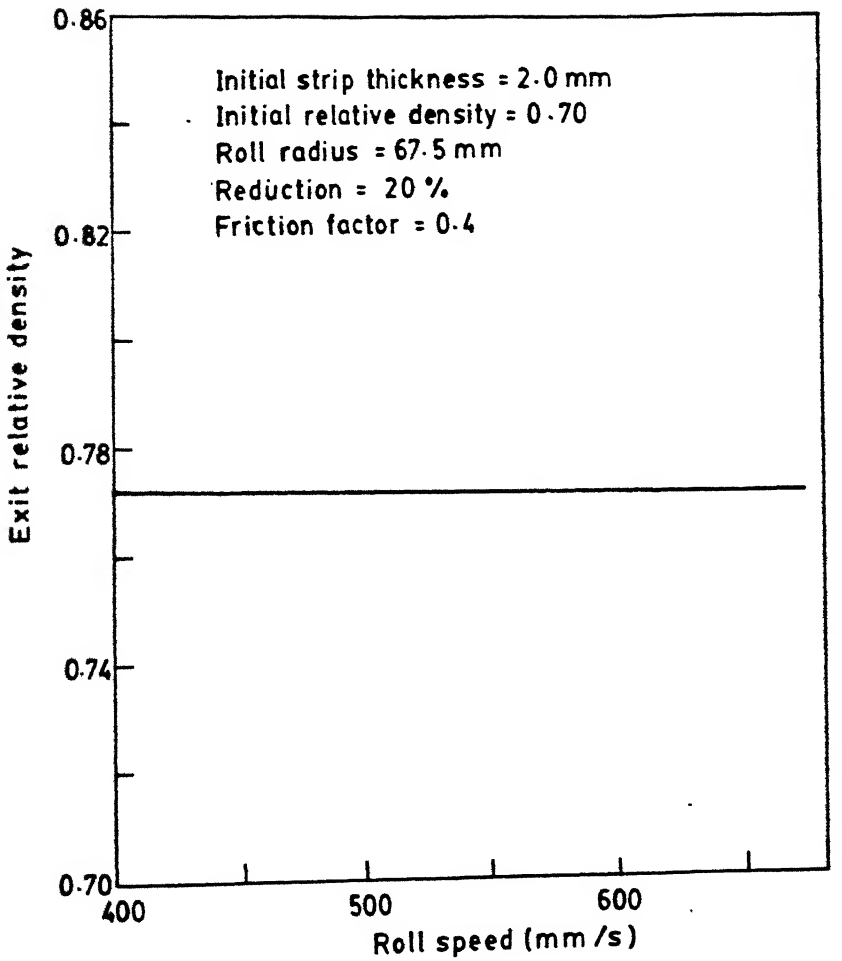

FIG. 5.11a EFFECT OF ROLL SPEED ON DENSIFICATION

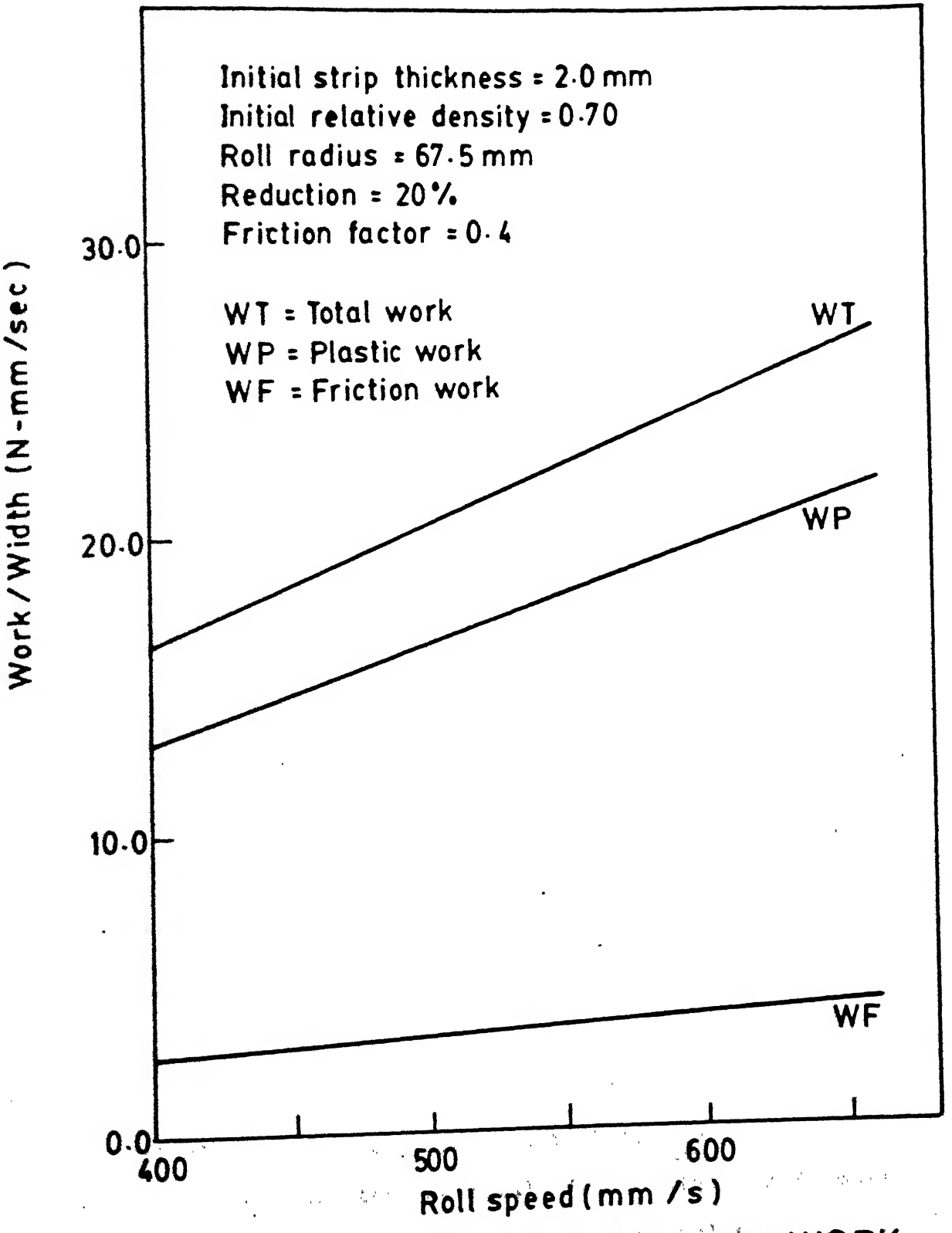

FIG. 5.11b EFFECT OF ROLL SPEED ON WORK

larger frictional dissipation. Of these two contributions, the change in plastic deformation power is more as compared to that of the friction power. These results are summarised in Tables 5.7 and 5.8.

(v) Strip Thickness: Figure 5.12a shows that larger densification occurs for smaller strip thickness. This can be attributed to the smoother entry of the strip between the rolls when it is thin. Consequently the entrance strip velocity is also larger.

The plastic work increases steeply with initial thickness of the strip (Figure 5.12b). This is obviously a consequence of larger material volume undergoing plastic deformation. The friction work also increases due to larger arc of contact and an increase in the magnitude of backward slip. The total rolling power, therefore, exhibits a sharp linear increase with initial slip thickness. The results are shown in Tables 5.9 and 5.10.

(vi) Initial Relative Density of the Strip: The incremental change in relative density from the entrance to the exit sections is shown in figure 5.13a as a function of the initial relative density. It is observed that the percentage increase in density decreases for higher initial relative density. This is because of larger contact area and smaller available void space for a larger initial relative density. Due to these two factors, the resistance offered by the material for further deformation increases resulting in a higher yield stress value. On the other hand the work per unit width increases with initial

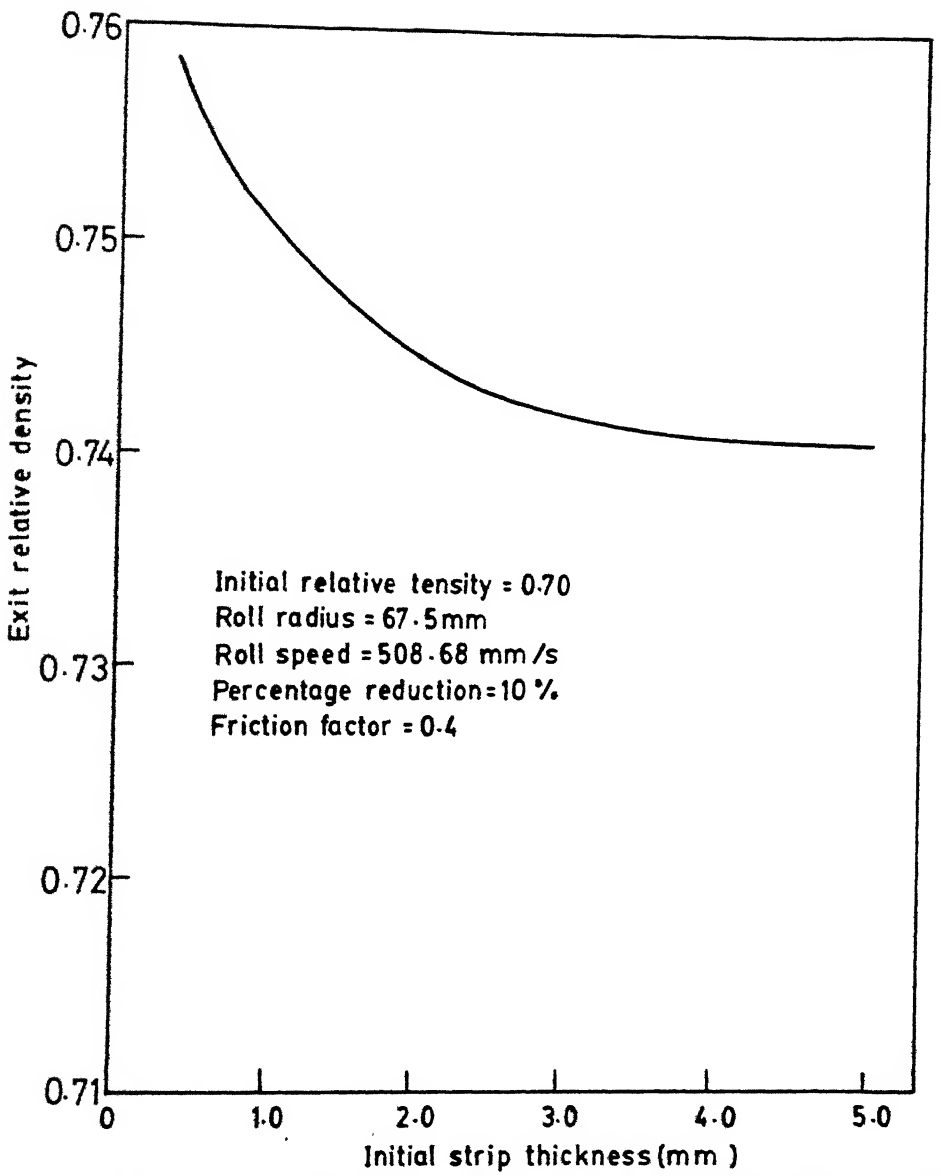

FIG. 5.12a EFFECT OF INITIAL STRIP THICKNESS ON DENSIFICATION

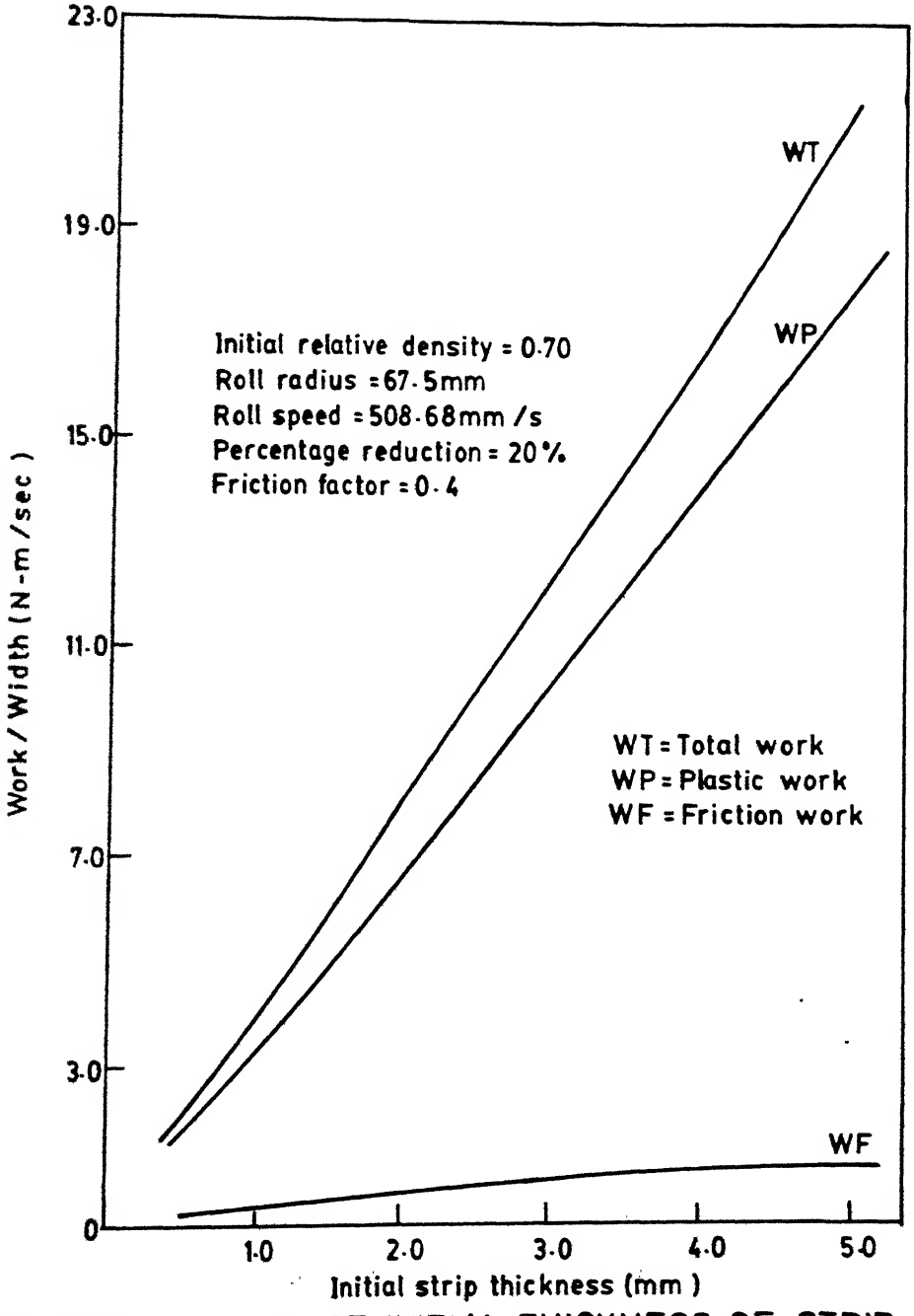

FIG. 5.12b EFFECT OF INITIAL THICKNESS OF STRIP ON WORK

relative density (Fig. 5.13b). Evidently the higher yield stress value increases the plastic work contribution. Also, because of larger actual contact area between the rolls and the porous strip at higher relative density as well as the higher yield stress value, the friction work will also increases. The results are shown in Tables 5.11 and 5.12.

5.4 COMPARISON BETWEEN THEORY AND EXPERIMENTS

For multipass cold densification rolling, the exit density and linear dimensions of the strip were measured after each pass. A theoretical study of multipass rolling with conditions similar to those of the experiments was also conducted, in order to validate the present theoretical approach and the numerical solution procedure. The measured and predicted exit relative density values after each pass have been plotted against the cumulative percentage reduction in Fig. (5.14a). It is observed that, there is reasonable agreement between theory and experiment, especially at higher cumulative percentage reductions. It is to be noted, however, that the actual friction factor (which has a significant effect upon densification) could not be measured and the value of 0.4 used for obtaining the results is only an assumed value. This value of friction factor seems to be a reasonable one for the present study in view of the fact that the roll srface was not smooth one and the rolling was performed under unlubricated condition. Also, there is a slight scatter in the experimental results which is represented by the difference between the actual measured points and the experimental curve fit (dotted curve). With the above two facts

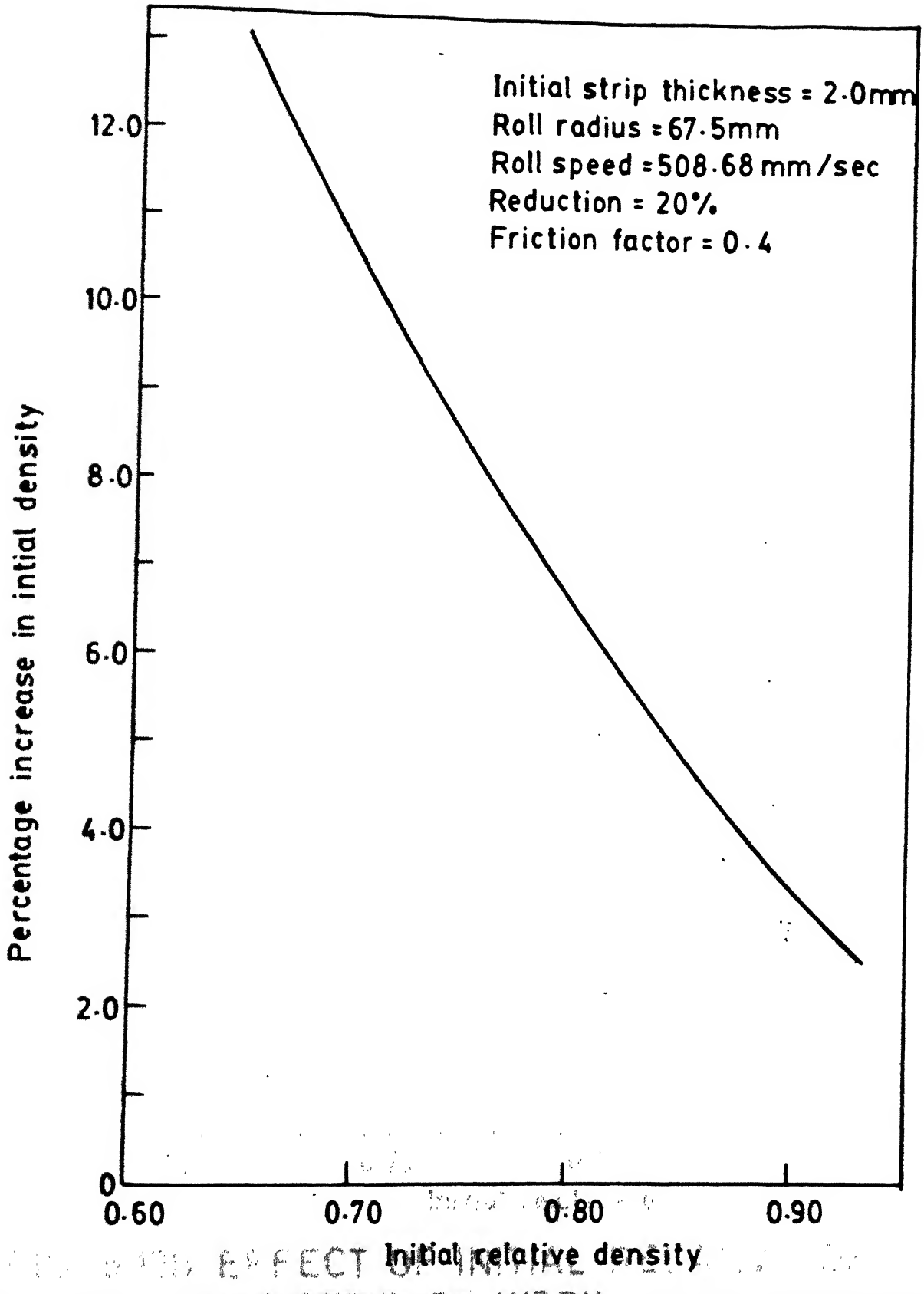

FIG. 5.13a EFFECT OF INITIAL RELATIVE DENSITY OF STRIP ON DENSIFICATION

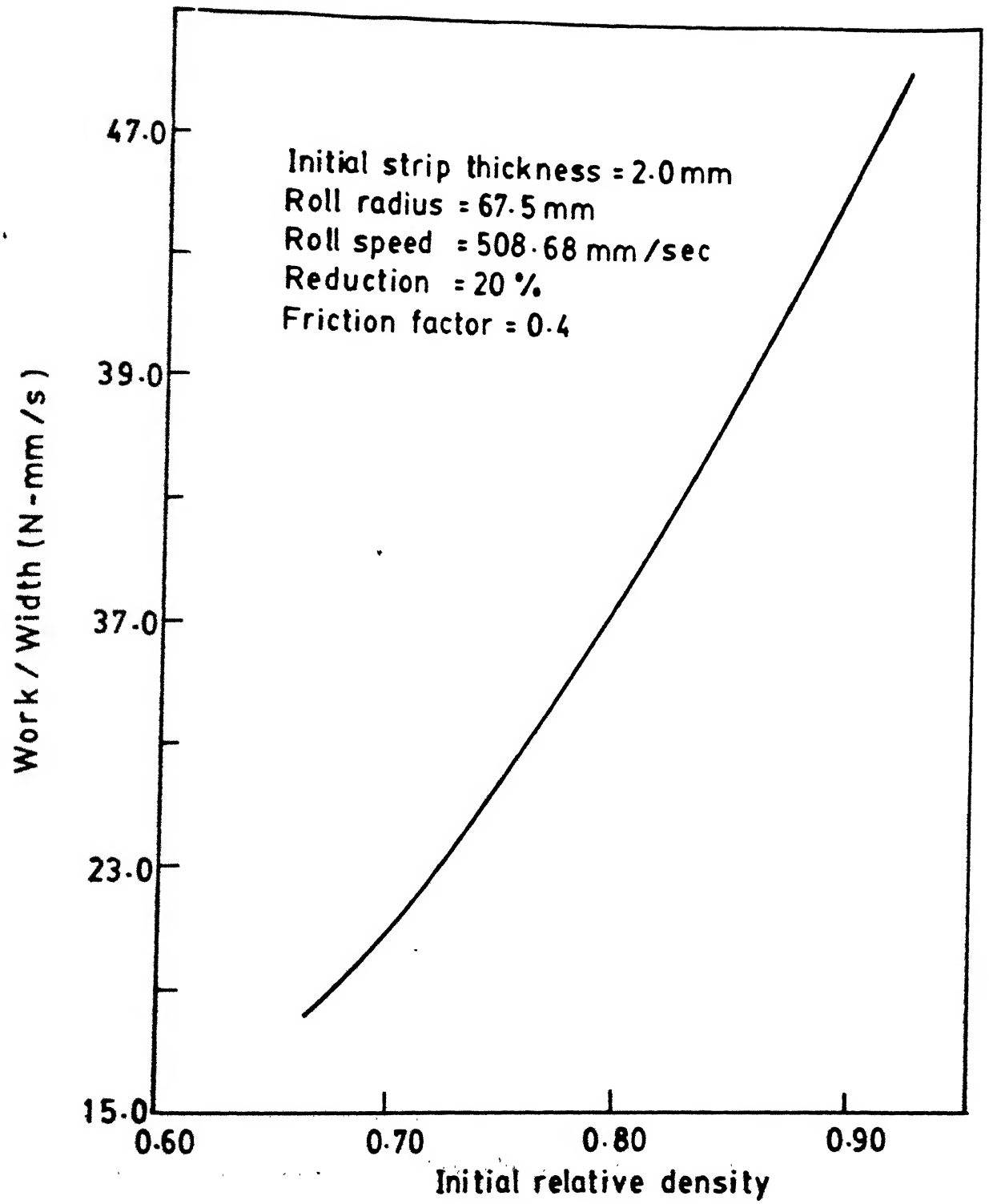

FIG. 5.13b EFFECT OF INITIAL RELATIVE DENSITY OF STRIP ON WORK

in mind, it can abe said that the agreement between theory and experiment is satisfactory for the prediction of exit relative density.

From the measured dimensions of the strip before and after each pass the true length and thickness strains have been calculated. These are plotted against each other in Figure 5.14b. The figure also includes the corresponding theoretical predictions and the curve for a fully dense material undergoing ideal plane strain rolling. It is observed that the ratio $\varepsilon_x / \varepsilon_y$ is less than one for porous strip, while it is equal to one for fully dense material. When the solid metal undergoes rolling deformation under plane strain condition, the true strains in both longitudinal and thickness directions are same. However, when a porous metal is rolled under plane strain situation, most of the deformation initially takes place in thickness direction which leads to closing of pores and thereby increasing the density of the strip. Very little elongation of the strip takes place. As the rolling continues further, a stage comes when the strip starts deforming both in thickness direction and longitudinal direction. When the porouus strip has been fully densified, then the true longitudinal strain (ε_x) Vs. tre thickness strain (ε_y) curve becomes parallel to that of the solid metal. A good correspondence is observed between the theoretical and experimental curves shown in the figure. The experimental curve lies slightly above that of the theoretical curve. The following reasons can be attributed for this behaviour: (i) the existence of strain in the third direction (ε_z) i.e. width direction for the experimental situation as can

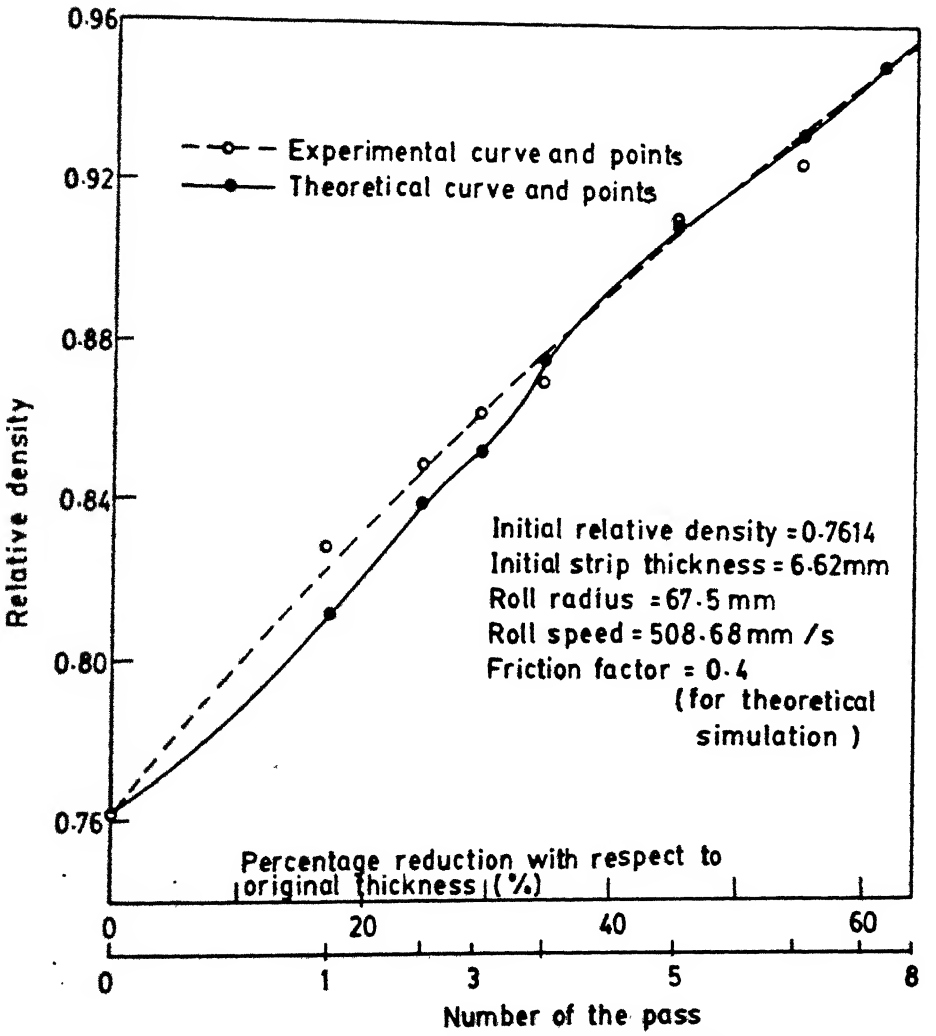

FIG. 5.14a COMPARISON BETWEEN EXPERIMENTAL AND THEORETICAL RESULTS FOR RELATIVE DENSITY FOR MULTI-PASS ROLLING OF SINTERED COPPER STRIP

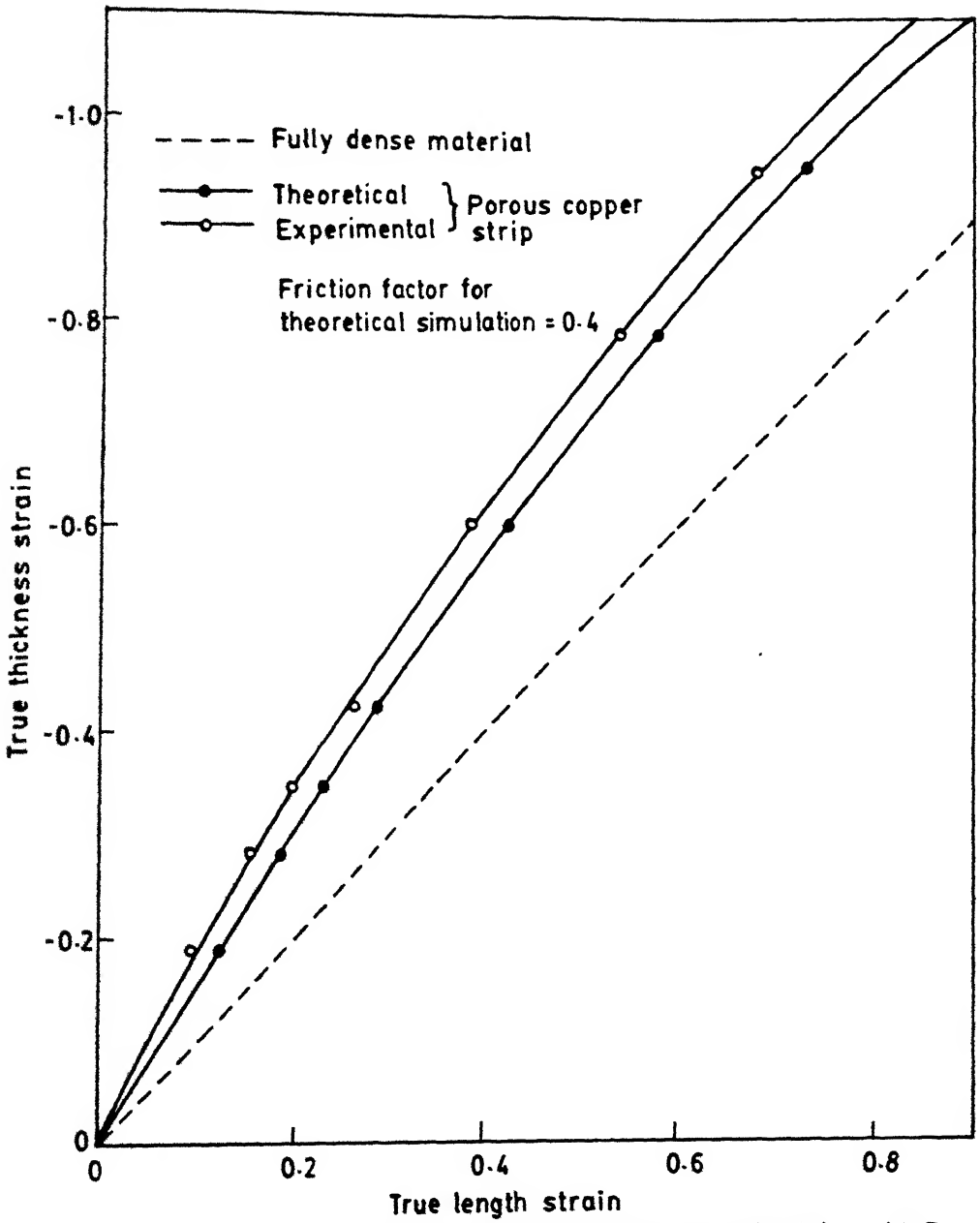

FIG. 5.14b COMPARISON BETWEEN EXPERIMENTAL AND THEORETICAL RESULTS FOR STRAINS FOR MULTI PASS ROLLING OF COPPER STRIP

be seen from Table 5.13 which leads to a reduction of the length strain (ε_{yy}); (ii) the actual friction factor under experimental conditions is not known and only an assumed value of 0.4 has been used in the theoretical calculations. The results are summarised in Tables 5.13 and 5.14.

5.5 ANALYSIS OF MULTI-PASS ROLLING WITH AND WITHOUT INTERMEDIATE ANNEALING:

Figure (5.15), the path followed by the density curve as a function of reduction has been shown for multi-pass cold rolling with intermediate annealing. It has been assumed, while predicting the results shown in the figure, that relative density is unaltered by intermediate annealing. It is evident from the figure that, the incremental change in relative density for a given percentage reduction decreases after each pass. This is because of the larger resistance to the deformation offered at higher material density, which was discussed earlier.

A comparison between the exit density predictions for multi-pass rolling with and without intermediate annealing is shown in Figure 5.16. It is clear from the figure that the theoretically predicted values of the relative density of the strip after cold densification rolling with and without intermediate annealing are approximately same. A similar observation has been found experimentally while hot rolling sponge iron strip of density 1.9 gm/c.c. at 850^{0}C and 1130^{0}C. It was observed that the density is independent of hot rolling temperature, while the ductility of the strip hot rolled at 1130^{0}C was higher than that of hot rolled at 850^{0}C [19]. A

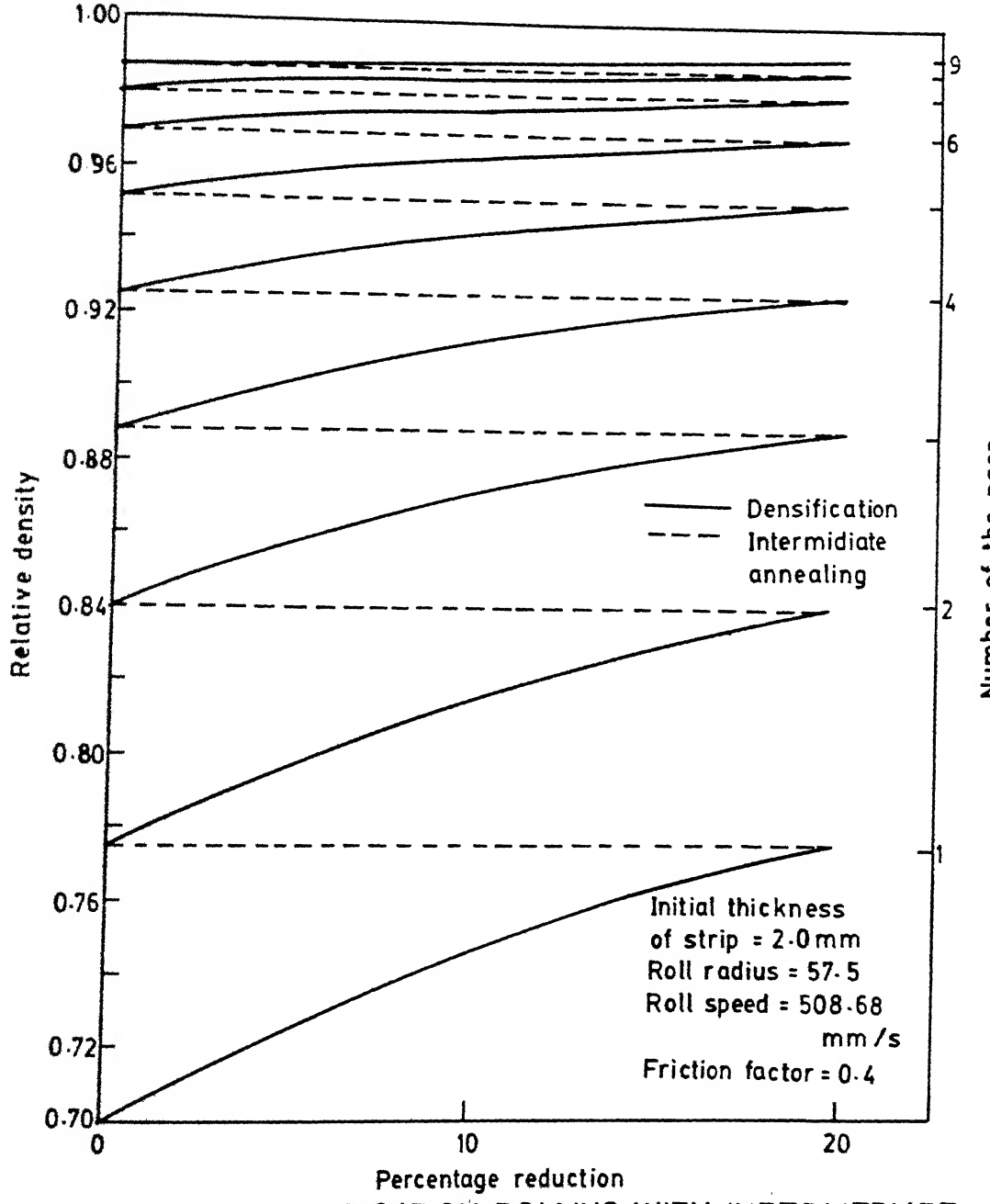

FIG. 5.15 COLD DENSIFICATION ROLLING WITH INTERMEDIATE ANNEALING.

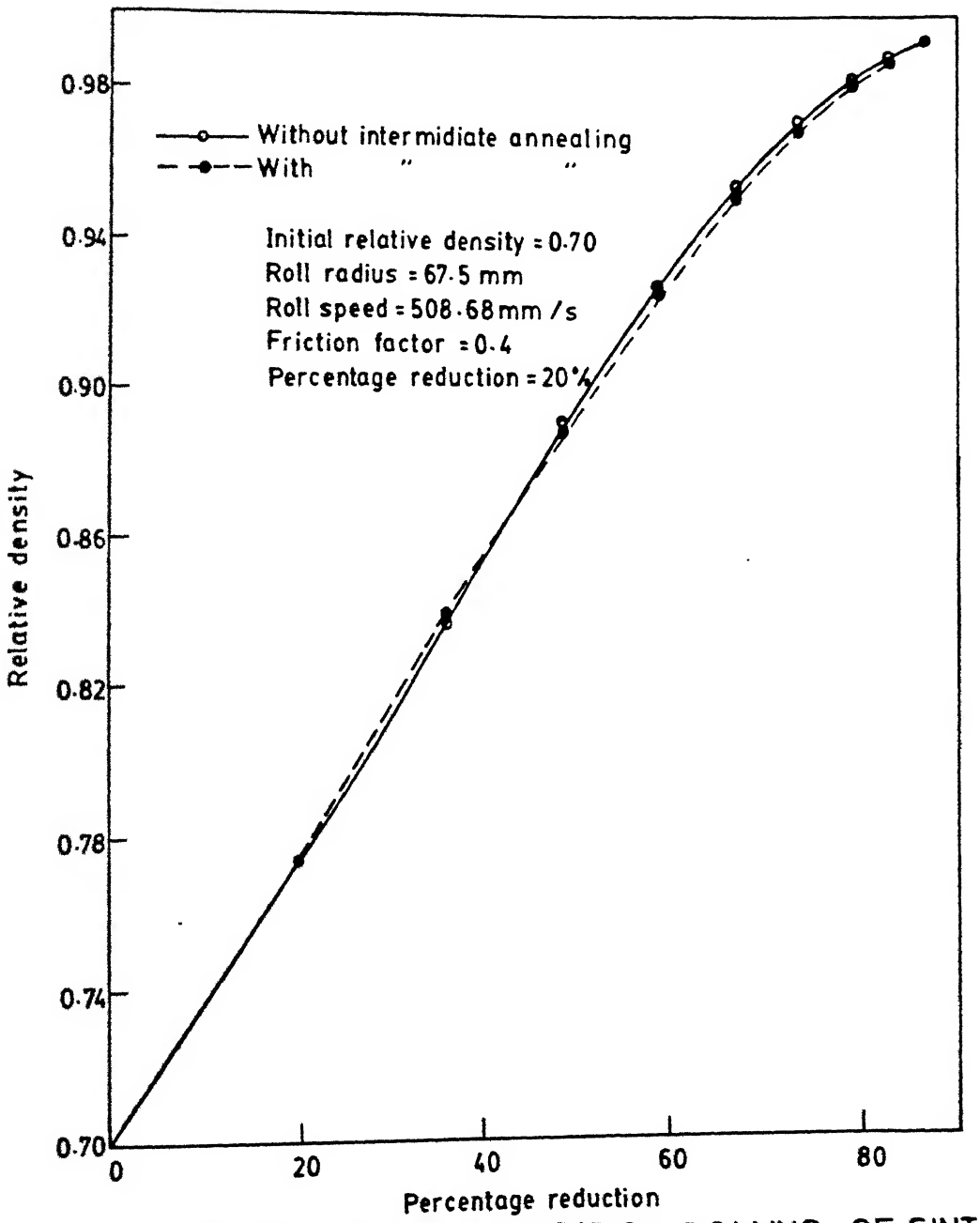

FIG. 5.16 MULTI-PASS COLD DENSIFICATION ROLLING OF SINTERED COPPER STRIP WITH AND WITHOUT ANNEALING

similar trend was also found while cold rolling a copper strip with and without annealing [20]. From this present analysis it seems that the densification of porous copper strip is not affected by the mode of cold rolling , i.e. cold rolling with intermediate annealing or cold rolling without intermediate annealing. However, from the point of view of the properties achieved in the rolled strip the mode of rolling is an important factor.

A comparison of the incremental work for each pass for rolling with and without intermediate annealing is shown in Figure 5.17. Although, densification is not significantly affected by annealing it is seen that work almost increases by factor of two, if annealing is not performed. This difference is because of work hardening effect. It is also observed that the work per pass decreases at later stages of the multi-pass rolling process. This can be attributed to the reduction in the strip thickness as evident from Fig. 5.12b. The results for cold densification rolling with and without intermediate annealing are shown in Tables 5.15 and 5.16 respectively.

CHAPTER VI

CONCLUSIONS

6.1 CONCLUSIONS OF THE PRESENT STUDY

(i) The simplified upper bound technique based on streamline approach is shown to be successful for the prediction of density and velocity fields and other parameters of interest in rolling.

(ii) It is demonstrated that, there exists a global minimum value for rolling power which corresponds to proper densification and metal flow rate.

(iii) The velocity, density and strain distributions indicate that compression is essentially homogeneous.

(iv) The backward and forward slip and the roll pressure increase with percentage reduction. The neutral point occurs closer to the exit side than to the entry for all reductions. It is seen that the roll pressure is much smaller as compared that of a solid material under similar rolling conditions.

(v) Exit relative density increases with friction factor, especially at higher percentage reductions. The rolling power also increases with friction factor. With percentage reduction density reaches a maximum with other conditions remaining the same. The power, on the other hand increases with reduction also. The roll speed and roll radius have insignificant effect upon densification. The rolling power was found to increase linearly with roll speed. For a higher initial strip density, the

densification is less and rolling power is more. It also be seen that thinner strips experience greater densification.

(vi) The comparison between theoretical predictions and the experimental measurements shows reasonable agreement for densification as well as strains.

(vii) The densification trend remains same for multi-pass rolling with and without intermediate annealing. The work on the other hand is much smaller for annealed strip.

SCOPE FOR FUTURE WORK

(i) A detailed experimental study can be conducted to verify the effects of various rolling parameters upon densification.

(ii) The present results can be investigated by using more accurate FEM approach which takes into account realistic friction conditions.

(iii) The reason for the non-existence of global maximum of power consumed for higher percentage reduction in single pass rolling needs to be investigaed.

(iv) The study can be extended to hot densification rolling and also to include features such as front and back tension in cold rolling.

ABLE 5.1 : The Global Minimuum of Power Consumed for a given Set of Rolling Conditions

	u_1 = 435			u_2 = 445		
	WF	WP	WT	WF	WP	WT
.4	3.415	16.927	21.126	3.753	17.316	21.871
.5	3.322	16.769	20.87	3.565	17.155	21.522
6	3.253	16.625	20.66	3.396	17.007	21.205
.7	3.219	16.494	20.498	3.241	16.874	20.917
.8	3.226	16.377	20.38	3.110	16.754	20.66
.9	3.284	16.274	20.34	2.999	16.648	20.449
.0	3.413	16.184	20.382	2.916	16.556	20.275
.1	3.670	16.109	20.563	2.869	16.479	20.150
.2	4.034	16.047	20.865	2.859	16.416	20.078
.3	4.400	16.000	21.183	2.899	16.368	20.069
.4	4.767	15.966	21.517	3.006	16.333	20.01
.5	5.136	15.947	21.867	3.221	16.314	20.33
.6	5.507	15.942	22.233	3.581	16.308	20.69
.7	5.880	15.951	22.615	3.943	16.319	21.06
.8	6.255	15.974	23.013	4.307	16.341	21.450
.9	6.633	16.010	23.428	4.673	16.378	21.85
.0	7.013	16.061	23.858	5.041	16.430	22.27
.1	7.395	16.124	24.304	5.411	16.495	22.70
.2	7.780	16.202	24.766	5.783	16.574	23.16
.3	8.168	16.292	25.244	6.158	16.667	23.62
.4	8.558	16.395	25.737	6.535	16.772	24.10
.5	8.951	16.451	26.247	6.914	16.891	24.60
.6	9.346	16.639	26.670	7.296	17.022	25.12
.7	9.745	16.780	27.309	7.681	17.166	25.64

2.8	10.146	16.932	27.862	8.067	17.321	26.19
2.9	10.550	17.096	28.430	8.457	17.489	26.74
3.0	10.957	17.271	29.012	8.853	17.668	27.31

b	u_1 = 460			u_2 = 475		
	WF	WP	WT	WF	WP	WT
0.4	4.943	17.899	23.671	6.739	18.483	26.07
0.5	4.680	17.733	23.242	6.446	18.311	25.61
0.6	4.424	17.581	22.834	6.152	18.154	25.16
0.7	4.179	17.442	22.451	5.859	18.011	24.72
0.8	3.936	17.318	22.084	5.571	17.883	24.31
0.9	3.705	17.209	21.743	5.285	17.770	23.91
1.0	3.487	17.114	21.430	5.005	17.673	23.53
1.1	3.227	17.035	21.140	4.727	17.590	23.17
1.2	3.083	16.969	20.882	4.453	17.523	22.83
1.3	2.902	16.919	20.651	4.184	17.471	22.51
1.4	2.743	16.884	20.456	3.924	17.435	22.21
1.5	2.601	16.864	20.294	3.668	17.414	21.93
1.6	2.487	16.858	20.174	3.421	17.408	21.68
1.7	2.404	16.868	20.101	3.185	17.418	21.45
1.8	2.355	16.892	20.076	2.959	17.443	21.25
1.9	2.349	16.930	20.109	2.747	17.483	21.08
2.0	2.398	16.985	20.211	2.548	17.537	20.94
2.1	2.523	17.051	20.404	2.368	17.607	20.83
2.2	2.788	17.133	20.750	2.210	17.691	20.75
2.3	3.144	17.228	21.202	2.075	17.790	20.72
2.4	3.501	17.338	21.668	1.970	17.903	20.72

2.5	3.860	17.460	22.149	1.900	18.029	20.78
2.6	4.221	17.596	22.646	1.872	18.170	20.89
2.7	4.584	17.744	23.158	1.894	18.323	21.07
2.8	4.949	17.905	23.684	1.986	18.489	21.33
2.9	5.317	18.078	24.225	2.180	18.668	21.70
3.0	5.686	18.263	24.779	2.524	18.859	22.23

b	u_1 = 453		
	WF	WP	WT
0.4	4.297	17.627	22.741
0.5	4.064	17.463	22.344
0.6	3.844	17.313	21.974
0.7	3.630	17.177	21.624
0.8	3.431	17.055	21.303
0.9	3.243	16.947	21.007
1.0	3.075	16.854	20.745
1.1	2.923	16.775	20.515
1.2	2.796	16.711	20.324
1.3	2.690	16.662	20.169
1.4	2.618	16.627	20.062
1.5	2.581	16.607	20.005
1.55	2.580	16.603	19.999
1.6	2.290	16.602	20.008
1.7	2.656	16.611	20.083
1.8	2.803	16.635	20.254
1.9	3.105	16.673	20.594
2.0	3.463	16.725	21.005

2.1	3.824	16.792	21.432
2.2	4.186	16.872	21.875
2.3	4.550	16.966	22.333
2.4	4.917	17.074	22.807
2.5	5.285	17.194	23.296
2.6	5.656	17.328	23.801
2.7	6.029	17.474	24.320
2.8	6.404	17.633	24.854
2.9	6.782	17.803	25.402
3.0	7.162	17.985	25.964

Table 5.2 : Effect of Friction Factor on Exit Relative Density

Percentage Reduction %	Friction Factor (m)			
	0.3	0.4	0.5	0.6
	Exit Relative Density (s)			
5	0.7241	0.7250	0.7259	0.7267
10	0.7443	0.7447	0.7489	0.7508
15	0.7564	0.7635	0.7682	0.7737
20	0.7673	0.7744	0.7782	0.7832

Table 5.3 : Effect of Friction Factor on Work

Percentage Reduction %	Friction Factor							
	0.3		0.4		0.5		0.6	
	Work/Width (N-mm/s)							
	WF	WT	WF	WT	WF	WT	WF	WT
5	0.109	3.512	0.135	3.548	0.157	3.582	0.175	3.613
10	0.479	7.878	0.636	8.038	0.695	8.180	0.786	8.315
15	1.306	13.382	1.560	13.790	1.816	14.175	2.010	14.541
20	2.580	19.999	3.218	20.844	3.911	21.643	4.506	22.412

Table 5.4 : Effect of Percentage Reduction on Exit Relative Density for Different Friction Factors

Percentage Reduction (%)	Friction Factor (m)			
	0.3	0.4	0.5	0.6
	Exit Relative Density (ρ)			
5	0.7241	0.7250	0.7259	0.7267
10	0.7443	0.7447	0.7489	0.7508
15	0.7564	0.7635	0.7682	0.7737
20	0.7673	0.7744	0.7782	0.7832
25	0.7677	0.7763	0.7797	0.7825
30	0.7543	0.7628	0.7761	0.7810

TABLE 5.5 : Effect of Roll Radius on Exit Relative Density

Sl.No.	Roll Radius (mm)	Exit Relative Density (ρ)
1	67.50	0.7744
2	80.00	0.7744
3	90.00	0.7744
4	100.00	0.7744
5	150.00	0.7817
6	200.00	0.7892
7	350.00	0.7999

TABLE 5.6 : Effect of Roll Radius on Work

Sl.No.	Roll Radius (mm)	Work/Width (N-mm/s)		
		WF	WP	WT
1	67.50	3.218	16.800	20.844
2	80.00	3.516	16.742	21.017
3	90.00	3.737	16.707	21.159
4	100.00	3.946	16.678	21.303
5	150.00	4.598	16.796	21.952
6	200.00	4.985	17.051	22.525
7	350.00	6.057	17.494	23.925

TABLE 5.7 : Effect of Roll Speed on Exit Relative Density

Sl.No.	Roll Speed (mm/s)	Exit Relative Density (ρ)
1	400.00	0.7720
2	508.68	0.7744
3	525.00	0.77126
4	550.00	0.77126
5	650.00	0.77126
6	800.00	0.77126

TABLE 5.8 : Effect of Roll Speed on Work

Sl.No.	Roll Speed (mm/s)	Work/Width (N-mm/s)		
		WF	WP	WT
1	400.00	2.581	13.161	16.388
2	508.68	3.218	16.800	20.844
3	525.00	3.437	17.228	21.512
4	550.00	3.576	18.071	22.535
5	650.00	4.211	21.370	26.632
6	800.00	5.205	26.282	32.779

Table 5.9 : Effect of Initial Strip Thickness on Exit Relative Density

Sl.No.	Initial Strip Thickness (mm)	Exit Relative Density (ρ)
1	5.0	0.7406
2	4.0	0.7406
3	3.0	0.7419
4	2.0	0.7447
5	0.5	0.7571

Table 5.10 : Effect of Initial Strip Thickness on Work

Sl.No.	Initial Strip Thickness (mm)	Work/Width (N-mm/s)		
		WP	WF	WT
1	5.0	17.831	1.095	21.380
2	4.0	14.008	0.994	16.758
3	3.0	10.327	0.837	12.306
4	2.0	6.761	0.636	8.038
5	0.5	1.706	0.214	2.000

Table 5.11 : Effect of Initial Relative Density of Strip on Densification

Sl.No.	Initial Relative Density of Strip (ρ_1)	Exit Relative Density (ρ)	Percentage Increase In Relative Density (%)
1	0.70	0.7744	10.630
2	0.80	0.8566	7.084
3	0.90	0.9299	3.322

Table 5.12 : Effect of Initial Relative Density of Strip on Work

Sl.No.	Initial Relative Density of Strip (ρ_1)	Work/Width (N-mm/s)		
		WP	WF	WT
1	0.70	16.800	3.218	20.844
2	0.80	24.861	5.725	31.706
3	0.90	35.122	9.526	46.102

TABLE 5.13 : Experimental Results for Multi-pass Rolling of Sintered Copper Strip

Number of the pass	Percentage Thickness reduction with respect to original thikness	Length l(cm)	Width W(cm)	Thickness t(cm)	Relative Density (ρ)	True length strain ε_x	True thick-ness strain ε_y	True width strain ε_z
1	17.09	7.350	4.600	0.5488	0.8281	0.09259	-0.1875	0.01092
2	24.6	7.800	4.653	0.4990	0.8484	0.1520	-0.2826	0.02238
3	29.116	8.143	4.665	0.4692	0.862	0.1951	0.3441	0.02496
4	34.5	8.700	4.686	0.4332	0.869	0.2612	-0.4239	0.02945
5	45.2	9.850	4.720	0.3627	0.9111	0.3853	-0.6015	0.03668
6	54.83	11.525	4.777	0.3017	0.9249	0.5425	-0.7857	0.04868
7	61.4	13.200	4.808	0.255	0.9494	0.6781	-0.9540	0.05515

Table 5.14 : Theoretical Results for Multi-pass Rolling of Sintered Copper Strip

Number of the Pass	Percentage Thickness Reduction with Respect to Original Thickness (%)	Relative Density (ρ)	Length Strain (ε_x)	Thickness Strain (ε_y)	Width Strain (ε_z)
1	17.09	0.8095	0.12613	-0.18741	0
2	24.6	0.8393	0.1854	-0.2826	0
3	29.116	0.8506	0.2335	-0.3440	0
4	34.5	0.8748	0.2852	-0.4238	0
5	45.2	0.9079	0.4256	-0.6013	0
6	54.83	0.9318	0.5837	-0.7855	0
7	61.4	0.9509	0.7316	-0.9536	0

Table 5.15: Multi-pass Cold Densification Rolling with Intermediate Annealing

Sl.No.	Percentage Reduction with respect to original thickness (%)	Optimal Entrance Velocity (u_o) (mm/sec)	Exponent (b)	Relative Density (ρ)	Work/Width (N-mm/s)			
					WP	WF	WS	WT
1	20.00	458	1.73	0.7744	16.800	3.218	0.825	20.844
2	36.00	450	1.88	0.8392	18.077	4.397	0.746	23.221
3	48.80	440	1.84	0.8873	18.216	5.632	0.638	24.488
4	59.04	435	2.02	0.9251	17.218	6.297	0.519	24.034
5	67.23	430	2.02	0.9509	15.583	6.705	0.407	22.695
6	73.78	428	2.18	0.9692	13.582	6.661	0.331	20.554
7	79.03	425	1.98	0.9800	11.494	6.468	0.231	18.195
8	83.22	424	2.05	0.9873	9.534	6.043	0.169	15.748
9	86.57	423	1.70	0.9917	7.820	5.577	0.123	13.521

Table 5.16 : Multi-pass Cold Densification Rolling without Intermediate Annealing

Sl.No.	Percentage Reduction with respect to original thickness (%)	Optimal Entrance Velocity (u_o) (mm/sec)	Exponent (b)	Relative Density (ρ)	Work/Width (N-mm/s)			
					WP	WF	WS	WT
1	20.00	458	1.73	0.7744	16.800	3.218	0.825	20.844
2	36.00	450	1.80	0.8368	25.075	6.405	1.779	33.260
3	48.80	445	2.03	0.8896	29.418	9.100	1.941	40.460
4	59.04	438	2.10	0.9279	31.088	11.724	1.851	44.663
5	67.23	433	2.22	0.9548	30.451	13.562	1.626	45.640
6	73.78	430	2.20	0.9718	28.338	14.578	1.354	44.272
7	79.03	429	2.42	0.9834	25.399	14.766	1.085	41.251
8	83.22	427	2.12	0.9896	22.147	14.635	0.845	37.629
9	86.57	426	1.62	0.9927	18.928	14.084	0.645	33.658

REFERENCES

[1] I. Davis, W.M. Gibbon, and A.G. Harris, "Thin strips from powders", Powder Metall. 11, 295 (1968).

[2] H.A. Kuhn and C.L. Downey, "Deformation characteristics and plasticity theory of sintered powder materials", Int. J. Powder Mater. 7, 5 (1971).

[3] R.J. Green, "A plasticity theory for poros metals", Int. J. Mech. Sci. 14, 215 (1972).

[4] S. Shima and M. Oyane, "Plasticity theory for porous metals", Int. J. Mech. Sci. 18, 285 (1976).

[5] B. Avitzur, "An Upper-Bound Approach to cold-strip rolling", Journal of Engineering for Industry. 31 (1964).

[6] B. Avitzur, W. Gordon and S. Talbert, "Analysis of strip rolling by the Upper Bound Approach", Transactions of the ASME. 109, 338 (1987).

[7] S.S. Rao and Alok Kumar, "Finite element analysis of cold strip rolling", Int. J. Mach. Tool Des. Res. 17, 159 (1977).

[8] C. Liu, P. Hartley, C.E.N. Sturgess and G.W. Rowe, "Elastic-plastic element modelling of cold rolling of strip", Int. J. Mech. Sci. 27, 531 (1985).

[9] C. Liu, P. Hartley, C.E.N. Sturgess and G.W. Rowe, "Simulation of cold rolling of strip using an elastic-plastic finite element technique", Int. J. Mech. Sci. 27, 829 (1985).

[10] K. Osakada, J. Nakano and K. Mori, "Finite element method for rigid-plastic analysis of metal forming - formulation

for finite deformation", Int. J. Mech. Sci. 24, 459 (1982).

[11] K. Mori and K. Osakada, "Simulation of three-dimensional deformation in rolling by the finite element method", Int. J. Mech. Sci. 26, 515 (1984).

[12] Ya. Tarnovskii, A.A. Pozdeyev and V.B. Lyashkov, Deformation of metals during rolling.

[13] Betzalel Avitzur, Handbook of Metal Forming Processes.

[14] Johnson, W., and Mellor, P.B., Engineering Plasticity.

[15] K. Mori and K. Osakada, "Analysis of the forming process of sintered powder metal by a rigid-plastic finite-element method", Int. J. Mech. Sci. 29, 229 (1987).

[16] K. Mori, S. Shima and K. Osakada, "Finite element method for analysis of plastic deformation of porous metals", Bull. JSME 23, 516 (1980).

[17] K. Mori, S. Shima and K. Osakada, "Analysis of free forging by Rigid plastic finite element method based on the plasticity equation for porous metals", Bull. JSME. 23, 523 (1980).

[18] Dr. S. Bhargava, communicated to metallurgical transaction.

[19] R.K. Dube and A. R. E. Singer, "Reduction, sintering and hot rolling of preformed iron oxide superconcentrate strip", Metal Technology, 5 (7), 270 (1978).

[20] S. Bhargava and R.K. Dube, "Cold densification rolling of porous copper strip obtained directly from cuprous preform", Mater. Sci. Technol. 4, 267 (1988).

```
C        ^^^^^^^^^^^^^^^^^^^^^^^^^^^^^^^^^^^^^^^^^^^^^^^^^^^^^^^^^^^^^^^^
C        ****************************************************************
C        ****************************************************************
C        PROGRAMME TO EVALUATE STRAIN,DENSITY AND VELOCITY DISTRIBUTIONS
C        IN THE DEFORMATION ZONE FOR PLANE STRAIN ROLLING OF POROUS METAL
C        STRIP USING UPPER BOUND TECHNIQUE
C        ****************************************************************
C        ****************************************************************
C        ^^^^^^^^^^^^^^^^^^^^^^^^^^^^^^^^^^^^^^^^^^^^^^^^^^^^^^^^^^^^^^^^

C        Y1=STRIP THICKNESS AT THE ENTRY SECTION
C        UO=STRIP VELOCITY AT THE ENTRY
C        U=ROLL SPEED
C        FR=FRICTION FACTOR
C        S=EQUIVALENT STRESS FOR THE GIVEN MATERIAL
C        Y2OLD=STRIP THICKNESS AT THE EXIT
C        EPS=CONVERGENCE CRITERION
C        NU=NUMBER OF ITERATIONS
C        EL=LENTH OF CONTACT
C        WORKI=TOTAL WORK FUNCTION
C        RHOO=DENSITY AT THE ENTRY
C        XSI=STREAM LINE COORDINATE
C        R=RADIUS OF THE CIRCLE
C        RA=RADIUS OF THE ROLL
C        RHO=DENSITY IN THE DEFORMATION ZONE
C        U=AXIAL VELOCITY
C        V=TRANSVERSE VELOCITY
C        X=X-CORDINATE
C        Y=Y-CORDINATE
C        SI=MASS FLOW RATE
C        XNODE=X-CORDINATE OF THE NODE
C        YNODE=Y-CORDINATE OF THE NODE
C        RHONOD=DENSITY AT THE NODE
C        UNODE=AXIAL VELOCITY OF THE NODE
C        VNODE=TRANSVERSE VELOCITY OF THE NODE
C        V1=DERATIVE OF THE STREAM FUNCTION WITH RESPECT TO Y-CORDINATE
C        V2=DERATIVE OF THE STREAM FUNCTION WITH RESPECT TO X-CORDINARE
C        FRICT=WORK LOSS DUE TO FRICTION
C        DISCT=WORK LOSS AT THE VELOCITY DISCONTINUTY
C        DEFORM=WORK REQUIRED FOR PLASTIC DEFORMATION
C        FF=DERATIVE OF WORK FUNCTION WITH RESPECT TO Y2OLD
C        DFF=SECOND DERATIVE OF WORK FUNCTION WITH RESPECT TO Y2OLD

         IMPLICIT REAL * 8(A-H,O-Z)

         RA=67.5
         Y1=1.0
         Y2=0.80
         FR=0.4
         UO=450.00
         UX=508.68
         RHOO=0.70

         EPS=0.0001
         BMAX=8.0
         DELB=0.0001
         DB=0.1
         B1=0.1
         NUM=50

         CALL WORK(RHOO,Y1,UO,Y2,FR,RA,UX,B1,WORKI)
         WORKI1=WORKI
         B11=B1+DELB
         CALL WORK(RHOO,Y1,UO,Y2,FR,RA,UX,B11,WORKI)
         WORKI11=WORKI
```

```
      B12=B1-DELB
      CALL WORK(RHOO,Y1,UO,Y2,FR,RA,UX,B12,WORKI)
      WORKI12=WORKI
      FF1=(WORKI11-WORKI12)/(2.0*DELB)
      DFF1=(WORKI11+WORKI12-(2.0*WORKI1))/(DELB**2)

629   B2=B1+DB
      CALL WORK(RHOO,Y1,UO,Y2,FR,RA,UX,B2,WORKI)
      WORKI2=WORKI
      B21=B2+DELB
      CALL WORK(RHOO,Y1,UO,Y2,FR,RA,UX,B21,WORKI)
      WORKI21=WORKI
      B22=B2-DELB
      CALL WORK(RHOO,Y1,UO,Y2,FR,RA,UX,B22,WORKI)
      WORKI22=WORKI
      FF2=(WORKI21-WORKI22)/(2.0*DELB)
      DFF2=(WORKI21+WORKI22-(2.0*WORKI2))/(DELB**2)
      IF (FF1*FF2)10,20,30

30    B1=B2
      FF1=FF2
      IF(B2.GT.BMAX)GO TO 9243
      GO TO 629
9243  TYPE *,'QUEST'
      GO TO 2456

10    PAUSE'IN TO ITERATION'

      BOLD=B1
      FF=FF1
      DFF=DFF1
      ITERATION=1
60    BNEW=BOLD-(FF/DFF)
      CALL WORK(RHOO,Y1,UO,Y2,FR,RA,UX,BNEW,WORKI)
      WORKIN=WORKI
      BX1=BNEW+DELB
      CALL WORK(RHOO,Y1,UO,Y2,FR,RA,UX,BX1,WORKI)
      WORKIM=WORKI
      BX2=BNEW-DELB
      CALL WORK(RHOO,Y1,UO,Y2,FR,RA,UX,BX2,WORKI)
      WORKIL=WORKI
      FF=(WORKIM-WORKIL)/(2.0*DELB)
      DFF=(WORKIM+WORKIL-(2.0*WORKIN))/(DELB**2)
      WRITE(5,*)'ITERATION=',ITERATION
      IF(DABS(FF).LE.EPS)STOP
C     IF(DFF.LT.0.0)STOP
      ITERATION=ITERATION+1
      IF(ITERATION.GE.NUM)STOP
      BOLD=BNEW
      GO TO 60

20    BNEW=B2

2456  STOP
      END

C     XXXXXXXXXXXXXXXXXXXXXXXXXXXXXXXXXXXXXXXXXXXXXXXXXXXXXXXXXXXXXXXXXXXXXXXXXXXXXXX
      SUBROUTINE WORK(RHOO,Y1,UO,Y2,FR,RA,UX,B,WORKI)
C     XXXXXXXXXXXXXXXXXXXXXXXXXXXXXXXXXXXXXXXXXXXXXXXXXXXXXXXXXXXXXXXXXXXXXXXXXXXXXXX
C     SUBROUTINE TO CALCULATE DENSITY,VELOCITY FIELD IN THE DEFORMATION
C     ZONE AND WORK REQUIRED FOR PLASTIC DEFORMATION FOR STRIP ROLLING
C     UNDER PLANE STRAIN
C
C     ---------------------------------------
C     --------   EXTERNAL SUBROUTINE  --------
C     -    SHAPE4                           -
```

```
C       -   DJACOB                              -
C       -   DRIVES                              -
C       -   PLASTIC                             -
C       ----------------------------------------

        IMPLICIT REAL * 8(A-H,O-Z)

        DIMENSION POSGB(2),WEIGB(2),SHAPI(4)
     1  ,X(11,22),Y(11,22),XSI(11,22),SI(11,22)
     2  ,R(11,22),F(11,22),Z(11,22),RHO(11,22),U(11,22),V(11,22)
     3  ,RHOI(22),YI(22),XI(22),RI(22),EQS(11,22),AVSY(11,22)
     4  ,SX(210,4),SY(210,4),SXY(210,4),EQSR(11,22),AVSX(11,22)
     6  ,EX(11,22),EY(11,22),EXY(11,22),EQSS(210,4),AVSXY(11,22)
     7  ,ROLL(1,22),VELO(11,22)

        COMMON/FEM/XNODE(210,4),YNODE(210,4)
        COMMON/GEM/UNODE(210,4),VNODE(210,4),RHONOD(210,4)

C       M IS NO. OF GRID POINTS IN X-DIRECTION
C       N IS NO. OF GRID POINTS IN Y-DIRECTION
        N=11
        M=22

        EL=DSQRT((RA-((Y1-Y2)/2.0))*2.0*(Y1-Y2))
        DXSI=1.0/DFLOAT(N-1)
        DX=EL/DFLOAT(M-1)
C       ------------------------------------------------------------------
C               EVALUATION OF DENSITY AT THE SURFACE USING DENSITY
C               EXPRESSION
C       ------------------------------------------------------------------
        TXVAL=-DX
        DO 908 I=1,22
        TXVAL=TXVAL+DX
        XI(I)=TXVAL
        RI(I)=((EL**2)/(2.0*(Y1-Y2)))+((Y1-Y2)/2.0)
        YR=RI(I)+Y2
        YI(I)=-DSQRT(RI(I)**2-(XI(I)-EL)**2)+YR
        RNIT=(1.0-RHOO)/RHOO
        VARI=(YI(I)/Y1)**B
        RHOI(I)=1.0/(1.0+(RNIT*VARI))
        IF(RHOI(I).GT.0.998)RHOI(I)=0.998
908     CONTINUE
C       ------------------------------------------------------------------
C               EVALUATION OF DENSITY IN THE DOMAIN
C       ------------------------------------------------------------------
        XSIVAL=-DXSI
        DO 100 J=1,N
        XVAL=-DX
        XSIVAL=XSIVAL+DXSI
        DO 150 K=1,M
        XVAL=XVAL+DX
        X(J,K)=XVAL
        XSI(J,K)=XSIVAL
        IF(J.EQ.1)GO TO 42
        R(J,K)=((EL**2)/(2.0*XSI(J,K)*(Y1-Y2)))+(XSI(J,K)
     1  *(Y1-Y2)/2.0)
        YO=R(J,K)+XSI(J,K)*Y2
        Y(J,K)=-DSQRT(R(J,K)**2-(X(J,K)-EL)**2)+YO
        SI(J,K)=RHOO*UO*Y1*XSI(J,K)
        T1=Y(J,K)-YO
        T2=Y2*(Y(J,K)-YO)
        T3=R(J,K)+Y(J,K)-YO
        T4=-EL**2/(2.0*(Y1-Y2)*XSI(J,K)**2)
        T5=(Y1-Y2)/2.0
        V1=T1/(T2+(T3*(T4+T5)))
        T6=X(J,K)-EL
```

```
      V2=T6/(T2+(T3*(T4+T5)))
      F(J,K)=RHO0*U0*Y1*V1
      Z(J,K)=-RHO0*U0*Y1*V2
      RHO(J,K)=RHOI(K)
      U(J,K)=F(J,K)/RHO(J,K)
      V(J,K)=Z(J,K)/RHO(J,K)
      GO TO 33
42    V(J,K)=0.0000
      RHO(J,K)=RHOI(K)
33    SI(J,K)=RHO(J,K)*U(J,K)*Y(J,K)
150   CONTINUE
100   CONTINUE

      J=1
      DO 352 I=1,22
      U(J,I)=U(2,I)
352   CONTINUE

      DO 663 J=1,11
      DO 530 K=1,22
      VELO(J,K)=DSQRT(U(J,K)**2+V(J,K)**2)
530   CONTINUE
663   CONTINUE
C     ------------------------------------------------------------------
C           NUMBERING THE NODES AND SETTING THE CORDINATES
C     ------------------------------------------------------------------
      NEL=0
      DO 1238 J=1,10
      DO 1200 K=1,21
      NEL=NEL+1
      XNODE(NEL,1)=X(J,K)
      YNODE(NEL,1)=Y(J,K)
      RHONOD(NEL,1)=RHO(J,K)
      UNODE(NEL,1)=U(J,K)
      VNODE(NEL,1)=V(J,K)
      XNODE(NEL,2)=X(J,K+1)
      YNODE(NEL,2)=Y(J,K+1)
      RHONOD(NEL,2)=RHO(J,K+1)
      UNODE(NEL,2)=U(J,K+1)
      VNODE(NEL,2)=V(J,K+1)
      XNODE(NEL,3)=X(J+1,K+1)
      YNODE(NEL,3)=Y(J+1,K+1)
      RHONOD(NEL,3)=RHO(J+1,K+1)
      UNODE(NEL,3)=U(J+1,K+1)
      VNODE(NEL,3)=V(J+1,K+1)
      XNODE(NEL,4)=X(J+1,K)
      YNODE(NEL,4)=Y(J+1,K)
      RHONOD(NEL,4)=RHO(J+1,K)
      UNODE(NEL,4)=U(J+1,K)
      VNODE(NEL,4)=V(J+1,K)
1200  CONTINUE
1238  CONTINUE
C     ------------------------------------------------------------------
C           WORK FUNCTION FOR PLASTIC DEFORMATION
C     ------------------------------------------------------------------
C     EX= STRAIN IN X-DIRECTION
C     SX= STRAIN RATE IN X-DIRECTION
C     AVSX= AVERAGE STRAIN RATE IN X-DIRECTION
C     EY= STRAIN IN Y-DIRECTION
C     SY= STRAIN RATE IN Y-DIRECTION
C     AVSY= AVERAGE STRAIN RATE IN Y-DIRECTION
C     EXY= SHEAR STRAIN
C     SXY= SHEAR STRAIN RATE
C     AVSXY= AVERAGE SHEAR STRAIN
C     EQSR= EQUIVALENT STRAIN
C     EQS= EQUIVALENT STRAIN
```

```
C
C       EVALUATION OF STRAIN RATES IN THE DOMAIN USING STRAIN SUBROUTINE
C
        DO 111 IELEM=1,210
        NELEM=210
        NNODL=4
        NODE=4
        CALL STRAIN(NELEM,IELEM,NODE,NNODL,SX,SY,SXY)
111     CONTINUE
C
C       EVALUATION OF AVERAGE STRAIN RATE AT A NODE INSIDE THE DOMAIN
C
        DO 702 J=1,9
        DO 703 K=1,20
        I=(J-1)*21+K
        AVSX(J+1,K+1)=(SX(I,3)+SX(I+1,4)+SX(I+21,2)+SX(I+22,1))/4.0
        AVSY(J+1,K+1)=(SY(I,3)+SY(I+1,4)+SY(I+21,2)+SY(I+22,1))/4.0
        AVSXY(J+1,K+1)=(SXY(I,3)+SXY(I+1,4)+SXY(I+21,2)+SXY(I+22,1))
     1  /4.0
703     CONTINUE
702     CONTINUE
C
C       EVALUATION OF AVERAGE STRAIN AT A NODE AT THE CENTRE LINE
C
        J=1
        DO 704 K=1,20
        AVSX(J,K+1)=(SX(K,2)+SX(K+1,1))/2.0
        AVSY(J,K+1)=(SY(K,2)+SY(K+1,1))/2.0
        AVSXY(J,K+1)=(SXY(K,2)+SXY(K+1,1))/2.0
704     CONTINUE
C
C       EVALUATION OF STRAIN RATE AT THE SURFACE
C
        J=10
        DO 705 K=1,20
        I=(J-1)*21+K
        AVSX(J+1,K+1)=(SX(I,3)+SX(I+1,4))/2.0
        AVSY(J+1,K+1)=(SY(I,3)+SY(I+1,4))/2.0
        AVSXY(J+1,K+1)=(SXY(I,3)+SXY(I+1,4))/2.0
705     CONTINUE
C
C       EVALUATION OF THE STRAIN RATE AT THE ENTRY SECTION
C
        K=1
        DO 706 J=1,9
        I=(J-1)*21+K
        AVSX(J+1,K)=(SX(I,4)+SX(I+21,1))/2.0
        AVSY(J+1,K)=(SY(I,4)+SY(I+21,1))/2.0
        AVSXY(J+1,K)=(SXY(I,4)+SXY(I+21,1))/2.0
706     CONTINUE
C
C       EVALUATION OF STRAIN RATE AT EXIT SECTION
C
        K=21
        DO 707 J=1,9
        I=(J-1)*21+K
        AVSX(J+1,K+1)=(SX(I,3)+SX(I+21,2))/2.0
        AVSY(J+1,K+1)=(SY(I,3)+SY(I+21,2))/2.0
        AVSXY(J+1,K+1)=(SXY(I,3)+SXY(I+21,2))/2.0
707     CONTINUE
C
C       EVALUATION OF STRAIN RATES AT THE CORNERS OF THE DOMAIN
C
        AVSX(1,1)=SX(1,1)
        AVSY(1,1)=SY(1,1)
        AVSXY(1,1)=SXY(1,1)
```

```
      AVSX(11,1)=SX(190,4)
      AVSY(11,1)=SY(190,4)
      AVSXY(11,1)=SXY(190,4)
      AVSX(1,22)=SX(21,2)
      AVSY(1,22)=SY(21,2)
      AVSXY(1,22)=SXY(21,2)
      AVSX(11,22)=SX(210,3)
      AVSY(11,22)=SY(210,3)
      AVSXY(11,22)=SXY(210,3)
C
C     EVALUATION OF EQUIVALENT STRAIN AT NODES
C
      DO 611 J=1,11
      DO 633 K=1,22
      TT1=(AVSX(J,K)-AVSY(J,K))**2
      TT2=AVSX(J,K)+AVSY(J,K)
      TT3=(AVSX(J,K))**2
      TT4=(AVSY(J,K))**2
      TT5=(RHO(J,K))**1.5
      TT6=1.0/(2.49*(1.0-RHO(J,K))**0.514)
      TT7=(AVSXY(J,K))**2
      EQSR(J,K)=TT5*DSQRT(((2.0/9.0)*(TT1+TT3+TT4+(3.0*TT7)))
     1 +((TT6*TT2)**2))
633   CONTINUE
611   CONTINUE
C
C     EVALUATION OF CUMULATIVE STRAINS
C
      DO 353 J=1,11
      DO 412 K=1,22
      IF(K.EQ.1)GO TO 815
      AVEQSR=(EQSR(J,K-1)+EQSR(J,K))/2.0
      AVEX=(AVSX(J,K-1)+AVSX(J,K))/2.0
      AVEY=(AVSY(J,K-1)+AVSY(J,K))/2.0
      AVEXY=(AVSXY(J,K-1)+AVSXY(J,K))/2.0
      AVUVAL=(U(J,K-1)+U(J,K))/2.0
      EQS(J,K)=EQS(J,K-1)+(AVEQSR*((X(J,K)-X(J,K-1))/AVUVAL))
      EX(J,K)=EX(J,K-1)+(AVEX*((X(J,K)-X(J,K-1))/AVUVAL))
      EY(J,K)=EY(J,K-1)+(AVEY*((X(J,K)-X(J,K-1))/AVUVAL))
      EXY(J,K)=EXY(J,K-1)+(AVEXY*((X(J,K)-X(J,K-1))/AVUVAL))
      GO TO 521
815   EX(J,K)=0.0
      EY(J,K)=0.0
      EQS(J,K)=0.0
      EXY(J,K)=0.0
521   CONTINUE
412   CONTINUE
353   CONTINUE
C
C     NUMBERING THE NODES FOR EQUIVALENT STRAIN
C
      IELEM=0
      DO 8238 J=1,10
      DO 8200 K=1,21
      IELEM=IELEM+1
      EQSS(IELEM,1)=EQS(J,K)
      EQSS(IELEM,2)=EQS(J,K+1)
      EQSS(IELEM,3)=EQS(J+1,K+1)
      EQSS(IELEM,4)=EQS(J+1,K)
8200  CONTINUE
8238  CONTINUE
C     ------------------------------------------------------------
C               EVALUATION OF ROLL PRESSURE
C     ------------------------------------------------------------
      J=11
      DO 6309 K=1,22
```

```
      P10=RHO(J,K)**4.0
      P11=431.00*((EQS(J,K)+0.01)**0.32)
      P12=(2.0*AVSY(J,K))/3.0
      FO=1.0/(2.49*(1.0-RHO(J,K))**0.514)
      P14=2.0/(9.0*FO**2)
      P15=FO**2
      P16=AVSX(J,K)+AVSY(J,K)
      P17=(P10*P11)/EQSR(J,K)
      P18=(2.0*AVSX(J,K))/3.0
      P19=P17*(P12+((1.0-P14)*P15*P16))
      P20=P17*(P18+((1.0-P14)*P15*P16))
      ROLL(J,K)=DSQRT(P19**2+P20**2)
6309  CONTINUE
C     ------------------------------------------------------------------
C               EVALUATION OF PLASTIC WORK
C     ------------------------------------------------------------------
      FI=0.0
      DO 641 IELEM=1,210
      NELEM=210
      NNODL=4
      NGAUS=2
      CALL DRIVES(NELEM,EQSS,
     1 NGAUS,NNODL,SUM,IELEM)
      FI=FI+SUM
641   CONTINUE
      DEFORM=FI
C     ------------------------------------------------------------------
C       WORK LOSSES AT THE ROLL SURFACE AND AT THE DISCONTINUITY
C     ------------------------------------------------------------------
      POSGB(1)=0.5773502692
      POSGB(2)=-POSGB(1)
      WEIGB(1)=1.0000000
      WEIGB(2)=1.0000000
      SHAPI(1)=(1.0-POSGB(1))/2.0
      SHAPI(2)=(1.0+POSGB(1))/2.0
      SHAPI(3)=(1.0-POSGB(2))/2.0
      SHAPI(4)=(1.0+POSGB(2))/2.0
C
C     WORK FUNCTION AT THE ROLL SURFACE
C
      G=0.0
      J=11
      DO 888 K=1,21
      DDX=X(J,K+1)-X(J,K)
      DDY=Y(J,K)-Y(J,K+1)
      DDL=DSQRT(DDX**2+DDY**2)
      DETJL=DDL/2.0
      E1=(SHAPI(1)*RHO(J,K)+SHAPI(2)*RHO(J,K+1))**2.5
      E2=(SHAPI(3)*RHO(J,K)+SHAPI(4)*RHO(J,K+1))**2.5
      D1=DSQRT(((SHAPI(1)*U(J,K)+SHAPI(2)*U(J,K+1))**2)+
     1 ((SHAPI(1)*V(J,K)+SHAPI(2)*V(J,K+1))**2))
      D2=DSQRT(((SHAPI(3)*U(J,K)+SHAPI(4)*U(J,K+1))**2)+
     1 ((SHAPI(3)*V(J,K)+SHAPI(4)*V(J,K+1))**2))
      EF1=SHAPI(1)*EQS(J,K)+SHAPI(2)*EQS(J,K+1)
      RF1=431.00*((EF1+0.01)**0.32)
      G1=E1*DABS(UX-D1)*WEIGB(1)*DETJL*RF1
      EF2=SHAPI(3)*EQS(J,K)+SHAPI(4)*EQS(J,K+1)
      RF2=431.00*((EF2+0.01)**0.32)
      G2=E2*DABS(UX-D2)*WEIGB(2)*DETJL*RF2
      G=G+(G1+G2)
888   CONTINUE
      FRICT=(G*FR)/(SQRT(3.0))
C
C     WORK FUNCTION AT THE DISCONTINUITY
C
      Q=0.0
```

```
      K=1
      DO 444 J=1,10
      DFY=Y(J+1,K)-Y(J,K)
      DETJH=DFY/2.0
      E3=(SHAPI(1)*RHO(J,K)+SHAPI(2)*RHO(J+1,K))**2.5
      E4=(SHAPI(3)*RHO(J,K)+SHAPI(4)*RHO(J+1,K))**2.5
      D3=DSQRT((SHAPI(1)*V(J,K)+SHAPI(2)*V(J+1,K))**2)
      D4=DSQRT((SHAPI(3)*V(J,K)+SHAPI(4)*V(J+1,K))**2)
      EF3=SHAPI(1)*EQS(J,K)+SHAPI(2)*EQS(J+1,K)
      RF3=431.00*((EF3+0.01)**0.32)
      G3=E3*D3*WEIGB(1)*DETJH*RF3
      EF4=SHAPI(3)*EQS(J,K)+SHAPI(4)*EQS(J+1,K)
      RF4=431.00*((EF4+0.01)**0.32)
      G4=E4*D4*WEIGB(2)*DETJH*RF4
      Q=Q+(G3+G4)
444   CONTINUE
      DISCT=Q/(SQRT(3.0))
      WORKI=DEFORM+FRICT+DISCT
      RETURN
      END
C     XXXXXXXXXXXXXXXXXXXXXXXXXXXXXXXXXXXXXXXXXXXXXXXXXXXXXXXXXXXXXXXXXX
      SUBROUTINE SHAPE4(DERIV,SHAPE,XEQIV,YEQIV)
C     XXXXXXXXXXXXXXXXXXXXXXXXXXXXXXXXXXXXXXXXXXXXXXXXXXXXXXXXXXXXXXXXXX
C     DERIV=DERATIVE OF SHAPE FUNCTION WITH RESPECT TO LOCAL COORDINATES
C     XEQIV,YEQIV=LOCAL COORDINATES
C     X,Y=LOCAL NAME FOR XEQIV AND YEQIV

      IMPLICIT REAL * 8(A-H,O-Z)
      DIMENSION DERIV(2,8),SHAPE(8)

      X=XEQIV
      Y=YEQIV
      XY=X*Y
      SHAPE(1)=(1.-X-Y+XY)*.25
      SHAPE(2)=(1.+X-Y-XY)*.25
      SHAPE(3)=(1.+X+Y+XY)*.25
      SHAPE(4)=(1.-X+Y-XY)*.25
      DERIV(1,1)=(-1.+Y)*.25
      DERIV(1,2)=(1.-Y)*.25
      DERIV(1,3)=(1.+Y)*.25
      DERIV(1,4)=(-1.-Y)*.25
      DERIV(2,1)=(-1.+X)*.25
      DERIV(2,2)=(-1.-X)*.25
      DERIV(2,3)=(1.+X)*.25
      DERIV(2,4)=(1.-X)*.25
      RETURN
      END
C     XXXXXXXXXXXXXXXXXXXXXXXXXXXXXXXXXXXXXXXXXXXXXXXXXXXXXXXXXXXXXXXXXX
      SUBROUTINE DJACOB(DERIV,DETJB,DJACK,DJACI,NNODL
     1  ,IELEM,NELEM)
C     XXXXXXXXXXXXXXXXXXXXXXXXXXXXXXXXXXXXXXXXXXXXXXXXXXXXXXXXXXXXXXXXXX
C     DETJB=DETERIMINANT OF JACOBIAN MATRIX
C     DJACI=INVERSE OF JACOBIAN MATRIX
C     DJACK=JACOBIAN MATRIX
C     NNODL=NUMBER OF NODES IN LINEAR ELEMENT
C     NELEM=NUMBER OF ELEMENTS IN MESH

      IMPLICIT REAL * 8(A-H,O-Z)
      DIMENSION DERIV(2,8),DJACI(2,2),DJACK(2,2)
      COMMON/FEM/XNODE(210,4),YNODE(210,4)

C     SET UP TEMPORARY MATRIX TO ALLOW THE JACOBIAN TO BE FORMED
C
      TEMPY1=0.0
      TEMPY2=0.0
      TEMPY3=0.0
```

```
      TEMPY4=0.0
      DO 20 INODL=1,4
      XNODI=XNODE(IELEM,INODL)
      YNODI=YNODE(IELEM,INODL)
      TEMPY1=TEMPY1+DERIV(1,INODL)*XNODI
      TEMPY2=TEMPY2+DERIV(1,INODL)*YNODI
      TEMPY3=TEMPY3+DERIV(2,INODL)*XNODI
      TEMPY4=TEMPY4+DERIV(2,INODL)*YNODI
20    CONTINUE
      DJACK(1,1)=TEMPY1
      DJACK(1,2)=TEMPY2
      DJACK(2,1)=TEMPY3
      DJACK(2,2)=TEMPY4
      DETJB=DJACK(1,1)*DJACK(2,2)-DJACK(1,2)*DJACK(2,1)
C
C     CHECK FOR ZERO OR NEGATIVE DETERMINANT
C
      IF(DETJB)30,30,40
30    CONTINUE
      WRITE(5,2000)IELEM
      STOP
40    CONTINUE
C
C     INVERT TEMPORARY MATRIX TO FORM JACOBIAN
C
      DJACI(1,1)=DJACK(2,2)/DETJB
      DJACI(2,2)=DJACK(1,1)/DETJB
      DJACI(1,2)=-DJACK(1,2)/DETJB
      DJACI(2,1)=-DJACK(2,1)/DETJB
C     FORMAT(3X,'IELEM=',I4)
      RETURN
      END
C     XXXXXXXXXXXXXXXXXXXXXXXXXXXXXXXXXXXXXXXXXXXXXXXXXXXXXXXXXXXXXXXX
      SUBROUTINE STRAIN(NELEM,IELEM,NODE,NNODL,SX,SY,SXY)
C     XXXXXXXXXXXXXXXXXXXXXXXXXXXXXXXXXXXXXXXXXXXXXXXXXXXXXXXXXXXXXXXX

      IMPLICIT REAL * 8(A-H,O-Z)
      DIMENSION DERIV(2,8),SHAPE(8),
     1 DJACI(2,2),DJACK(2,2),CARTL(2,4),
     2 SX(210,4),SY(210,4),SXY(210,4)
      COMMON/FEM/XNODE(210,4),YNODE(210,4)
      COMMON/GEM/UNODE(210,4),VNODE(210,4),RHONOD(210,4)
C
C     SX(IELEM,NODE)= X-STRAIN RATE AT NODE
C     SY(IELEM,NODE)= Y-STRAIN RATE AT NODE
C     SXY(IELEM,NODE)= SHEAR-STRAIN RATE AT NODE
C
      DO 545 NODE=1,4
      IF(NODE.EQ.1) GO TO 4444
      IF(NODE.EQ.2) GO TO 4445
      IF(NODE.EQ.3) GO TO 4446
      IF(NODE.EQ.4) GO TO 4447
4444  XEQIV=-1.0
      YEQIV=-1.0
      GO TO 4888
4445  XEQIV=1.0
      YEQIV=-1.0
      GO TO 4888
4446  XEQIV=1.0
      YEQIV=1.0
      GO TO 4888
4447  XEQIV=-1.0
      YEQIV=1.0
      GO TO 4888
4888  CONTINUE
      CALL SHAPE4(DERIV,SHAPE,XEQIV,YEQIV)
```

```
      CALL DJACOB(DERIV,DETJB,DJACK,DJACI,NNODL,IELEM,NELEM)
      DO 300 IDIME=1,2
      DO 300 INODL=1,4
      CARTL(IDIME,INODL)=0.0
      DO 934 JDIME=1,2
      CARTL(IDIME,INODL)=CARTL(IDIME,INODL)+DJACI(IDIME,JDIME)*
     1 DERIV(JDIME,INODL)
934   CONTINUE
300   CONTINUE
      DUDX=0.0
      DUDY=0.0
      DVDX=0.0
      DVDY=0.0
      DO 429 INODL=1,4
      DUDX=DUDX+CARTL(1,INODL)*UNODE(IELEM,INODL)
      DUDY=DUDY+CARTL(2,INODL)*UNODE(IELEM,INODL)
      DVDX=DVDX+CARTL(1,INODL)*VNODE(IELEM,INODL)
      DVDY=DVDY+CARTL(2,INODL)*VNODE(IELEM,INODL)
429   CONTINUE
      SX(IELEM,NODE)=DUDX
      SY(IELEM,NODE)=DVDY
      SXY(IELEM,NODE)=DUDY+DVDX
545   CONTINUE
      RETURN
      END
C     XXXXXXXXXXXXXXXXXXXXXXXXXXXXXXXXXXXXXXXXXXXXXXXXXXXXXXXXXXXXXXXXXXXXXXX
      SUBROUTINE DRIVES(NELEM,EQSS,
     1 NGAUS,NNODL,SUM,IELEM)
C     XXXXXXXXXXXXXXXXXXXXXXXXXXXXXXXXXXXXXXXXXXXXXXXXXXXXXXXXXXXXXXXXXXXXXXX
C     NGAUS=NUMBER OF GAUSS POINTS IN RULE
C     POSGL(NGAUS)=POSITION OF GAUSS POINT IN LOCAL COORDINATES
C     WEIGL(NGAUS)=GAUSS WEIGHING FACTORS AT SAMPLING POINTS
C     AREAW=PRODUCT OF ELEMENT AREA AND GAUSS WEIGHING FUNCTIONS

C     --------------------------------
C     -    EXTERNAL SUBROUTINE       -
C     -    SHAPE4                    -
C     -    DJACOB                    -
C     -    PLASTIC                   -
C     --------------------------------

      IMPLICIT REAL * 8(A-H,O-Z)

      DIMENSION DERIV(2,8),AREAW(4),SHAPE(8),
     1 DJACI(2,2),DJACK(2,2),CARTL(2,4),
     2 POSGL(2),
     3 WEIGL(2),W(4),EQSS(210,4),SUMY(4),
     4 SUM1(4),SUM2(4),SUM3(4),SUM4(4),SUMI(4)
      COMMON/FEM/XNODE(210,4),YNODE(210,4)
      COMMON/GEM/UNODE(210,4),VNODE(210,4),RHONOD(210,4)
C
C     SET UP POSITIONS AND WEIGHTS FOR 2 POINT GAUSS RULE
C
      POSGL(1)=0.5773502
      POSGL(2)=-POSGL(1)
      WEIGL(1)=1.0
      WEIGL(2)=WEIGL(1)
C
C     CALCULATE SHAPE FUNCTION AND DERIVATIVES FOR ELEMENTS
C
      LGAUS=0
      DO 50 IGAUS=1,NGAUS
      DO 50 JGAUS=1,NGAUS
      LGAUS=LGAUS+1
      XEQIV=POSGL(IGAUS)
      YEQIV=POSGL(JGAUS)
```

```
C
C       USE GAUSS POSITIONS TO CALCULATE LOCAL VALUES
C
        CALL SHAPE4(DERIV,SHAPE,XEQIV,YEQIV)
C
C       SET UP JACOBIAN MATRIX AND INVERSE
C
        CALL DJACOB(DERIV,DETJB,DJACK,DJACI,NNODL,
     1  IELEM,NELEM)
C
C       CALCULATE GLOBAL DERIVATIVES FOR LINEAR FUNCTIONS
C
        DO 30 IDIME=1,2
        DO 30 INODL=1,4
        CARTL(IDIME,INODL)=0.0
        DO 10 JDIME=1,2
        CARTL(IDIME,INODL)=CARTL(IDIME,INODL)+DJACI(IDIME,JDIME)*
     1  DERIV(JDIME,INODL)
10      CONTINUE
30      CONTINUE
        DUDX1=0.0
        DUDY1=0.0
        DVDX1=0.0
        DVDY1=0.0
        DO 329 INODL=1,4
        DUDX1=DUDX1+CARTL(1,INODL)*UNODE(IELEM,INODL)
        DUDY1=DUDY1+CARTL(2,INODL)*UNODE(IELEM,INODL)
        DVDX1=DVDX1+CARTL(1,INODL)*VNODE(IELEM,INODL)
        DVDY1=DVDY1+CARTL(2,INODL)*VNODE(IELEM,INODL)
329     CONTINUE
        SUM1(LGAUS)=DUDX1
        SUM2(LGAUS)=DVDX1
        SUM3(LGAUS)=DUDY1
        SUM4(LGAUS)=DVDY1
        SUMI(LGAUS)=0.0
        DO 16 INODL=1,4
        SUMI(LGAUS)=SUMI(LGAUS)+RHONOD(IELEM,INODL)*SHAPE(INODL)
16      CONTINUE
        SUMY(LGAUS)=0.0
        DO 17 INODL=1,4
        SUMY(LGAUS)=SUMY(LGAUS)+EQSS(IELEM,INODL)*SHAPE(INODL)
17      CONTINUE
        AREAW(LGAUS)=DETJB*WEIGL(IGAUS)*WEIGL(JGAUS)
C
C       CALCULATION OF PLASTIC WORK FUNCTION
C
        CALL PLASTIC(LGAUS,SUM1,SUM2,SUM3,SUM4,SUMY,SUMI,AREAW,W)

50      CONTINUE
        SUM=(W(1)+W(2)+W(3)+W(4))
        RETURN
        END
C       XXXXXXXXXXXXXXXXXXXXXXXXXXXXXXXXXXXXXXXXXXXXXXXXXXXXXXXXXXXXXXXXXXXXXX
        SUBROUTINE PLASTIC(LGAUS,SUM1,SUM2,SUM3,SUM4,SUMY,SUMI,
     1  AREAW,W)
C       XXXXXXXXXXXXXXXXXXXXXXXXXXXXXXXXXXXXXXXXXXXXXXXXXXXXXXXXXXXXXXXXXXXXXX

        IMPLICIT REAL * 8(A-H,O-Z)

        DIMENSION SUM1(4),SUM2(4),SUM3(4),SUM4(4),
     1  SUMI(4),AREAW(4),W(4),SUMY(4)

        W1=(SUM1(LGAUS)-SUM4(LGAUS))**2
        W2=(SUM2(LGAUS)+SUM3(LGAUS))**2
        W3=SUM1(LGAUS)+SUM4(LGAUS)
        W4=SUM1(LGAUS)
```

```
      W5=SUM4(LGAUS)
      W6=SUMI(LGAUS)
      W7=(2.0/9.0)*(W1+W4**2+W5**2+
     1  (3.5*W2))
      W8=(1.0-W6)**0.514
      W9=(W3/(2.49*W8))**2
      SQT1=431.00*((SUMY(LGAUS)+0.01)**0.32)
      W(LGAUS)=(W6**2.5)*DSQRT(W7+W9)*
     1  AREAW(LGAUS)*SQT1
      RETURN
      END
C     ******************************************************************
C     ******************************************************************
```

ME-1990-M-DES-ANA